987

Université de Neuchâtel
Institut de Microtechnique

ELECTRONIC FRINGE INTERPOLATION IN HOLOGRAPHIC INTERFEROMETRY

APPLIED TO DEFORMATION MEASUREMENT OF SOLID OBJECTS

THESE

présentée à la Faculté des Sciences
pour obtenir le grade de Docteur ès Sciences

par

RUEDI THALMANN

IMPRIMATUR POUR LA THÈSE

Electronic Fringe Interpolation in

Holographic Interferometry Applied to

Deformation Measurement of Solid Objects

de M*onsieur Rudolf THALMANN*

UNIVERSITÉ DE NEUCHATEL

FACULTÉ DES SCIENCES

La Faculté des sciences de l'Université de Neuchâtel, sur le rapport des membres du jury,

Messieurs R. Dändliker, H. Beck, W. Schumann (EPF-Zurich) et R. Pryputniewicz (Worcester, USA)

autorise l'impression de la présente thèse.

Neuchâtel, le *6 novembre 1986*

Le doyen:

François Sigrist

François Sigrist

Les tirés à part ci-joints représentent l'essentiel de la thèse de doctorat dont le titre et le nom de l'auteur sont repris en page de garde.
Le texte complet du manuscrit peut être consulté à la bibliothèque de l'Institut de Microtechnique, rue A.-L.-Breguet 2, 2000 Neuchâtel.

FRINGE INTERPOLATION BY TWO-REFERENCE-BEAM HOLOGRAPHIC INTERFEROMETRY: REDUCING SENSITIVITY TO HOLOGRAM MISALIGNMENT

R. DÄNDLIKER, R. THALMANN and J.-F. WILLEMIN
Institut de Microtechnique de l'Université, CH-2000 Neuchâtel, Switzerland

Received 19 April 1982

Accurate fringe interpolation in holographic interferometry requires two-reference-beam holographic recording. Using two reference sources close together, the sensitivity to (angular) misalignement of the hologram is drastically reduced (10° instead of 0.01°). Overlapping of the cross-reconstructions can be tolerated, unless extreme precision and spatial resolution are demanded. Experimental results obtained by video processing of such holograms show an accuracy of better than 1/100 of a fringe. The optical setup becomes nearly as compact and simple as in classical holographic interferometry.

1. Introduction

Double exposure holographic interferometry requires for accurate deformation measurement interpolation of the interference fringes. Interpolation independent of fringe position and intensity variations in the reconstructed image is only possible by applying two-reference-beam holography [1,2], which allows to vary the relative phase of the interfering wavefields during reconstruction. Two kinds of methods to evaluate the interference phase are known. In heterodyne methods [1] the relative phase increases linearly in time and the interference phase is measured electronically at the beat frequency of the reconstructed wavefields. "Quasi-heterodyne" techniques change the relative phase stepwise, using at least three different values [3–6]. Compared with classical double exposure holographic interferometry the necessity to use two-reference-beam holography introduces unfortunately some additional difficulties with unwanted reconstructions and repositioning of the hologram [2].

In holographic interferometry of diffusely scattering objects the repositioning requirements can be drastically reduced by choosing the two reference beams very close together, as it was already proposed for heterodyne holographic interferometry [7,8]. In this arrangement, however, the undesired cross reconstructions overlap with the desired reconstructions. As a consequence, the fringe contrast is reduced and an additional statistical phase error is introduced, respectively.

In this paper we will show that the two arrangements with reference beams well separated and very close together give results of equally good accuracy when used for a quasi-heterodyne system with TV image processing. We will present a setup for holographic interferometry with high quality fringe interpolation, which is optically nearly as simple as classical double exposure holography and uses standard video-electronic equipment for information processing.

2. Two-reference-beam holographic interferometry

The optical arrangements for two-reference-beam holographic interferometry are sketched in fig. 1a for well separated reference sources and in fig. 1b for reference sources close together. Except for the two references, this setup is the same as for classical holographic interferometry. In both arrangements, the object is illuminated by a point source, and an imaging system permits to observe the interferogram on a screen by a TV-camera. Consecutively, the first object state O_1 is recorded by reference R_1 and the second object state O_2 by reference R_2 on the same hologram plate. A mirror on a piezo mounting allows to vary the path length of one reference beam and hereby to control the relative phase of the two reference beams during reconstruction.

0 030-4018/82/0000–0000/$ 02.75 © 1982 North-Holland

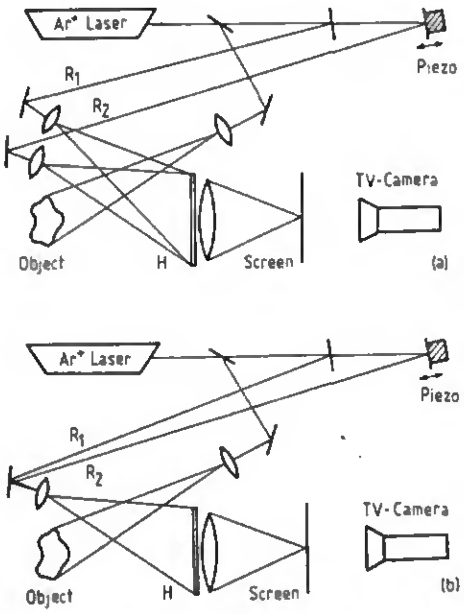

Fig. 1. Setup for two-reference-beam holographic interferometry with (a) well separated reference sources and (b) reference sources close together.

As described in ref. [2], two-reference-beam holography requires special attention to the multiplicity of the reconstructed images and the influence of misalignement of the hologram with respect to the reference beams. Illuminating the hologram with both reference beams R_1 and R_2 yields eight reconstructions. Four of them are conjugate reconstructions. The other ones are the two desired primary self-reconstructions ($R_1 R_1^* O_1$ and $R_2 R_2^* O_2$), which give rise to the interference pattern, and the two undesired cross-reconstructions ($R_2 R_1^* O_1$ and $R_1 R_2^* O_2$). The direction of propagation of the various reconstructed waves depends on the geometry of the optical setup. The primary reconstructions are shown for both cases in fig. 2a and fig. 2b.

To avoid disturbing overlapping of the different reconstructions (fig. 2a) the two reference sources must be chosen on the same side of the object with a mutual separation just larger than the angular size of the object in the corresponding direction (fig. 1a). However, the consequence of large separation of the reference sources is high sensitivity to repositioning errors, as described hereafter. Therefore reference sources close together (fig. 1b) would be prefered if,

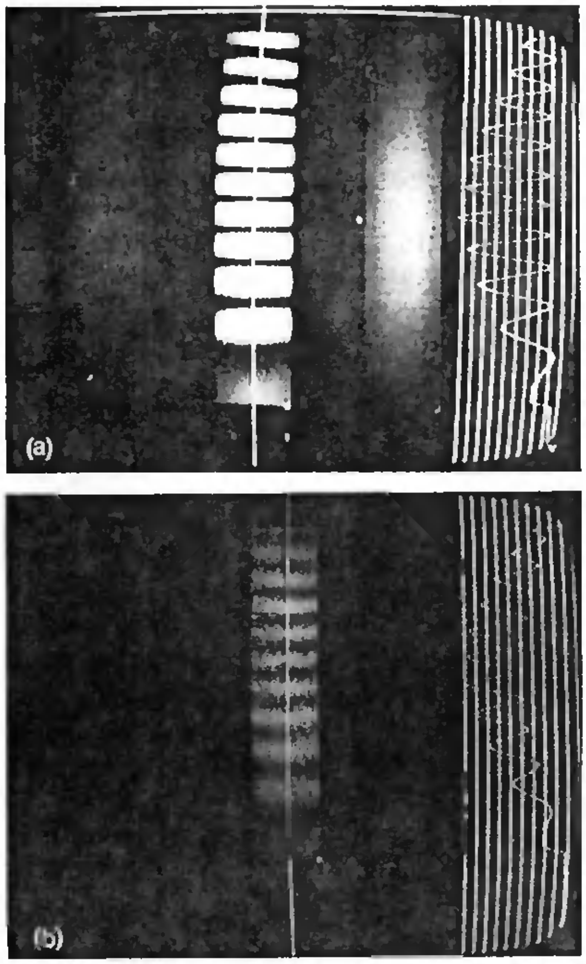

Fig. 2. Primary reconstructed images on TV screen. (a) Well separated reference sources yield separated cross-reconstructions $R_2 R_1^* O_1$ and $R_1 R_2^* O_2$. (b) Reference sources close together yield overlapping reconstructions. The extracted intensity profiles show the difference in fringe contrast.

under certain conditions, overlapping (fig. 2b) of the cross-reconstructions could be tolerated without undue loss of accuracy for the interference phase measurement.

The sensitivity to repositioning for two-reference-beam holographic interferometry occurs because the propagations of the two reconstructed wavefields are differently affected. For small changes of the hologram position from recording to reconstruction the resulting additional phase difference $\psi(x_H)$ in the hologram plane between the reconstructed waves corresponding to the objects O_1 and O_2 is given by [1]

$$\psi(x_H) \approx \{(k_1 - k_2) \times w\} x_H, \quad (1)$$

where $w = (\Delta\alpha, \Delta\beta, \Delta\gamma)$ is the rotation vector for small hologram rotations $\Delta\alpha, \Delta\beta, \Delta\gamma$ around the x, y, z axes, respectively, and x_H are the coordinates in the hologram plane. Note that a pure translation of the hologram causes only a constant phase shift and can be ignored. It is seen from eq. (1) that a rotation of the hologram introduces a linear phase deviation across the hologram plane which depends only on the difference vector $\Delta k = k_1 - k_2$ of the two references. This means that the repositioning sensitivity is much smaller for reference sources close together. The effect of a linear phase deviation in the hologram plane results mainly in a mutual transverse shift between the two desired reconstructions in the image plane [1], given by

$$u_I = (d_I/k)|\mathrm{grad}_H\ \psi| = (d_I/k)$$

$$\times [(\Delta k_y \Delta\gamma - \Delta k_z \Delta\beta)^2 + (\Delta k_z \Delta\alpha - \Delta k_x \Delta\gamma)^2]^{1/2} \quad (2)$$

where d_I is the distance from the lens to the image plane and $\mathrm{grad}_H\ \psi$ is the component of **grad** ψ in the hologram plane.

The magnitude of the interference term depends essentially on the autocorrelation $C_h(u_I)$ of the impulse response function of the imaging system, which defines also the speckle size in the image. The interference fringes are only visible as long as the mutual shift of the speckle patterns is smaller than the speckle size. For a circular aperture of diameter D, the fringe contrast $\gamma(u_I) = C_h(u_I)$ is given by the well known Airy function

$$\gamma(u_I) = 2J_1(\pi D u_I/\lambda d_I)/(\pi D u_I/\lambda d_I), \quad (3)$$

where $J_1(\cdot)$ is the first order Bessel function. The fringe contrast decreases with transverse shift u_I in terms of the diffraction limited optical resolution $(\Delta x)_I = \lambda d_I/D$.

In fig. 3 theoretical and experimental results for the fringe contrast versus hologram rotation $\Delta\gamma$ are presented. The two reference waves had an angular separation of $\Delta k_y/k = 0.19$, which is necessary to separate the reconstructions (figs. 1a and 2a) in a typical holographic setup. A one-to-one image of the reconstructed object was formed by an objective of $f = 300$ mm ($d_I = 600$ mm) and of $D = 9$ mm ($f/32$) effective aperture. The repositioning error for a reduction of the fringe contrast γ to 50% as obtained from eqs. (2) and (3) is found to be only $\Delta\gamma = 0.013°$, (see also fig. 3).

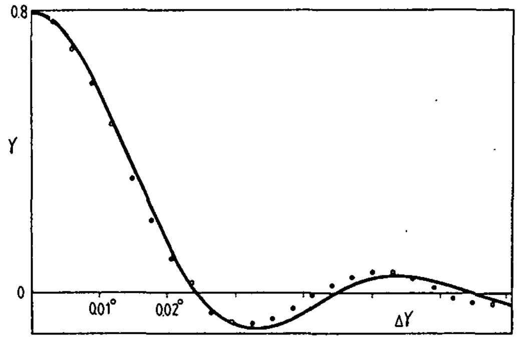

Fig. 3. Fringe contrast γ versus angular misalignement $\Delta\gamma$ of the hologram for well separated reference sources ($\Delta k_y/k = 0.19$). The theoretical curve of eq. (3) is normalized to the maximum measured contrast $\gamma_{max} = 0.8$.

On the other hand, as long as the lateral separation of the cross-reconstructions $R_2R_1^*O_1$ and $R_1R_2^*O_2$ is just larger than the speckle size $(\Delta x)_I$, the speckle patterns of the desired and undesired images are uncorrelated and their superposition does not produce any macroscopic interference. The required minimum angular separation between the two reference sources is given by the diffraction limit of the resolution imposed by the circular aperture D of the imaging lens. In other words, the two reference sources must produce more than one interference fringe across the lens aperture. The sensitivity to misalignement in such a setup (fig. 1b) is reduced to less than $\Delta\gamma = 10°$, compared to the 0.01° for the well separated cross-reconstructions.

However, the overlapping with the uncorrelated cross-reconstructions reduces the overall fringe contrast by a factor two, as can be seen by comparing figs. 2a and 2b, and introduces a statistical error to the interference phase. This error can be adequately reduced by spatial averaging using a detection area which covers many speckles [1], as it is the case in TV processing due to the limited camera resolution.

3. Interferogram processing

To determine the phase in the interferogram, a quasi-heterodyne technique is used [3–6]. The hologram is reconstructed three times, the mutual phase of the two reference beams is changed each time between two reconstructions by a well controlled phase-shift. The local intensities $I_k(x)$ in the interferogram of the reconstructions $k = 1,2,3$ are given by the three equations

$$I_k(x) = a(x)\,\{1 + m(x)\cos(\phi(x) + \phi_k)\}, \qquad (4)$$

where $a(x)$ denotes the local mean intensity, $m(x)$ the fringe contrast and $\phi(x)$ the interference phase. The additional phases ϕ_k are adjusted differently for each reconstruction k. For the interference phase $\phi(x)$ one gets from eqs. (4)

$$\tan\phi(x) = \frac{(I_3-I_2)\cos\phi_1 + (I_1-I_3)\cos\phi_2 + (I_2-I_1)\cos\phi_3}{(I_3-I_2)\sin\phi_1 + (I_1-I_3)\sin\phi_2 + (I_2-I_1)\sin\phi_3}. \qquad (5)$$

The other unknown values are given by

$$a(x)\,m(x) = \frac{(I_1 - I_2)}{\cos(\phi(x)+\phi_1) - \cos(\phi(x)+\phi_2)}, \qquad (6)$$

$$a(x) = I_1 - a(x)\,m(x)\cos(\phi(x) + \phi_1). \qquad (7)$$

Data acquisition and processing is carried out with a video-system and a micro-computer (fig. 4). The interferogram, projected on a ground glass screen, is observed with a TV-camera. The silicon target Ultricon camera guarantees a linear response for the detected signal. A video-analyser extracts an analog signal along a straight line through the object. This signal is converted into digital and the micro-computer takes the average of the three successive scans as input. This process is repeated for three hologram reconstructions with different relative phases ϕ_k of the reference beams. These phases are adjusted carefully with a piezo mounted mirror (fig. 1) to become $\phi_1 = 0°$, $\phi_2 = 120°$, $\phi_3 = 240°$. Finally the interference phase $\phi(x)$ along the scanned

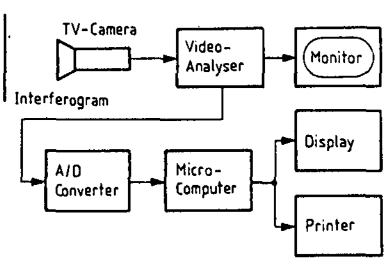

Fig. 4. Block diagram of the video-electronic processing.

line is calculated, displayed and plotted by the computer.

To estimate the accuracy of the phase measurement one has to distinguish between systematical and statistical sources of errors. A systematic error is introduced by wrong phase shifts ϕ_k. It gives rise to a periodic error for $\phi(x)$. For three measurements with phase shifts ϕ_k in steps of 120°, the maximal error of $\phi(x)$ is of the same order as the errors for the ϕ_k. It is important to point out, that the absolute value of the ϕ_k must be guaranteed with the same precision as desired for the phase $\phi(x)$. It will be discussed later, how to control the phase shifts ϕ_k in the cases of reference sources close together or well separated.

For the statistical error $\Delta\phi$ the expression

$$(\Delta\phi)^2 = (2/3\,m^2)\,(\Delta I/I)^2 + \tfrac{1}{2}\,(\Delta\phi_k)^2 \qquad (8)$$

can be derived from eq. (5). It depends on the relative fluctuations $\Delta I/I$ of the intensities measured by the TV-camera and on the statistical fluctuations $\Delta\phi_k$ of the relative phases between the reference beams due to thermal perturbations and mechanical instabilities. To avoid disturbing fluctuations of the ϕ_k, the phase between the two reference beams had to be stabilized by a feed back loop acting on the piezo electric mirror.

In the case of two reference sources close together (fig. 1b) the relative phase of the two reference beams can be detected and controlled very effectively by a twin-photodiode placed in the hologram plane, just outside the field used for the reconstruction. This is possible easily and accurately since the two reference beams produce on the hologram a pattern of parallel and equidistant interference fringes of typically 2 to 5 mm separation. The twin-photodiode detects the fringe maximum and an integrating feed back loop to the piezo electric mirror keeps the fringes stable. The different phases ϕ_k for the three reconstructions can be established very accurately by moving the twin-photodiode in steps of 1/3 of the fringe separation. With this stabilization device $\Delta\phi_k$ of less than 1° for a time constant of 10 ms have been achieved.

This method does not work for well separated reference sources (fig. 1a), since no macroscopic fringe pattern is available in the hologram plane. Therefore one has to use for the stabilization feed back the fringe pattern due to the object deformation in the reconstructed image, which is not always practicable and does not allow easily and accurately to control the steps of the phases ϕ_k by moving the detector.

The average electric noise ratio $\Delta I/I$ of the TV-camera was determined experimentally to be about 2.5%. Averaging over three independent scans reduces this value by a factor $1/\sqrt{3}$. So one can expect a phase error of $\Delta\phi = 1.7°$, calculated with eq. (8) for a fringe contrast of $m = 0.4$.

4. Experimental results

The capability of the described method was experimentally verified with a cantilever under bending load (length = 200 mm, width = 40 mm) as test object. This object was illuminated with a 600 mW single frequency Ar-laser (λ = 514 nm). As shown in fig. 1, the intensity ratios between object illumination and references R_1 and R_2 can be adjusted independently by two variable beam splitters to get first optimum recording conditions and afterwards maximum power in the reconstructing reference waves. The double exposure hologram was recorded on a Millimask plate (50 X 50 mm).The interferogram was reconstructed through an objective with 300 mm focal length and $f/5.6$ on a ground glass screen at unit magnification and observed by a silicon target Ultricon TV-camera.

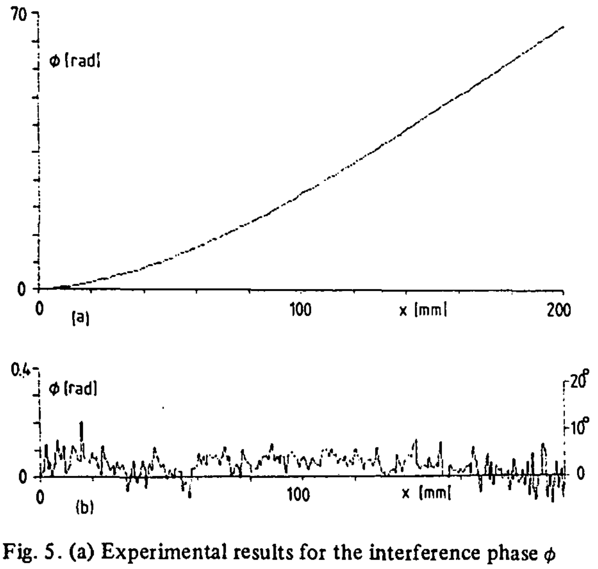

Fig. 5. (a) Experimental results for the interference phase ϕ (deformation) of a bent cantilever versus length x. (b) Phase variations (statistical error) measured for the undeformed cantilever.

The experimental result for the bent cantilever, clamped at the base and loaded at the end, is given in fig. 5a. The same result was obtained with both optical arrangements, shown in fig. 1.

The normal displacement of the cantilever surface can be deduced from the interference phase $\phi(x)$. As shown in eq. (8), the statistical phase error is due first to intensity fluctuations and second to reference phase fluctuations. Besides this statistical errors, additional errors may occur in the measured interference phase $\phi(x)$, mainly caused by optical and mechanical instabilities between the recording of the two object states. To determine the statistical errors (variance) of the phase measurement independently of these perturbations between the two exposures, the same object was recorded simultaneously with the two reference beams to give a two-reference-beam hologram of an undeformed object. The result of the analyzed reconstruction is shown in fig. 5b.

From the measured phase along the undeformed object (fig. 5b), the statistical phase error was determined to be $\Delta\phi = 1.6°$. This agrees very well with the expected value. Note that the phase error is slightly larger at the extremities of the object due to the lower mean intensity I, which yields a reduction of the TV signal-to-noise ratio.

5. Conclusions

It has been demonstrated how two-reference-beam holographic interferometry with video-electronic processing, offering an accuracy of 1/100 of a fringe at TV resolution, can be operated nearly as easily as classical double exposure holography. The misalignement sensitivity of two-reference-beam holograms is drastically reduced to about 10° angular positioning (compared to about 0.01° for conventional arrangements) by using two reference sources very close together (about 0.01° angular separation). It has been shown that the overlapping of the cross-reconstructions can be tolerated for objects with rough surfaces, unless extreme precision and spatial resolution are demanded. The described system combines effectively the simplicity of standard double exposure holography, video-electronic processing, and the power of heterodyne holographic interferometry.

References

[1] R. Dändliker, in: Progress in optics, Vol. 17, ed. E. Wolf (North-Holland, Amsterdam, 1980) pp. 1–84.
[2] R. Dändliker, E. Marom and F.M. Mottier, J. Opt. Soc. Am. 66 (1976) 23.
[3] G.E. Sommargren, Appl. Optics 16 (1977) 1736.
[4] F. Lanzl and M. Schlüter, SPIE 136 (1977) 166.
[5] J.H. Bruning, D.R. Herriott, J.E. Gallagher, D.P. Rosenfeld, A.D. White and D.J. Brangaccio, Appl. Optics 13 (1974) 2693.
[6] L.M. Frantz, A.A. Sawschuk and W. von der Ohe, Appl. Optics 18 (1979) 3301.
[7] R. Dändliker, in: Applications of holography and optical data processing (Pergamon Press, Oxford, 1977) pp. 169–181.
[8] Ref. [1], pp. 40–44.

High resolution video-processing for holographic interferometry applied to contouring and measuring deformations

R. Thalmann, R. Dändliker
Institut de Microtechnique de l'Université
CH-2000 Neuchâtel, Switzerland

Abstract

An opto-electronic system for the evaluation of double-exposure and double-pulse holographic interferograms is presented. Video-electronic detection with quasi-heterodyne fringe interpolation (step-wise phase shifting) is employed and yields a resolution of 1/100 of a fringe. Automated quantitative determination of object shape and object deformation is possible in the same set-up.

Introduction

The automated evaluation of holographic interferograms for quantitative determination of displacement and strain of arbitrarily shaped objects is a problem still not resolved satisfactorily. It requires accurate interference phase measurement, independent of fringe position and intensity variations in the reconstructed image. In many interferometric set-ups, heterodyne or quasi-heterodyne [1] techniques have become a powerful tool for high resolution interference fringe interpolation. In holographic interferometry, these techniques have been applied to real-time [2,3] as well as to double-exposure [2,4,5] holography. For double-exposure holography two reference beams are required [6]. During reconstruction a change of the relative phase between the two reference beams allows to shift the fringes in the interferogram at will.

In heterodyne methods, the relative phase increases linearly in time and the interference phase is measured electronically at the beat frequency of the reconstructed wavefields. Heterodyne holographic interferometry offers high spatial resolution and interpolation up to 1/1000 of a fringe. However, it requires sophisticated electronic equipment and mechanical scanning of the image by photodetectors [4]. In quasi-heterodyne methods, the relative phase is changed step-wise, using at least three different values. The interference phase can then be computed from the different measured intensity values. Quasi-heterodyne techniques are more adequate for digital processing and TV detection. Two-reference-beam holography with reference sources close together and video-electronic processing allow to measure the interference phase with an accuracy of 1/100 of a fringe at any point in the TV image. This system combines effectively the simplicity of standard double-exposure holography, video-electronic processing, and the power of heterodyne holographic interferometry.

In this paper, we present first some fundamental considerations concerning quasi-heterodyne fringe evaluation. Then the experimental set-up with two reference sources close together, interference fringe stabilization and video-electronic processing is described. The limitations for the accuracy of the phase measurement are discussed in detail. Finally, experimental results for holographic contouring are reported to illustrate the possibilities of the described measuring technique.

Interferometry and fringe interpolation

Interferometry is used to transform phase differences of wavefields into detectable intensity variations, i.e. interference fringes. Assuming that the two wavefields to be compared are given by

$$V_1(\vec{x}) = a_1(\vec{x}) \cos[\omega t + \phi_1(\vec{x})], \qquad V_2(\vec{x}) = a_2(\vec{x}) \cos[\omega t + \phi_2(\vec{x}) + \psi], \tag{1}$$

where ψ is an additional constant phase. The local intensity $I(\vec{x})$ of their superposition becomes

$$I(\vec{x}) = |V_1 + V_2|^2 = a(\vec{x}) \{1 + m(\vec{x}) \cos[\phi(\vec{x}) + \psi]\}, \tag{2}$$

where $a(\vec{x})$ is the local mean intensity, $m(\vec{x})$ the fringe contrast, and $\phi(\vec{x}) = \phi_2(\vec{x}) - \phi_1(\vec{x})$ the phase difference of the two wavefields.

In classical interferometry, interpolation of the phase $\phi(\vec{x})$ between dark fringes is not accurately possible, because mean intensity $a(\vec{x})$ and fringe contrast $m(\vec{x})$ may change as well with position $\vec{x}$. As mentioned in the introduction, this problem can be solved by heterodyne interferometry [4]. However, it requires sophisticated electronic equipment and mechanical scanning of the image by photodetectors.

For moderate accuracy and spatial resolution, quasi-heterodyne techniques have been developped, which allow electronic scanning of the image by photodiode-arrays (CCD) or TV-cameras and use microprocessor controlled digital phase evaluation [3]. For this purpose, the additional phase ψ, in Eqs.(1) and (2), is changed step-wise. To determine the interference phase $\phi(\vec{x})$, the interferogram is analyzed at least three times and the mutual phase ψ is changed each time by a well controlled phase-shift. The local intensities $I_k(\vec{x})$ are then given by

$$I_k(\vec{x}) = a(\vec{x}) \{1 + m(\vec{x}) \cos[\phi(\vec{x}) + \psi_k]\}, \tag{3}$$

which correspond for k = 1, 2, 3 to a system of three equations with three unknown quantities: the mean intensity $a(\vec{x})$, the fringe contrast $m(\vec{x})$ and the interference phase $\phi(\vec{x})$. From Eqs.(3) one gets

$$\tan \phi(\vec{x}) = \frac{(I_3-I_2)\cos\psi_1 + (I_1-I_3)\cos\psi_2 + (I_2-I_1)\cos\psi_3}{(I_3-I_2)\sin\psi_1 + (I_1-I_3)\sin\psi_2 + (I_2-I_1)\sin\psi_3}, \tag{4}$$

which allows to calculate the interference phase $\phi(\vec{x})$ mod π. Inserting $\phi(\vec{x})$ again into the Eqs.(3), the phase can be determined modulo 2π. The complete phase is evaluated using the continuity of the phase function, assuming that it changes less than π between adjacent points. The other unknown quantities are given by

$$a(\vec{x})\cdot m(\vec{x}) = (I_1 - I_2)/\{\cos[\phi(\vec{x}) + \psi_1] - \cos[\phi(\vec{x}) + \psi_2]\}, \tag{5}$$

$$a(\vec{x}) = I_1 - a(\vec{x})\cdot m(\vec{x}) \cos[\phi(\vec{x}) + \psi_1]. \tag{6}$$

The interference fringe contrast $m(\vec{x})$ determined this way allows to control very efficiently the interferogram evaluation. Any inaccuracy in reference phase shifting and intensity measurement or any extraneous fringe patterns in the image plane show up as considerable fluctuations in the fringe contrast function.

For both heterodyne and quasi-heterodyne fringe evaluation, independent access to the two wavefields is necessary in order to control their relative phase. For holographic interferometry, this implies independent recording of each wavefield by using different reference sources. The frequency offset or the change of the phase ψ of the reconstructed wavefields can be introduced by acting on the respective reference beams.

Description of the experimental set-up

The optical set-up for double-exposure holographic interferometry with quasi-heterodyne interferogram processing is sketched in Fig.1. It uses an arrangement with two reference sources lying very close together [5]. Except for the two references, this set-up is the same as for classical holographic interferometry. The object is illuminated by a point source. An imaging system permits to observe the interferogram on a screen. Consecutively, the first object state O_1 is recorded by reference R_1 and the second object state O_2 by reference R_2 on the same hologram plate. Two-reference-beam holography requires special attention to the multiplicity of the reconstructed images [6]. Illuminating the hologam with both references R_1 and R_2 yields four primary reconstructions, i.e. the two desired self-reconstructions ($R_1R_1^*O_1$ and $R_2R_2^*O_2$), which give rise to the interference pattern, and the two undesired cross-reconstructions ($R_2R_1^*O_1$ and $R_1R_2^*O_2$). The direction of propagation of the various reconstructed waves depends on the geometry of the optical set-up. Using reference sources close together results in an overlapping of the undesired cross-reconstructions in the interferogram. The overlapping reduces the overall fringe contrast by a factor two and introduces a statistical error to the interference phase. This error can be adequately reduced by spatial averaging using a detector area which covers many speckles (cf. following chapter).

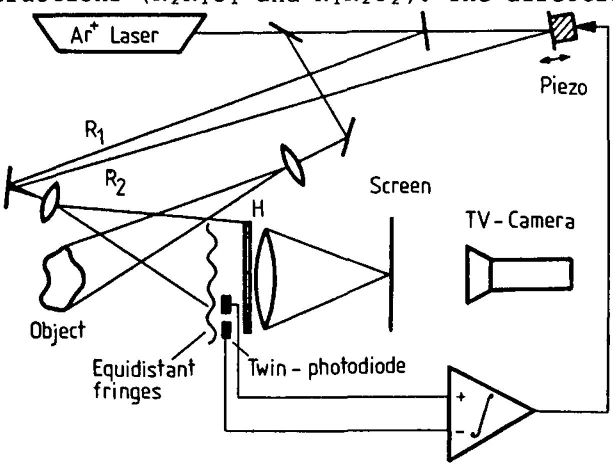

Figure 1. Optical set-up with reference sources close together and fringe stabilization.

The advantages of a set-up with reference sources close together are: First, the sensitivity for repositioning of the hologram plate is very low (about 10° of angular misalignement, compared to 0.01° for well separated reference sources). This makes it possible to reconstruct the hologram anywhere in a similar optical set-up. Even holograms recorded by a ruby laser can be realigned for reconstruction with a He-Ne laser. Second, the reference waves produce in the hologram plane a pattern of parallel macroscopic fringes which can be used to stabilize very efficiently the interference phase and to control accurately the shift of the mutual phase ψ of the reference beams. A twin-photodiode, which is placed just besides the hologram, detects a fringe maximum and an integrating feed back loop to a piezo mirror in one of the two reference beams keeps the fringes stable (Fig.1). The stabilizing twin-photodiode is mounted on a stepper-motor driven stage. By translating the photodiode, the interference fringes will move with it. This allows to adjust the phase steps ψ_k very accurately.

Data acquisition and processing is carried out with a video-system and a micro-computer. The interferogram is detected with a TV-camera. It can be observed either directly through the hologram or by projection on a screen. The silicon target Ultricon camera tube guarantees a linear response for the detected signal. A video-analyzer extracts an analog signal along a straight line through the object (fringe profile), which is converted into digital and stored in the micro-computer. This process is repeated for three hologram reconstructions with different relative phases ψ_k of the reference beams. Finally the interference phase $\phi(\vec{x})$ along the scanned line is calculated, displayed and plotted by the computer.

For a complete two-dimensional interferogram evaluation, a fast data-acquisition unit with a large memory, such as a video frame store, connected to a computer is required [3]. These features are usually offered by any kind of video image processing systems.

Limitations for the accuracy of the phase measurement

The limitations for the determination of the interference phase in holographic interferograms evaluated by a quasi-heterodyne fringe evaluation system as described above have been carefully investigated. The possible sources of errors can be summarized as follows:

Phase errors:
- fluctuations of the interference phase due to mechanical and thermal perturbations
- inaccuracy of the phase steps

Intensity errors (causing phase errors in the evaluated interferogram):
- additional interference patterns due to overlapping of the cross-reconstructions
- speckle noise
- electronic noise of the detector (TV-camera)
- non-linearity of the TV-camera

To investigate the errors, one has to distinguish between statistical and systematic errors. For the rms value of the statistical errors as a function of the intensity- and the phase-fluctuations, the following equation can be derived

$$\langle\delta\phi^2\rangle = (2/3\ m^2)\langle\delta I^2\rangle/\bar{I}^2 + (1/2)\langle\delta\psi^2\rangle. \qquad (7)$$

The systematic errors will generally be periodic. Equation (7) is still valid for the rms value of the periodic phase error.

Reference phase errors

The absolute value of the relative phases ψ_k between the two reference sources must be guaranteed during the measurements with the same precision as desired for the interference phase $\phi(\vec{x})$. Any error $\delta\psi$ in ψ_k cause systematic errors for $\phi(\vec{x})$ of the same magnitude as $\delta\psi$ (cf. Eq.(7)) and with the same periodicity as the interference fringes.

Since the relative phase ψ between the two references underlies important fluctuations due to mechanical vibrations of the optical set-up and due to thermal perturbations, it had to be stabilized. The employed stabilization, described above (Fig.1), reduces the fluctuations of the interference phase ψ with about 55 dB at 1 Hz and a slope of 20 dB/frequency decade. The residual rms fluctuations of ψ have been measured to be $\delta\psi = 0.4°$ rms for an integrating time constant of 20 ms (TV-camera), which corresponds to a bandwidth of 0 to 50 Hz. The systematic errors for the reference phase shifting can be kept very small due to the excellent periodicity of the macroscopic interference fringes which are used to control the phase shift by translating the stabilizing photodiode.

To summarize, the deviations of the mutual reference phases ψ_k can be expected to be less than 1°. By fitting more than three intensity profiles with different relative phases, as proposed e.g. in Ref.7, the reference phase errors could be reduced further. But comparing the achieved reference phase accuracy with other sources of errors (see the following sections) shows that this is not sensible.

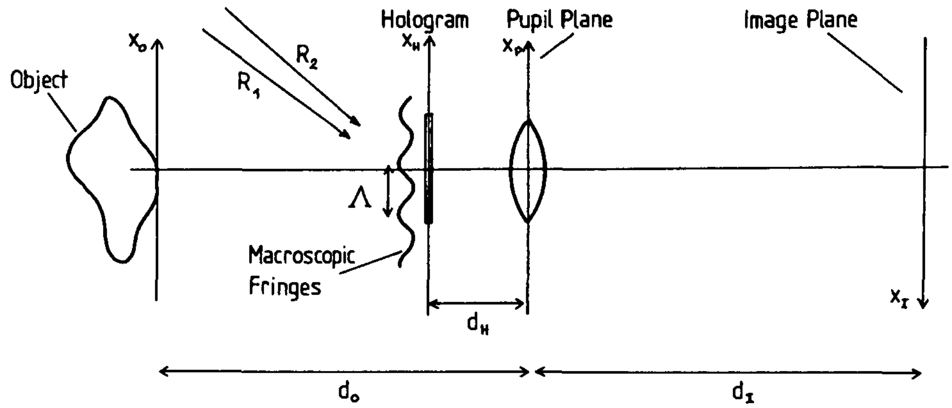

Figure 2. Schematic arrangement of the image formation system for hologram reconstruction.

Systematic errors due to the overlapping reconstructions

The overlapping of the cross-reconstructions can produce extraneous interference in the interferogram. The effect depends on the speckle size in the image, i.e. on the aperture of the image forming lens. If the aperture of this lens is too small to resolve completely the reference sources lying close together, the speckle patterns of the cross-reconstructions are not fully decorrelated and the reconstruction with one reference only produces already a fringe pattern in the interferogram. This will cause systematic phase errors with the same periodicity as the interference fringes in the interferogram. A second source of error is the fact, that the hologram plane lies not in the pupil plane of the imaging lens. Therefore the macroscopic fringe pattern of the reference beams on the hologram will be visible in the image plane. Its apparent periodicity depends on the distance between hologram and pupil plane, its visibility is determined by the aperture of the lens.

To examine these errors, one has to analyze the formation of the fringe pattern in the coherent image of the object (Fig.2). From a rigorous calculation of the superposition of all four primary reconstructions and averaging over the speckle statistics, one gets for the intensity in the image plane

$$I(\vec{x}_I) = 4\,|O|^2 \{1 + (1/2)\cos(\phi(\vec{x}_I) + \psi) + \gamma(\Delta x_I)\,[\cos(\phi(\vec{x}_I) + \vec{K}_H\cdot\vec{x}_I) + \cos(\psi - \vec{K}_H\cdot\vec{x}_I)] + (1/2)\gamma(2\Delta x_I)\,\cos(\phi(\vec{x}_I) + 2\vec{K}_H\cdot\vec{x}_I - \psi)\}. \tag{8}$$

Comparing with Eq.(3), one sees that the overlapping reconstructions reduce the fringe contrast m to (1/2) and introduces two additional fringe patterns with the visibilities $\gamma(\Delta x_I)$ and $(1/2)\gamma(2\Delta x_I)$, respectively. The function $\gamma(\Delta x_I)$ is given by the correlation between the speckle patterns of the desired reconstructions and the undesired cross-reconstructions which are laterally separated by Δx_I. This lateral shift can be expressed by the spacing Λ of the macroscopic interference fringes in the pupil plane due to the small separation of the reference sources (Fig.2): $\Delta x_I = \lambda d_I/\Lambda$. For a circular lens aperture, the correlation function $\gamma(\Delta x_I)$ is given by the Airy-function [4]

$$\gamma(\Delta x_I) = \frac{2J_1(\pi\Delta x_I D/\lambda d_I)}{(\pi\Delta x_I D/\lambda d_I)} = \mathrm{Airy}(\pi D/\Lambda). \tag{9}$$

The periodicity of these extraneous fringe patterns is essentially equal to the periodicity of the interference phase $\phi(\vec{x})$. In addition, a generally much slower periodic variation of the intensity is produced by the vector $\vec{K}_H = (2\pi/\Lambda)(d_H/d_O)$. This is the visibility of the macroscopic interference fringes on the hologram plane, seen through the imaging lens, if pupil plane and hologram plane are not identical.

The resulting systematic phase error depends on the visibility of the spurious fringes, i.e. on the value of the Airy function $2J_1(\pi D/\Lambda)/(\pi D/\Lambda)$, where D/Λ is the number of fringes (produced by the interference of the two references in the pupil plane) within the lens aperture. Since the rms value of periodic errors obeis Eq.(7), the expected average phase error can be estimated by introducing $\delta I/\bar{I} = \mathrm{Airy}(\pi D/\Lambda)$ into Eq.(7). This rms phase error has been calculated as a function of the lens aperture (Fig.3). To suppress the systematic phase errors, there exist two possibilities: either the lens aperture must contain enough fringes ($D/\Lambda \gg 1$, e.g. at least 7 fringes for a phase error of less than 2° rms), or the lens aperture has to be chosen to correspond to a zero of the Airy-function.

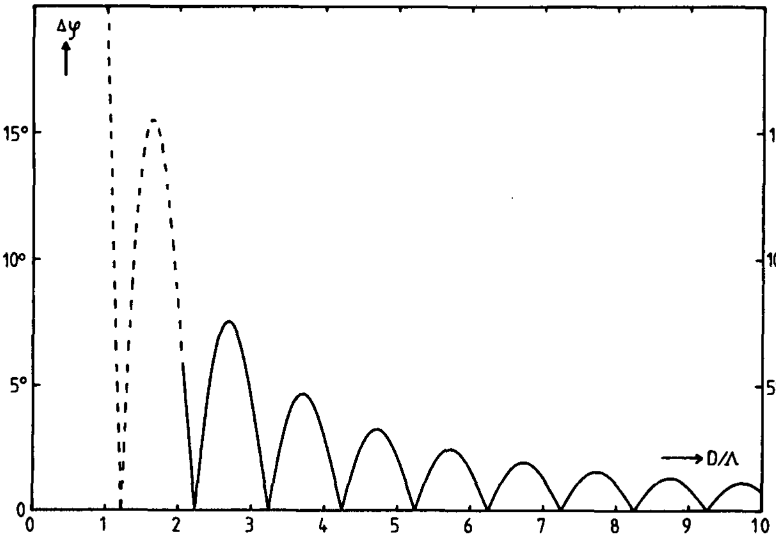

Figure 3. Systematic (periodic) phase error $\Delta\phi$ (rms value) due to overlapping reconstructions versus lens aperture (calculated for a fringe contrast $m = 0.4$).

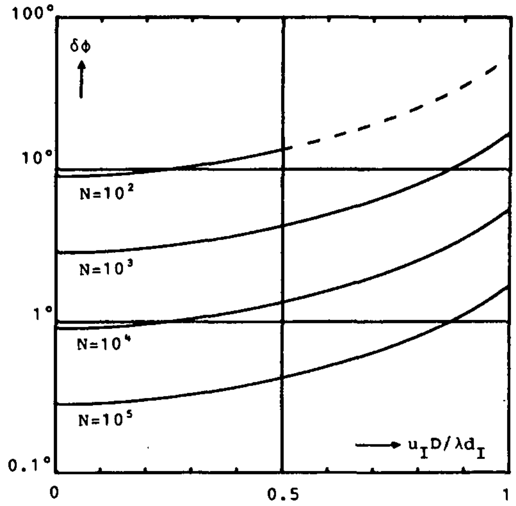

Figure 4. Statistical phase error $\delta\phi$ due to speckle decorrelation by transverse displacement ($u_I D/\lambda d_I$) and overlapping cross-reconstructions.

Speckle noise

Another source of intensity measurement errors is the speckle noise, which gives rise to a statistical phase error. The interference of non-correlated speckles (or non-correlated parts of speckles) introduces a random contribution to the phase of the mutual intensity of the interfering wavefields. The partial decorrelation of the speckle pattern is due to the transverse component u_I of the object displacement. In addition, the overlapping cross-reconstructions add two completely decorrelated speckle fields to the desired interfering reconstructions. The theoretical values of the statistical error $\delta\phi$ due to loss of fringe contrast by speckle decorrelation and overlapping reconstructions can be described by

$$\langle\delta\phi^2\rangle = \frac{6 - \gamma(2u)}{2(N+1)\,\gamma^2(u)}, \qquad (10)$$

where $\gamma(u) = \mathrm{Airy}(\pi u)$ and u is the normalized transverse displacement $u_I D/\lambda d_I$ in the image. This phase error depends essentially on the number N of independent speckles or correlation cells within the detector area A_D and decreases with $(1 + N)^{1/2}$ (cf.Fig.(4)). The minimum error for $u_I = 0$ has a finite value given by

$$\langle\delta\phi^2\rangle \approx 5/2(N+1). \qquad (11)$$

For practical purposes N can be estimated from the F-number and the focal length f of the imaging lens through the relation

$$N = A_D\pi(f/2F\lambda d_I)\ . \qquad (12)$$

An estimation of the expected phase error due to the speckle noise for the described system with video-electronic detection is difficult, because the resolution of the TV-camera is not well defined. Assuming 300 resolved lines/TV-field, one obtains a spatial resolution of about 16 µm for the vidicon tube. For an aperture of the TV-camera lens of $F = 2$, one gets from Eq.(12) $N \approx 650$ and $\delta\phi \approx 3.5°$. For $F = 5.6$, one gets $N \approx 80$ and $\delta\phi \approx 10°$. Experimentally, these two values were found to be about 3° and 8°, respectively. These errors can be adequately reduced by spatial averaging using a detector area which covers much more speckles, either "soft" (by computing the average over some neighbouring sample points), or "hard" (by electronically defocussing the TV-camera).

Errors due to the detector system

The detector introduces intensity measurement errors by electronic noise and non-linear response. In principle, both of these error sources can be eliminated. The noise can be arbitrarily reduced by averaging over many measurements. The non-linearity errors can be compensated numerically, if the exact detector response is known. These two sources of error will be discussed now for the detector used in the present system, namely a silicon target TV-camera, type RCA "Ultricon".

The camera noise has been determined experimentally to be 1.2 % rms of the maximum video signal. Calculating with a fringe contrast of m = 0.4, one obtains $\delta I/\bar{I}$ = 1.7 %, and by applying Eq.(7) $\delta\phi = 2°$ for the resulting phase error. Figure 5 shows the experimentally determined phase on an object without interference fringes. The intensity profiles have been averaged over three measurements, which reduces the error by a factor $\sqrt{3}$. One gets therefore $\delta\phi = 1.2°$ for the expected phase error in the central part of the interferogram, where the intensity is maximum. The corresponding experimental value is found to be 1.6° (Fig.5). (For this measurement, the speckle noise, which is normally of the order of some degrees, had to be supressed. This was done by elecronically defocussing the camera to reduce the spatial resolution).

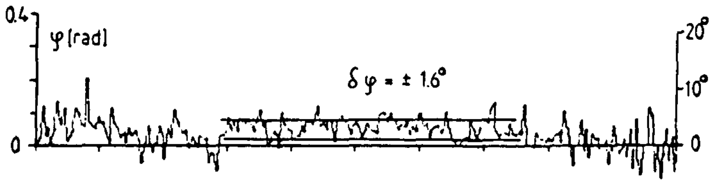

Figure 5. Statistical phase error due to electronic detector noise.

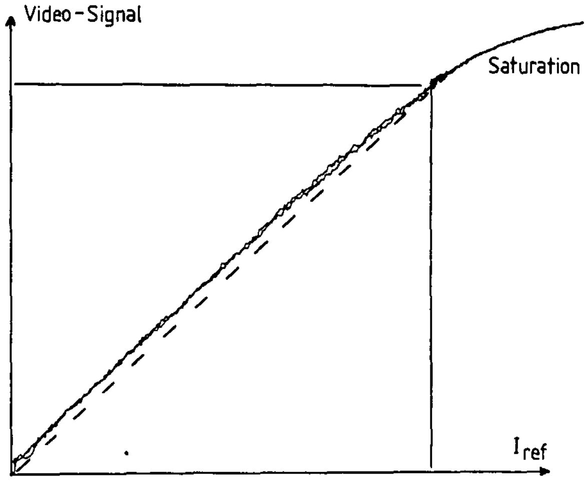

Figure 6. Response of the TV-camera. (Dashed line: linear fit).

The non-linearity of the detector produces systematic, periodic errors for the interference phase. Again, the error can be estimated with Eq.(7) by taking for δI the deviation of the detector response from the best linear function, fitted to the response over the dynamic range of measured intensity variations. The response of the TV-camera mentioned above is shown in Fig.6. It produces a maximum error of about 1° rms.

Experimental results

To demonstrate the capability of the described set-up, we show an experimental result of object shape measurement by holographic contouring. Since for simple object shapes the theoretically expected interference phase is well defined and can be calculated easily, the evaluation of contour fringes is more suitable to investigate the performance of a phase measurement system than the evaluation of interferograms from displaced or stressed objects. The contour fringes on the object are produced by two slightly different illumination beams S_1 and S_2 with each reference beam R_1 and R_2, respectively (Fig.7). The mean illumination direction was at an angle of about 26° with respect to the optical axis. The angular distance of the two illumination point sources was $6.8 \cdot 10^{-5}$ rad, which yields a contour fringe spacing of 8.4 mm in the transverse direction and of 16.8 mm in depth. To get the object contour, the measured interference phase has been evaluated respecting the change of illumination direction across the object due to the spherical waves. With this optical arrangement, a measurement error for the interference phase of $\delta\phi = 5°$ produces an error for the contour depth of δz = 0.25 mm. Figure 8 shows an experimental result for holographic contour determination of a cube edge. The accuracy for the object shape determination can be visually estimated to be better than 0.5 mm (rms).

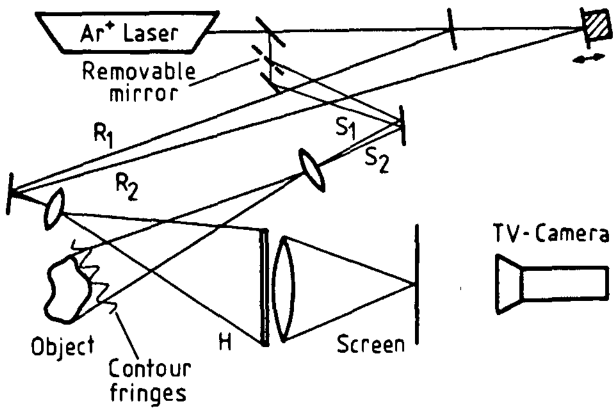

Figure 7. Optical set-up for holographic contouring by changing the illumination direction (S_1,S_2).

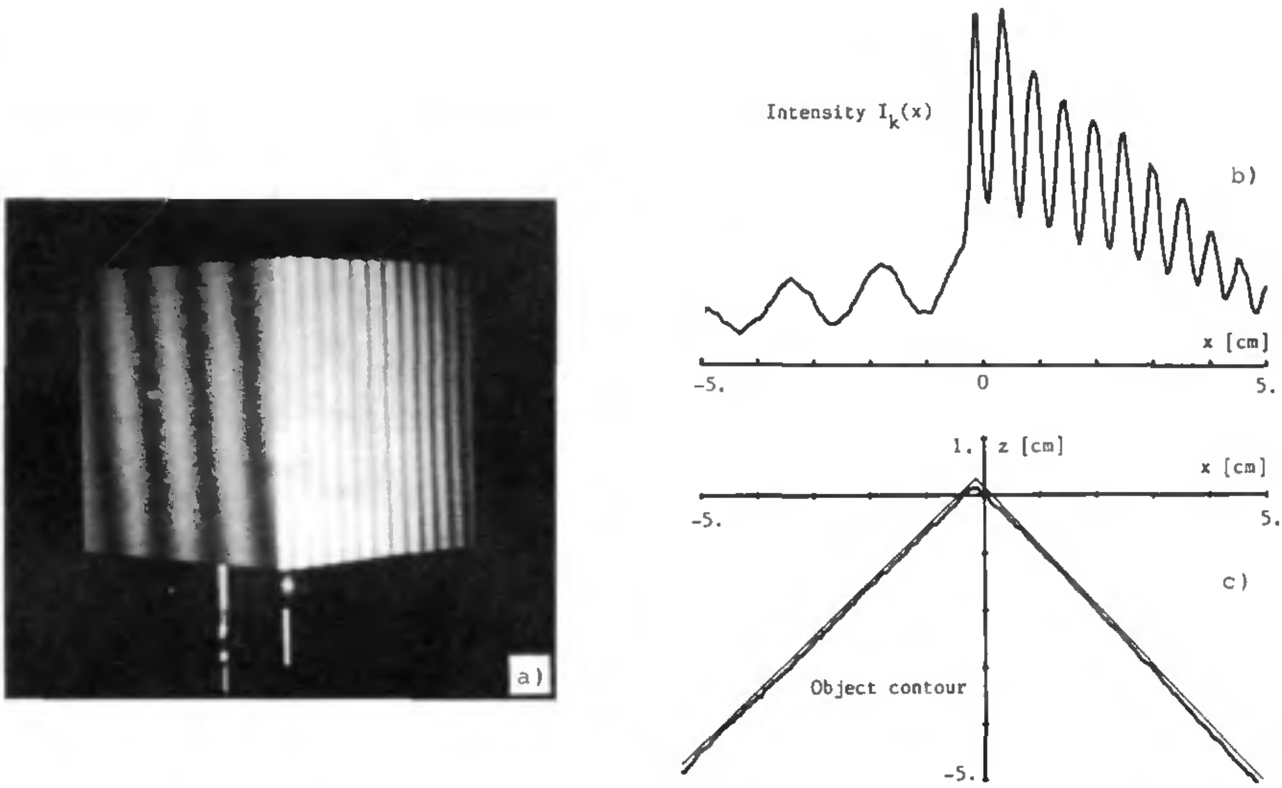

Figure 8. Holographic contouring of a cube: a) test object with contour fringes, b) intensity profile across the object, c) evaluated object contour.

The performances of the described system for holographic interferometry can be summarized as follows: The interferogram can be evaluated with a spatial resolution of about 300x300 points and an accuracy for fringe interpolation of about 1/100 rms. The measurement time for one interferogram (data acquisition of three images with mutually shifted phases) is some seconds. The time needed for the evaluation of the interference phase depends of course on the computer and the number of desired points; but one minute for the whole field will be sufficient [3].

Conclusions

In conclusion, quasi-heterodyne evaluation of holographic interferograms offers an accuracy of 1/100 of a fringe by using video-electronic processing. The required two-reference-beam holography can be operated as easily as classical double-exposure holography by using two reference beams close together. With this arrangement, the misalignment sensitivity of two-reference-beam holography is drastically reduced and even wavelength changes between recording and reconstruction, e.g. ruby laser for pulsed recording and He-Ne laser for reconstruction, can be tolerated. Moreover, the relative phase of the two reference waves during reconstruction can be stabilized and controlled very easily and accurately. The described system combines effectively the simplicity of standard double-exposure holography, video-electronic processing, and the power of heterodyne holographic interferometry.

The described set-up can be used for automated, rapid and quantitative evaluation of holographic interferograms with high spatial resolution. It can be applied to real-time, double-exposure and double-pulse holography. Using two different illumination beams S_1 and S_2 with each reference beam, holographic contouring can be performed in exactly the same experimental set-up (Fig.7). This allows the quantitative determination of displacement vector components on the surface of arbitrarily shaped objects. Using different illumination or observation directions, the high accuracy fringe interpolation offers also the possibility for automated determination of 3-D displacement vector fields from one and the same hologram plate [8].

References

1. Wyant, J. C., "Interferometric Optical Metrology: Basic Principles and New Systems", Laser Focus, May 1982, pp. 65-71.

2. Jüptner, W., Th. M. Kreis, M. Kreitlow, "Automatic Evaluation of Holographic Interferograms by Reference Beam Shifting", Proc. of SPIE, Vol. 398, pp. 22-29, 1983.

3. Hariharan, P., B. F. Oreb, N. Brown, "Real-time Holographic Interferometry: a Microcomputer System for the Measurement of Vector Displacements", Appl. Opt., Vol. 22, pp. 876-880, 1983.

4. Dändliker, R., "Heterodyne Holographic Interferometry", in Progress in Optics, Vol. XVII, E. Wolf, ed. (North Holland, Amsterdam, 1980), pp. 1-84.

5. Dändliker, R., R. Thalmann, J.-F. Willemin, "Fringe Interpolation by Two-Reference-Beam Holographic Interferometry: Reducing Sensitivity to Hologram Misalignement", Opt. Commun., Vol. 42, pp. 301-306, 1982.

6. Dändliker, R., E. Marom, F. M. Mottier, "Two-Reference-Beam Holographic Interferometry", J. Opt. Soc. Am., Vol. 66, pp. 23-30, 1976.

7. Schwider, J., et al., "Digital Wave-Front Measuring Interferometry: some Systematic Error Sources", Appl. Opt., Vol. 22, pp. 3421-3432, 1983.

8. Dändliker, R., R. Thalmann, "Determination of 3-D Displacement and Strain by Holographic Interferometry for Non-plane Objects", Proc. of SPIE, Vol. 398, pp. 11-16, 1983.

Heterodyne and quasi-heterodyne holographic interferometry

R. Dändliker
R. Thalmann
Institut de Microtechnique
Université de Neuchâtel
Rue de la Maladière 71
CH-2000 Neuchâtel 7, Switzerland

Abstract. The use of heterodyne and quasi-heterodyne techniques in holographic interferometry allows a quantitative evaluation of the interference phase with high accuracy and offers the possibility of automated interferogram processing. In this paper, the fundamentals of these electronic methods are reviewed, the possibilities and limitations are discussed, and some applications in the field of displacement and strain measurement are presented. Heterodyne holographic interferometry is well suited for scientific applications in which very high accuracy (1/1000 of a fringe) is needed. Quasi-heterodyne holographic interferometry with video processing is adequate for industrial applications in which high speed and medium accuracy (1/100 of a fringe) are required.

Subject terms: holographic interferometry; automatic fringe analysis; optical phase measurement; heterodyne; video data acquisition; speckles; displacement and strain measurement.

Optical Engineering 24(5), 824-831 (September/October 1985).

CONTENTS

1. INTRODUCTION

The automated quantitative evaluation of holographic interferograms requires accurate interference phase measurement independent of fringe position and intensity variations in the reconstructed image. In many interferometric arrangements, heterodyne or quasi-heterodyne techniques have become a powerful tool for high resolution interference fringe interpolation.[1] In holographic interferometry, these techniques have been applied to real-time[2,3] as well as to double-exposure[2,4–6] holography. For double-exposure holography two reference beams are required.[7,8] During reconstruction a change of the relative phase between the two reference beams allows one to shift the fringes in the interferogram at will.

Invited Paper HI-105 received March 13, 1985; revised manuscript received April 29, 1985; accepted for publication May 31, 1985; received by Managing Editor June 25, 1985.

In heterodyne methods, the relative phase increases linearly in time, and the interference phase is measured electronically at the beat frequency of the reconstructed wavefields. Heterodyne holographic interferometry offers high spatial resolution and interpolation up to 1/1000 of a fringe. However, it requires sophisticated electronic equipment and mechanical scanning of the image by photodetectors.[4,9] In quasi-heterodyne methods, the relative phase is changed step-wise, using at least three different values. The interference phase then can be computed from the different measured intensity values. Quasi-heterodyne techniques are more adequate for digital processing and TV detection. Two-reference-beam holography with reference sources close together and video electronic processing allows one to measure the interference phase with an accuracy of 1/100 of a fringe at any point in the TV image.

2. INTERFEROMETRY AND FRINGE INTERPOLATION

Interferometry is used to transform phase differences of wavefields into detectable intensity variations, i.e., interference fringes. Assuming that the two wavefields to be compared are given by

$$V_1(x) = a_1(x)\cos[\omega_1 t + \phi_1(x)] \ ,$$
$$V_2(x) = a_2(x)\cos[\omega_2 t + \phi_2(x) + \psi] \ , \tag{1}$$

where ψ is an additional constant phase, the local intensity $I(x)$ of their superposition becomes

$$I(x) = |V_1 + V_2|^2 = a(x)\left\{1 + m(x)\cos[\Delta\omega t + \phi(x) + \psi]\right\} \ , \tag{2}$$

where $a(x)$ is the local mean intensity, $m(x)$ is the fringe contrast, and $\phi(x) = \phi_2(x) - \phi_1(x)$ is the phase difference of the two wavefields.

In classical interferometry, the optical frequencies ω_1 and ω_2 are identical ($\Delta\omega = \omega_2 - \omega_1 = 0$) and the interference phase $\phi(x)$ is transformed into interference fringes independent of time. Interpolation of the phase $\phi(x)$ between dark fringes is not accurately possible because the mean intensity $a(x)$ and the fringe contrast $m(x)$ may change as well with position x.

2.1. Heterodyne

In heterodyne interferometry the two optical frequencies are chosen to differ by a small amount $\Delta\omega = \omega_2 - \omega_1$.[10] The superposition intensity is then time dependent, and the interference phase $\phi(x)$ is transformed into the phase of the beat frequency signal. Since the beat frequency $\Delta\omega$ is chosen low enough (<100 MHz) to be resolved by the optoelectronic detector employed, the interference phase can be measured with high accuracy independently of the amplitudes a_1 and a_2 using an electronic phasemeter. This way, both the interpolation problem and the sign ambiguity of classical interferometry are solved. This method requires special equipment, such as acousto-optical modulators and phasemeters. The image is scanned mechanically by photodetectors to measure the interference phase $\phi(x)$ locally. Therefore, the speed is relatively low (~1 s/point), but the accuracy ($\delta\phi \simeq 0.3°$, or 1/1000 of a fringe) and the spatial resolution (>10^6 resolvable points) are extremely high.[4]

2.2. Quasi-heterodyne

For moderate accuracy and spatial resolution, quasi-heterodyne techniques[11] have been developed, which allow electronic scanning of the image by photodiode arrays (CCDs) or TV cameras and use microprocessor-controlled digital phase evaluation.[3] For this purpose, the linear increase of the relative phase ($\phi_t = \Delta\omega t$) due to the heterodyne frequency offset $\Delta\phi$ is replaced by a stepwise change of ψ. To determine the interference phase $\phi(x)$, the interferogram is analyzed at least three times, and the mutual phase ψ is changed each time between two analyses by a well controlled phase shift. The local intensities $I_k(x)$ are then given by

$$I_k(x) = a(x)\Big\{1 + m(x)\cos[\phi(x) + \psi_k]\Big\} , \tag{3}$$

which correspond for k = 1, 2, 3 to a system of three equations with three unknown values: the mean intensity $a(x)$, the fringe contrast $m(x)$, and the interference phase $\phi(x)$. For the interference phase $\phi(x)$ one gets from Eq. (3)

$$\tan\phi(x) = \frac{(I_3 - I_2)\cos\psi_1 + (I_1 - I_3)\cos\psi_2 + (I_2 - I_1)\cos\psi_3}{(I_3 - I_2)\sin\psi_1 + (I_1 - I_3)\sin\psi_2 + (I_2 - I_1)\sin\psi_3} . \tag{4}$$

The other unknown values are given by

$$a(x)m(x) = \frac{I_1 - I_2}{\cos[\phi(x) + \psi_1] - \cos[\phi(x) + \psi_2]} , \tag{5}$$

$$a(x) = I_1 - a(x)m(x)\cos[\phi(x) + \psi_1] . \tag{6}$$

The mean intensity $a(x)$ and the fringe contrast $m(x)$ determined in this manner allow one to control the quality of the interferogram evaluation. In particular, they can be used to distinguish between true interference fringes and other structures in the image, such as shadows, contours, holes, etc. Considerable fluctuations of the fringe contrast versus position may also indicate inaccurate reference phase shifts and intensity measurements or extraneous fringe patterns in the image.

2.3. Holographic interferometry

For both heterodyne and quasi-heterodyne fringe evaluation, independent access to the two wavefields is necessary in order to control their relative phase. For holographic interferometry, this implies independent recording of each wavefield by using different reference sources.[4,8] The frequency offset $\Delta\omega$ or the change of the mutual phase ψ can be introduced by acting on the respective reference beams.

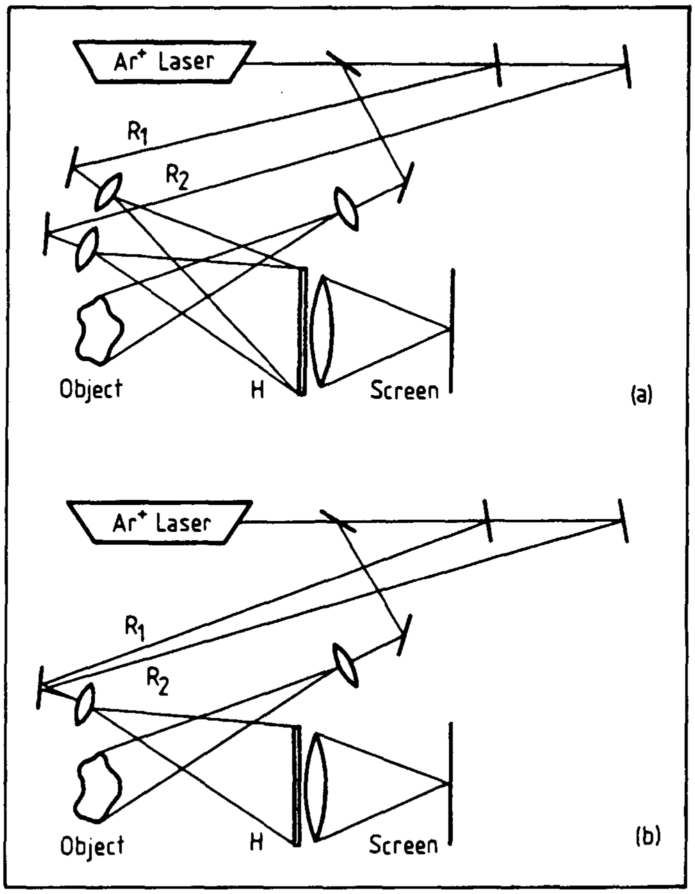

Fig. 1. Arrangements for two-reference-beam holographic interferometry. (a) Well separated reference sources; (b) reference sources close together.

3. TWO-REFERENCE-BEAM HOLOGRAPHIC INTERFEROMETRY

The optical arrangements for two-reference-beam holographic interferometry are sketched in Fig. 1(a) for well separated reference sources and in Fig. 1(b) for reference sources close together. Except for the two references, this setup is the same as for classical holographic interferometry. In both arrangements, the object is illuminated by a point source, and an imaging system permits one to observe the interferogram on a screen. Consecutively, the first object state O_1 is recorded by reference R_1 and the second object state O_2 by reference R_2 on the same hologram plate.

As described in Ref. 8, two-reference-beam holography requires special attention to the multiplicity of the reconstructed images and the influence of misalignment of the hologram with respect to the reference beams. Illuminating the hologram with both reference beams R_1 and R_2 yields eight reconstructions. Four of them are conjugate reconstructions. The other ones are the two desired primary self-reconstructions ($R_1R_1^*O_1$ and $R_2R_2^*O_2$), which give rise to the interference pattern, and the two undesired cross-reconstructions ($R_2R_1^*O_1$ and $R_1R_2^*O_2$). The direction of propagation of the various reconstructed waves depends on the geometry of the optical setup. The primary reconstructions are shown for both cases in Fig. 2(a) and Fig. 2(b).

To avoid disturbing overlapping of the different reconstructions [Fig. 2(a)], the two reference sources must be chosen on the same side of the object, with a mutual separation larger than the angular size of

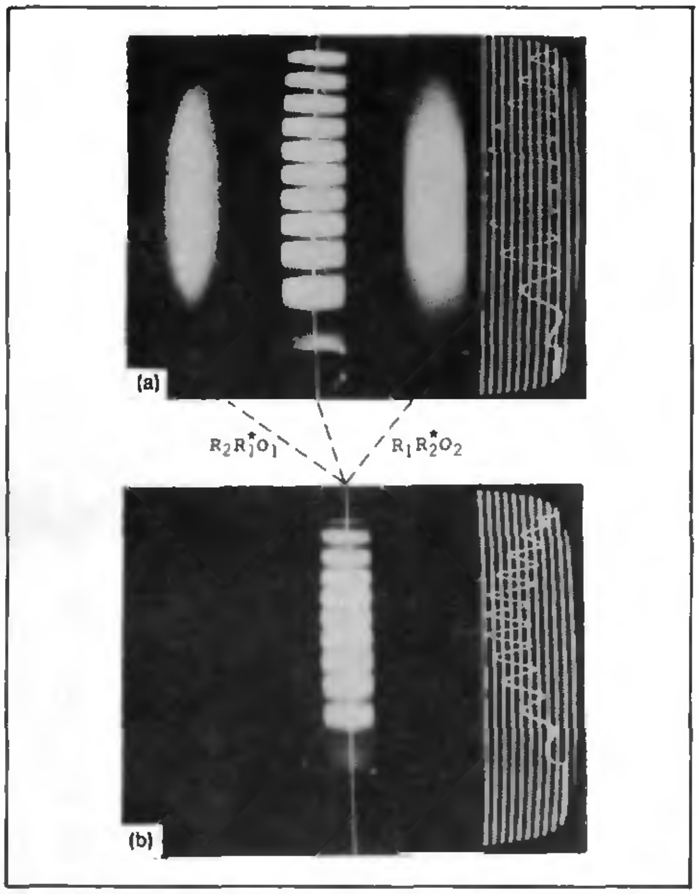

Fig. 2. Reconstructed images and intensity profiles on TV screen. (a) Separated cross-reconstructions $R_2R_1^*O_1$ and $R_1R_2^*O_2$; (b) overlapping reconstructions.

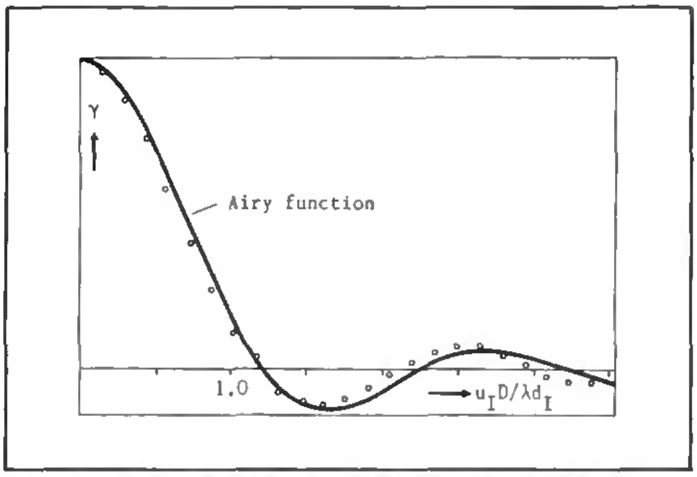

Fig. 3. Theoretical and experimental values of the fringe contrast γ versus transverse displacement u_I of the interfering speckle patterns, in terms of speckle size $\gamma d_I/D$.

the object in the corresponding direction [Fig. 1(a)]. However, the consequence of large separation of the reference sources is high sensitivity to repositioning errors, as described hereafter. Therefore, reference sources close together [Fig. 1(b)] would be preferred if, under certain conditions, overlapping of the cross-reconstructions [Fig. 2(b)] could be tolerated without undue loss of accuracy for the interference phase measurement.

3.1. Alignment and wavelength sensitivity

Two-reference-beam holographic interferometry is sensitive to repositioning errors and to wavelength changes, because the propagation directions of the reconstructed wavefields are differently affected by these alterations.[4,8] Wavelength changes or small rotations of the hologram plate result in an additional linear phase variation in the hologram plane, which is proportional to the difference $(\mathbf{k}_1 - \mathbf{k}_2)$ of the wave vectors of the two reference beams. If the imaging lens is placed close behind the hologram, this linear phase variation in the hologram plane produces a mutual transverse shift u_I between the two interfering reconstructions in the image plane. This results, as shown below, in a loss of fringe contrast in the interferogram.

The magnitude of the interference term depends essentially on the autocorrelation $C_h(u_I)$ of the impulse response function of the imaging system, which defines the speckle size in the image. The interference fringes are visible only as long as the mutual shift of the speckle patterns is smaller than the speckle size. For a circular aperture of diameter D, the fringe contrast $\gamma(u_I)$ is thus given by the well known Airy function:

$$\gamma(u_I) = C_h(u_I)\frac{2J_1(\pi D u_I/\lambda d_I)}{\pi D u_I/\lambda d_I} , \tag{7}$$

where $J_1(\cdot)$ is the first-order Bessel function and d_I is the distance from the lens to the image plane. Figure 3 shows the decrease of the fringe contrast versus the normalized transverse speckle shift $u = u_I D/\lambda d_I = u_I/(\Delta x)_I$, i.e., u_I in terms of the diffraction-limited optical resolution $(\Delta x)_I = \lambda d_I/D$ (speckle size in the image plane).

Wavelength changes and misalignment of the hologram plate and the reference sources thus result in a loss of interference fringe contrast. For well separated reference sources, to prevent overlapping cross-reconstructions, the difference $(\mathbf{k}_1 - \mathbf{k}_2)$ is quite large, and therefore the sensitivity to wavelength changes and hologram alignment is very high. Typically, a rotation of the hologram of only 0.01° about its surface normal is enough to reduce the fringe contrast to 50%.

3.2. Overlapping cross-reconstructions

On the other hand, the overlapping of the cross-reconstructions $R_2R_1^*O_1$ and $R_1R_2^*O_2$ for reference sources close together does not produce macroscopic interference, as long as the lateral separation of the cross-reconstructions is much larger than the speckle size $(\Delta x)_I$ and, therefore, the speckle patterns of the desired and undesired images are uncorrelated. To avoid systematic interference phase errors, the angular separation between the two reference sources must be several times larger than the diffraction limit, since the higher order maxima of the Airy function (Fig. 3) still give rise to some correlation with the undesired reconstructions.[6] In other words, the two reference sources must produce many interference fringes across the lens aperture to avoid disturbing phase errors, although in a typical setup with reference sources close together [Fig. 1(b)] the sensitivity to misalignment is less than 10°.

However, the overlapping with the uncorrelated cross-reconstructions reduces the overall fringe contrast by a factor of two, as can be seen by comparing Figs. 2(a) and 2(b), and introduces an additional statistical error to the interference phase measurement.[6] The minimum value of this phase error is given by

$$\delta\phi^2 = \frac{5}{2(N+1)} , \tag{8}$$

where N is the number of independent speckles or correlation cells within the detector area. Figure 4 shows theoretical and experimental values of the statistical phase error due to overlapping cross-reconstructions for different numbers N of speckles. For practical purposes N can be obtained from the F-number and the focal length f of the imaging lens through the relation

$$N = A_D \pi \left(\frac{f}{2F\lambda D_1}\right)^2 . \tag{9}$$

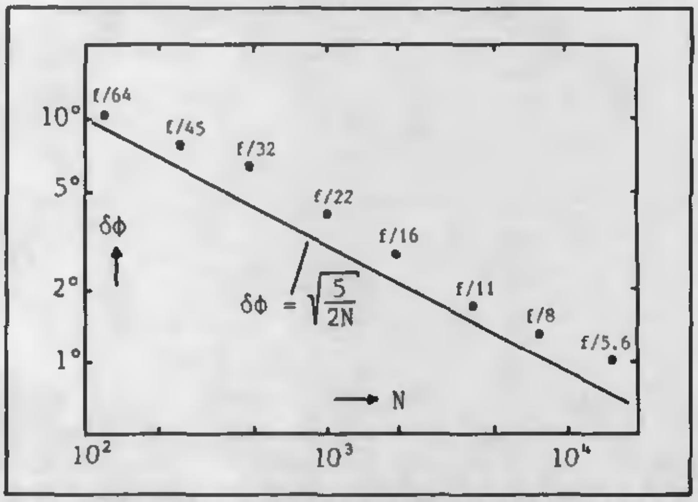

Fig. 4. Statistical phase error $\delta\phi$ due to the uncorrelated speckle fields of the overlapping cross-reconstructions versus the number N of speckles within the detector area. Experimental results for different lens apertures are shown.

where A_D is the detector area and d_I is the distance between the lens and the image plane.

3.3. Systematic errors

Additional errors of systematic nature may occur due to the fact that the hologram will usually not be exactly in the pupil plane of the imaging lens or due to nonlinear cross-talk in the hologram reconstruction.[4] The latter can be avoided by carefully cleaning the recorded scene of spurious reference light sources, such as parts of objects that remain unchanged between the two exposures.

4. HETERODYNE HOLOGRAPHIC INTERFEROMETRY

4.1. Experimental arrangement

A typical setup for double-exposure heterodyne holographic interferometry is shown in Fig. 5. The frequency difference $\Delta\omega/2\pi$ of about 100 kHz is realized by two commercially available acousto-optical modulators (AOMs) in cascade to give opposite frequency shifts. During recording, both modulators are driven with 40 MHz, so that the net shift is zero. During reconstruction, one modulator is driven with 40 MHz and the other with 40.1 MHz, so that the net shift is the desired beat frequency of 100 kHz. Figure 6 shows how the interference phase $\phi(\mathbf{x})$ is obtained by scanning the image of the object with a photodetector D_1 and measuring the phase of the beat frequency signal with respect to the reference phase obtained from a second detector D_r at a fixed point.

In practice an array of three detectors is used to determine the two phase differences $\Delta\phi_x$ and $\Delta\phi_y$ in the orthogonal directions x and y, rather than the interference phase $\phi(x,y)$ itself. The latter can be easily and accurately calculated by summation of the measured differences along a given path. All electronic amplifiers and filters in the signal path should be designed carefully to avoid phase distortion that could reduce the accuracy of the phase measurement.[12] The detector array can be realized by the ends of optical fibers of fiber bundles, which feed the light to three photomultiplier tubes. The beat frequency signals at 100 kHz are filtered with a bandwidth of 10 kHz, and the amplitudes are kept constant, independent of the intensity variations across the image, by a feedback control of the photomultiplier voltages. The phase differences $\Delta\phi_x$ and $\Delta\phi_y$ are measured with two zero-crossing phasemeters, which interpolate the phase angle to 0.1° and also count multiples of 360°, which correspond to the fringe numbers.[12] The detector array is mounted on a stepper-motor-driven stage to scan the image. Scanning and data acquisition is automated and computer controlled. The measuring time for one position, including displacement of the detector array, is about 1 s.

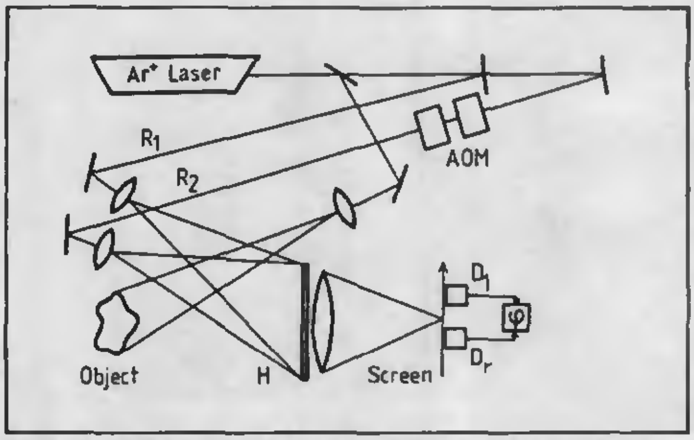

Fig. 5. Arrangement for heterodyne holographic interferometry using two acousto-optic modulators for the frequency offset.[4]

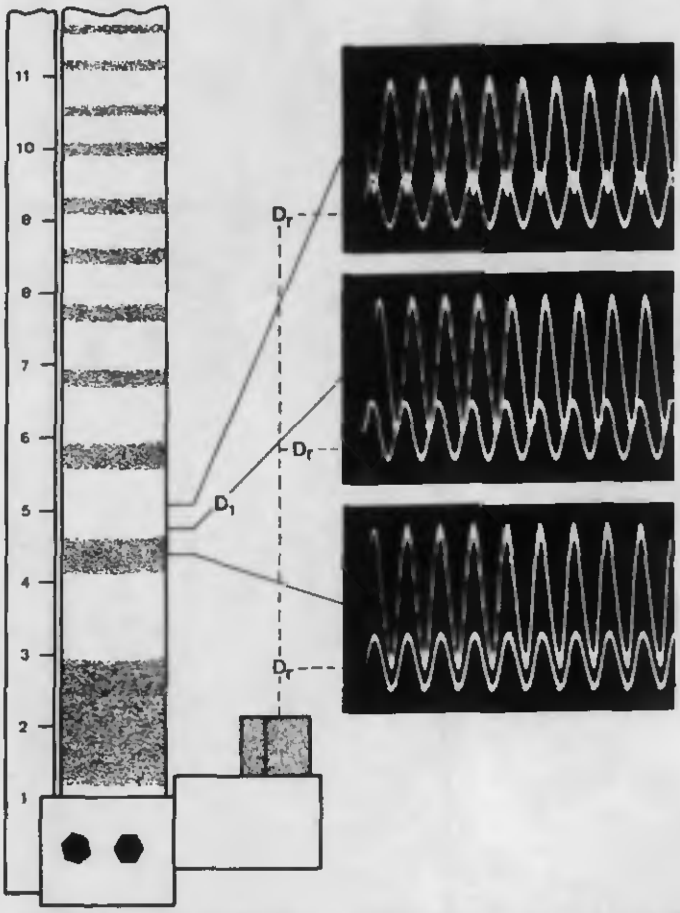

Fig. 6. Schematic representation of the interference fringes on a bent cantilever and the corresponding beat frequency signals from the two photodetectors D_r (fixed) and D_1 (scanning).[4]

4.2. Accuracy

The overall accuracy and reproducibility of heterodyne holographic interferometry depend mainly on the specification of the phasemeter, the signal-to-noise ratio (SNR) of the detector signals, and the mechanical stability of the optical setup.[13] Using good experimental equipment, a phase measurement accuracy of 0.2° to 0.5° can be

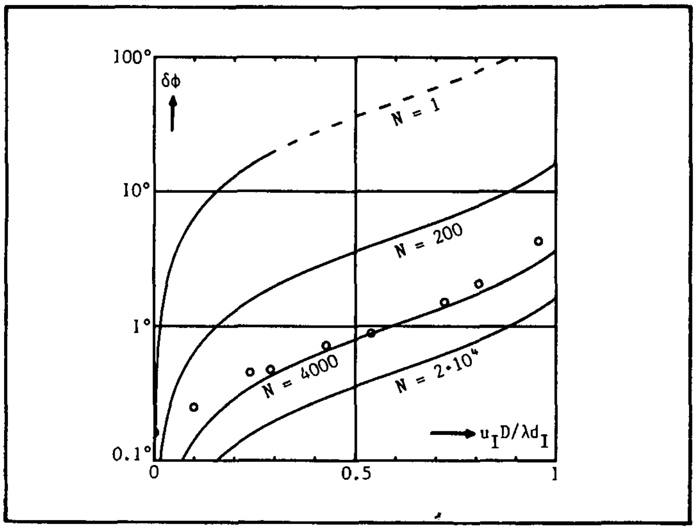

Fig. 7. Statistical phase error $\delta\phi$ due to partial speckle decorrelation versus transverse displacement u_l of the interfering speckle patterns, in terms of speckle size $\lambda d_l/D$. N is the number of speckles within the detector area. Experimental results for N = 4000 are shown.

obtained. The ultimate limits are due to loss of fringe contrast by speckle decorrelation and overlapping reconstructions, as already discussed in the preceding section. If high accuracy is required, the phase error due to overlapping cross-reconstructions from reference sources close together (Fig. 4) cannot be tolerated. For nonoverlapping cross-reconstructions, only a partial decorrelation of the interfering speckle fields (reduced fringe contrast, Fig. 3) due to a transverse component u_l of the object displacement gives rise to an additional random phase in the beat signal. The theoretical value of the statistical phase error $\delta\phi$ due to partial speckle decorrelation can be described by

$$\delta\phi^2 = \frac{1 - \gamma(2u)}{2(N+1)\gamma^2(u)} , \tag{10}$$

where $\gamma(u)$ is the fringe contrast [cf. Eq. (7) and Fig. 3] and $u = u_l D/\lambda d_l$ is the normalized transverse displacement in the image. Figure 7 shows the statistical phase error given by Eq. (10) for different speckle numbers N within the detector area. For completely correlated speckles ($u_l = 0$) this error becomes zero (no speckle noise).

The capability of heterodyne holographic interferometry is demonstrated by the experimental results given in Fig. 8.[4] The bending of a cantilever beam, clamped at the base and loaded at the end, was measured and compared with theory. The second derivative d^2u_z/dx^2 of the measured normal displacement $u_z(x)$ should follow a straight line, proportional to the bending moment M(x). The measurements were taken at intervals of $\Delta x = 3$ mm, and the comparison with theory indicates an accuracy for the interference phase of $\delta\theta = 0.3°$, corresponding to $\delta u_z = 0.2$ nm.

5. QUASI-HETERODYNE INTERFEROGRAM PROCESSING

5.1. Experimental arrangement

A typical setup for quasi-heterodyne holographic interferometry with two reference sources close together (c.f. Sec. 3.1) is shown in Fig. 9. The advantages of using reference sources close together are that, first, the requirements for correct repositioning of the hologram are low. This makes it possible to reconstruct the hologram anywhere in a similar optical setup. Even holograms recorded with a pulsed ruby laser can be realigned for reconstruction with a He-Ne laser. Second, the reference waves produce in the hologram plane a pattern

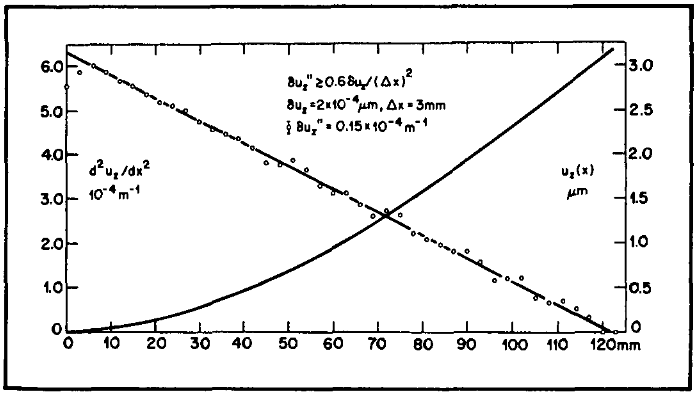

Fig. 8. Bending of a cantilever measured by heterodyne holographic interferometry. Comparison of the second derivatives d^2u_z/dx^2 of the normal displacement $u_z(x)$ with theory indicates an accuracy for the phase measurement of $\delta\phi = 0.3°$.[4]

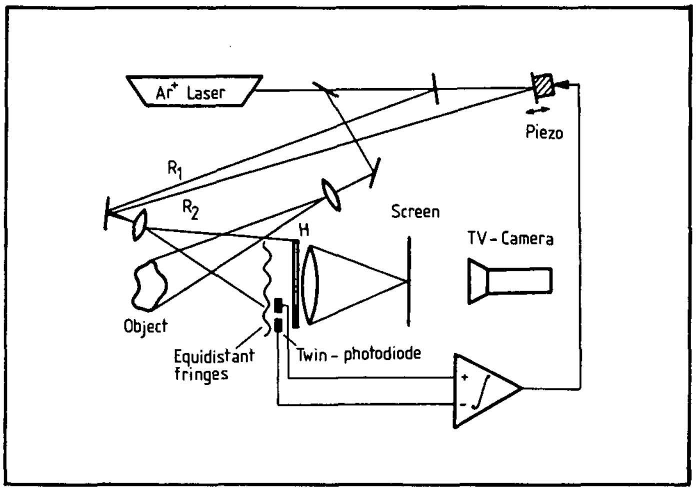

Fig. 9. Arrangement for quasi-heterodyne holographic interferometry with two reference sources close together, fringe stabilization, and TV observation.

of parallel macroscopic fringes of typically 1 to 2 mm separation, which can be used to stabilize the interference phase and to control the phase steps ψ very accurately. A twin photodiode placed just beside the hologram tracks the fringe maximum, and an integrating feedback loop to the piezoelectric mirror in one of the two reference beams keeps the fringes stable (Fig. 9). By translating the twin photodiode, the interference fringes will move with it. Accurate phase shifts of 120° are obtained by moving the photodiode, mounted on a stepper-motor-driven stage, in steps of 1/3 of the fringe separation.

Data acquisition and processing is carried out with a video system and a microcomputer. The interferogram is detected with a TV camera. It can be observed either directly through the hologram or by intermediate projection on a screen. A silicon target vidicon or CCD-array camera should be used to guarantee linear response for the intensity measurement. Three successive hologram reconstructions with different relative phases ψ of the reference beams are digitally stored and then analyzed pointwise by calculating the interference phase $\phi(x)$, the fringe contrast m(x), and the average intensity a(x) with the help of Eqs. (4) to (6). Video image processing systems with digital frame stores for fast data acquisition are readily available nowadays.

5.2. Accuracy

The limitations for the determination of the interference phase in quasi-heterodyne holographic interferometry as described above have been thoroughly investigated by the authors.[6] The possible sources of errors can be summarized as phase noise due to perturbations (mechanical, thermal), inaccuracy of the phase steps, speckle noise (mainly due to the overlapping cross-reconstructions), spurious interferences due to the overlapping cross-reconstructions, electronic noise of the detector (TV camera), and nonlinearity of the detector (TV camera).

To estimate the accuracy of the phase measurement, one has to distinguish between statistical and systematic errors. For the rms value of the statistical errors introduced by intensity and phase noise, $\delta I/\bar{I}$ and $\delta\psi$, respectively, the expression

$$(\delta\phi)^2 = \left(\frac{2}{3}\,m^2\right)\left(\frac{\delta I}{\bar{I}}\right)^2 + \frac{(\delta\psi)^2}{2} \tag{11}$$

can be derived from Eq. (4). The systematic errors will in general be periodic. Equation (11) is still valid for the rms value of the periodic phase errors.

5.2.1. Phase errors

The absolute value of the relative phases ψ_k between the two reference sources must be guaranteed with the same precision as desired for the interference phase $\phi(x)$. Any errors $\delta\psi$ in ψ_k cause systematic errors for $\phi(x)$ of the same magnitude as $\delta\psi$ [cf. Eq. (11)] and with the same periodicity as the interference fringes. With the stabilization scheme described above (Fig. 9), the phase noise was measured to be less than $\delta\psi = 0.4°$ rms for an integrating time of 20 ms (TV camera), and the deviations of the mutual phases ψ_k were found to be less than 1°.

5.2.2. Overlapping cross-reconstructions (cf. Sec. 3.2)

If the aperture of the imaging lens is too small compared with the angular separation of the two reference sources, the speckle patterns of the cross-reconstructions are not completely decorrelated [Eq. (7), Fig. 3]. This produces a spurious fringe pattern in the image, which will cause systematic phase errors with the same periodicity as the interference fringes. In addition, if the hologram is not exactly in the pupil plane of the imaging lens, the macroscopic fringe pattern of the reference beams on the hologram may be visible in the image. Its apparent periodicity depends on the distance between hologram and pupil plane; its visibility is determined by the aperture of the lens. To suppress these systematic phase errors, the lens aperture must be large enough to contain many fringes (at least seven fringes for a phase error of less than 2° rms).

The statistical phase error due to speckle noise is shown in Fig. 4 as a function of the number N of speckles integrated by the detector area. An estimation of the expected phase error for the described system with video electronic detection is difficult, because the resolution of the TV camera is not well defined. Assuming 300 resolved lines/TV-field, one obtains a spatial resolution of about 30 μm for the vidicon tube. For an aperture of the TV camera lens of F = 2, one gets from Eq. (9) N $\simeq$ 700 speckles within a spatial resolution cell, and by applying Eq. (8), $\delta\phi \simeq 3.5°$. This value agrees well with experimental results. The error due to speckle noise can be further reduced by spatial averaging using a detector area that covers more speckles, either "hard" (electronically defocusing the TV camera) or "soft" (numerically averaging over neighboring sample points).

5.2.3. Detector (TV camera)

The detector introduces intensity measurement errors by electronic noise and nonlinear response. On the contrary, variations of the sensitivity across the image, or from one pixel to another in CCD cameras, do not cause any error, since the calculation of the interference phase is based on three consecutive measurements of intensity at the same position [cf. Eq. (4)].

For a silicon target TV camera, such as the RCA Ultricon, the electrical signal-to-noise ratio has been determined experimentally to be about 35 dB. Assuming a fringe contrast of m = 0.4, one

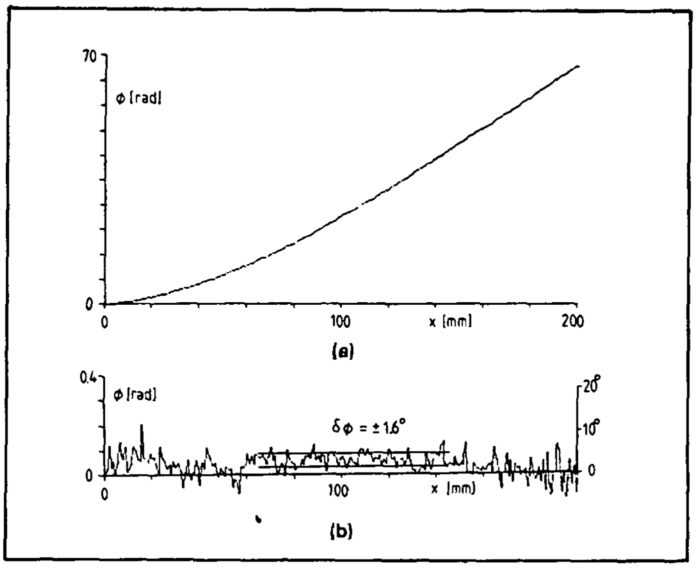

Fig. 10. Interference phase ϕ measured by quasi-heterodyne holographic interferometry. (a) Displacement of a bent cantilever versus length x. (b) Phase variations (statistical error) measured for the undeformed cantilever.[5]

obtains from Eq. (11) a statistical phase error of $\delta\phi = 2°$. Figure 10 shows the experimentally determined phase on an object without fringes. The intensity profiles have been averaged over three measurements, which reduces the expected error by a factor $\sqrt{3}$ to $\delta\phi = 1.2°$. The corresponding experimental value is found to be 1.6° (Fig. 10) in the central part of the image, where the average intensity is sufficiently high. (For this measurement, the speckle noise, which is normally of the order of some degrees, was further reduced by electronically defocusing the camera.)

A nonlinear response of the detector produces systematic errors of the same periodicity as the interference fringes. Again, the error can be estimated with Eq. (11) by taking for δI the deviation of the detector response from the best linear fit for the dynamic range of the measured intensities. The response of the TV camera mentioned above has been verified to be sufficiently linear to produce less than 1° error.

5.2.4. Conclusions

Quasi-heterodyne evaluation of holographic interferograms offers an accuracy of 1/100 of a fringe by using video electronic processing. The required two-reference-beam holography can be operated as easily as classical double-exposure holography by using two reference beams close together (about 0.5 mrad angular separation). The described system combines effectively the simplicity of standard double-exposure holography, the power of heterodyne holographic interferometry, and video electronic processing.

6. APPLICATIONS AND CONCLUSIONS

The described techniques for electronic processing of holographic interferograms can be applied to real-time, double-exposure, double-pulse, and stroboscopic holography. Both heterodyne and quasi-heterodyne methods offer high accuracy fringe interpolation, high spatial resolution, and the possibility for automated interferogram processing. They allow quantitative determination of displacement vector components on the surface of arbitrarily shaped objects. Using different illumination or observation directions, the high accuracy fringe interpolation also offers the possibility of automated determination of 3-D displacement and strain from a single hologram plate.[14,15] Moreover, using different illumination beams for each reference, holographic contouring can be performed in exactly the same setup.[6]

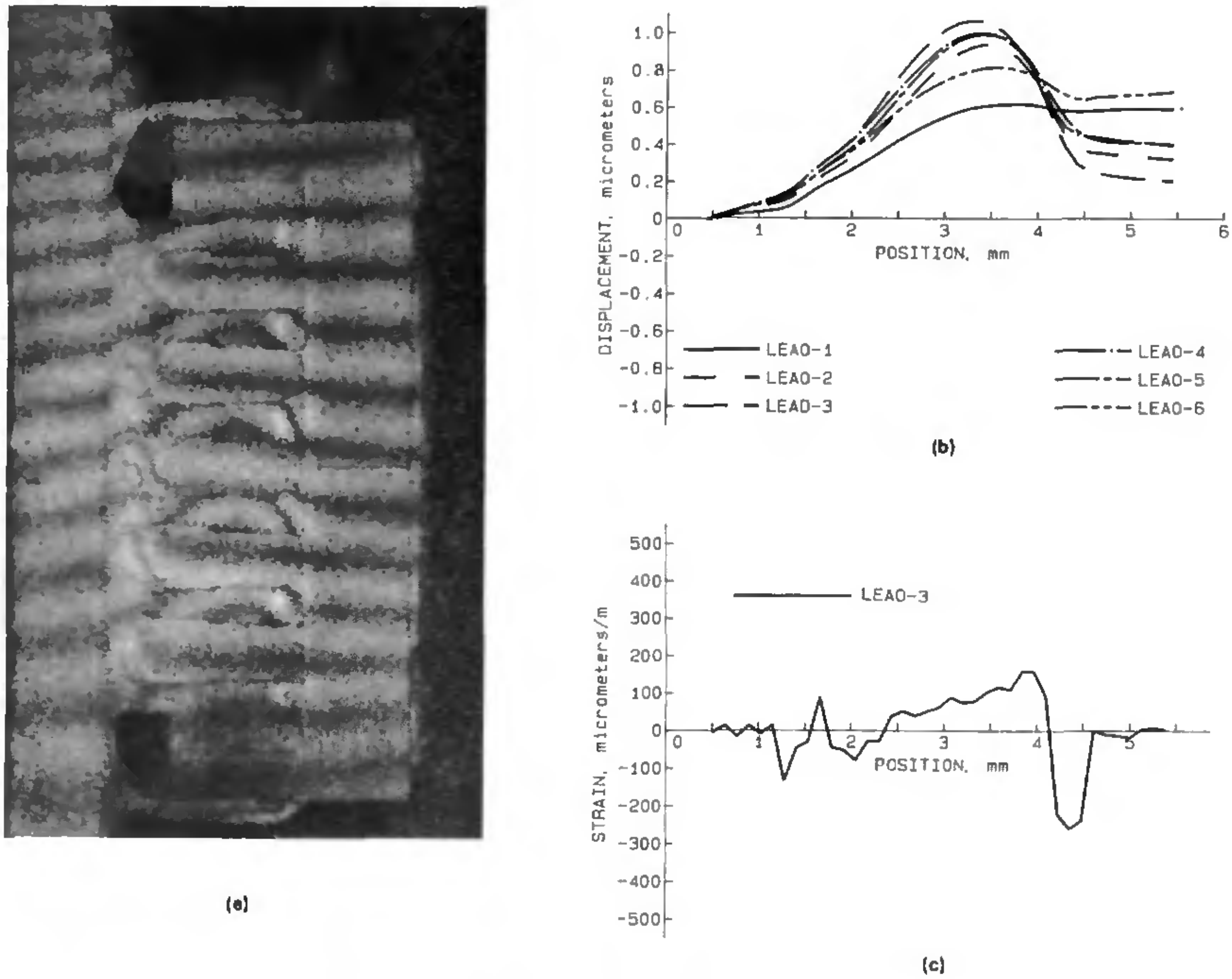

Fig. 11. Heterodyne holographic interferometry applied to displacement and strain measurements of computer chip carrier leads. (a) Typical fringe pattern. (b) Out-of-plane displacement component. (c) In-plane strain along one lead. (Figures courtesy of R. J. Pryputniewicz).

Heterodyne holographic interferometry requires sophisticated electronic equipment and mechanical scanning of the image by photodetectors. It is well suited for scientific applications in which very high resolution is needed. An application to quantitative displacement and strain measurements of computer chip carrier leads is presented in Fig. 11. The fringes were analyzed in the magnified image (about 8×) of the object with a heterodyne system similar to the one described in this paper (Sec. 4). Three different observation directions (about 20° difference) were used to determine the displacement vector at some 40 points along each lead, separated by about 0.13 mm. An accuracy of 0.5° for the measured interference phase would correspond to an error for the in-plane strain of about 10 μm/m.[15,16]

On the other hand, quasi-heterodyne holographic interferometry with TV detection is nearly as simple as standard double-exposure holography, and it does not require any special instrumentation apart from a video electronic data acquisition system. This method is very well suited for industrial applications in which high speed and medium accuracy are required. Applications to displacement and vibration measurements are shown in Fig. 12. The fringe patterns were analyzed with a quasi-heterodyne arrangement similar to the one described in this paper (Sec. 5.1) and a video image processing system with digital frame store. The deformation of the pressure-loaded CFC-panel of a radio telescope antenna [Fig. 12(a)], about 1.2 m by 1.4 m in size, was recorded by double-exposure, two-reference-beam holography using a cw argon laser. The vibration pattern of an oil pan [Fig. 12(b)] resonating at 1244 Hz was recorded with a synchronized double-pulse ruby laser in a holographic setup with reference sources close together. For the reconstruction and fringe analysis, however, a cw He-Ne laser was used. The effects of the wavelength change were compensated by readjusting the hologram and the angular separation of the reference sources.

7. ACKNOWLEDGMENTS

The authors would like to thank B. Breuckmann and R. Thieme of M.A.N. Neue Technologie, Munich, and R. Pryputniewicz, Worcester Polytechnic Institute, for making available some of their recent experimental results to illustrate the presented methods with actual applications. This work was supported in part by the Swiss Science Foundation.

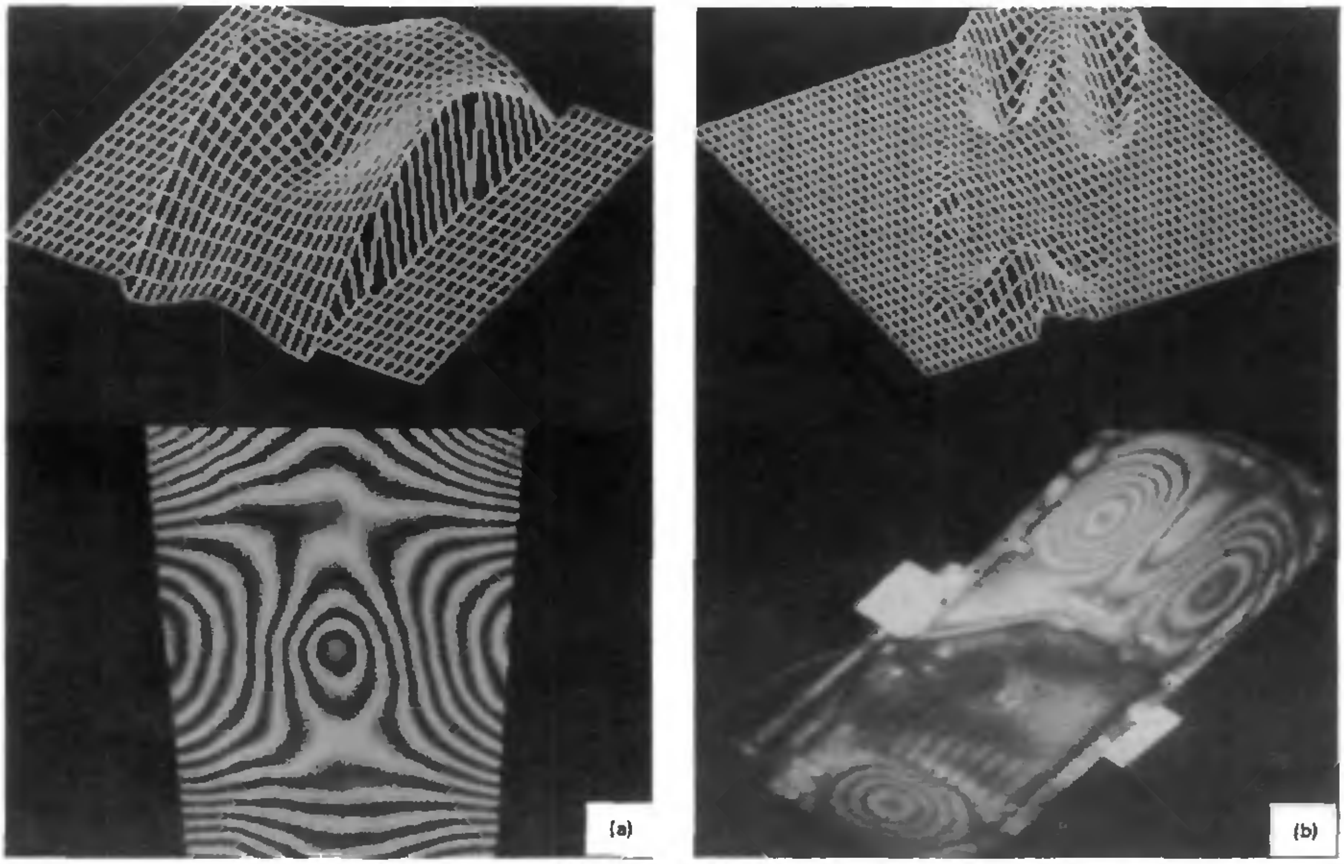

Fig. 12. Quasi-heterodyne holographic interferometry applied to displacement and vibration measurements. Typical examples of fringe patterns and deformation plots displayed on the monitor. (a) Out-of-plane displacement of a pressure-loaded CFC-panel of a radio telescope antenna. (b) Vibration amplitude of an oil pan resonating at 1244 Hz. (Figures courtesy of B. Breuckmann and W. Thieme.)

8. REFERENCES

1. Special issue on *Precision Surface Metrology*, J. C. Wyant, guest ed., Opt. Eng. 23(4), pp. 349-395 (1984).
2. W. Jüptner, T. M. Kreis, and M. Kreitlow, in *Industrial Applications of Laser Technology*, William F. Fagan, ed., Proc. SPIE 398, 22 (1983).
3. P. Hariharan, B. F. Oreb, and N. Brown, Appl. Opt. 22, 876 (1983).
4. R. Dändliker, in *Progress in Optics*, Vol. XVII, E. Wolf, ed., pp.1-84, North-Holland, Amsterdam (1980).
5. R. Dändliker, R. Thalmann, and J.-F. Willemin, Opt. Commun. 42, 301 (1982).
6. R. Thalmann and R. Dändliker, in *1984 European Conference on Optics, Optical Systems, and Applications*, B. Bölger and H. A. Ferwerda, eds., Proc. SPIE 492, 299 (1985).
7. G. S. Ballard, J. Appl. Phys. 39, 4846 (1968).
8. R. Dändliker, E. Marom, and F. M. Mottier, J. Opt. Soc. Am. 66, 23 (1976).
9. R. Dändliker, B. Ineichen, and F. M. Mottier, Opt. Commun. 9, 412 (1973).
10. R. Crane, Appl. Opt. 8, 538 (1969).
11. J. H. Bruning, D. R. Herriott, J. E. Gallagher, D. P. Rosenfeld, A. D. White, and D. J. Brangaccio, Appl. Opt. 13, 2693 (1974).
12. J. Mastner and V. Masek, Rev. Sci. Instrum. 51, 926 (1980).
13. R. Dändliker, in *Progress in Optics*, Vol. XVII, E. Wolf, ed., pp. 54-60, North-Holland, Amsterdam (1980).
14. R. Dändliker and R. Thalmann, in *Industrial Applications of Laser Technology*, William F. Fagan, ed., Proc. SPIE 398, 11 (1983).
15. R. J. Pryputniewicz, Int. Arch. Photogram. 24, 377 (1982).
16. R. Dändliker and B. Eliasson, Exp. Mech. 19(3), 93 (1979).

A reprint from

Optical Engineering

24(6), 930-935 (November/December 1985).

ISSN 0091-3286

HOLOGRAPHIC CONTOURING USING ELECTRONIC PHASE MEASUREMENT

R. Thalman
R. Dändliker

Institut de Microtechnique
Université de Neuchâtel
Rue de la Maladière 71
CH-2000 Neuchâtel, Switzerland

Holographic contouring using electronic phase measurement

R. Thalmann
R. Dändliker
Institut de Microtechnique
Université de Neuchâtel
Rue de la Maladière 71
CH-2000 Neuchâtel, Switzerland

Abstract. The application of heterodyne and quasi-heterodyne (stepwise phase shifting) fringe interpolation techniques to contouring for 3-D object shape measurement is discussed. A setup with two spherical illumination sources for contour fringe generation is described. The contour fringe pattern can be observed in real time or from a holographic reconstruction. The use of a microcomputer for automated data acquisition and processing allows one to determine the object shape for a large number of points and for arbitrarily shaped contour fringe surfaces. Experimental results are reported for both heterodyne and quasi-heterodyne phase measurement, offering a typical accuracy for object depth measurement of 0.2% of the lateral extension of the object.

Subject terms: 3-D sensing for inspection; holographic contouring; projected fringe contouring; automated fringe analysis; heterodyne; phase shifting interferometry; optical phase measurement; holographic interferometry.

Optical Engineering 24(6), 930-935 (November/December 1985).

CONTENTS

1. INTRODUCTION

Holographic contouring[1] is a well-known method to determine object shape based on the modulation of a regular fringe pattern by the object's surface. The contour fringe pattern is produced by the interference of the two reconstructed images of a double-exposure hologram in which some optical parameters have been modified between the two exposures. There exist various techniques for contour fringe generation: modifying either the illumination sources,[2-5] the observation points (hologram position),[3,4] the recording wavelength,[1,6] or the refractive index around the object.[7] The applications of holographic contouring may be divided into two categories: (a) inspection of very flat surfaces with high resolution and (b) recording of the surface shape of 3-D objects (with a depth of the object comparable to its lateral extension).

In this paper, the application of modern electronic interference fringe interpolation[8] methods and digital computers for 3-D object shape measurement by contouring will be discussed. In previous works, the methods of phase shifting interferometry have been applied to projected fringe contouring with two collimated sources[9] and to two-index holographic contouring.[7] Heterodyne phase measurement methods also have been used in moire surface contouring[10] and two-wavelength holographic contouring.[11] Electronic fringe processing provides not only a high accuracy for interference phase measurement but also represents the ideal interface between the optical interference fringe pattern and the digital computer; i.e., it offers the possibility for fully automated data acquisition and processing.

The arrangement described herein uses the simple geometry of two different spherical illumination beams for contour fringe generation. The interference phase can be measured in real time as well as in holographic reconstruction, using either a quasi-heterodyne system with video-electronic detection[8,12] or a heterodyne system[8,13] with mechanical scanning of the image by detectors. A computer controls the experiment and calculates the object contour from the measured phase data. The typical accuracy for depth measurement was found to be 0.2% of the lateral extension of the object.

2. CONTOUR FRINGE GENERATION

2.1. Two-illumination-source contouring

The contour fringe pattern on the object is generated by the interference of two different illumination sources.[2-5] The fringes can be observed in real time as well as holographically (by a single exposure with both sources simultaneously or by double exposure with the two illumination sources consecutively).

The fringe pattern due to the interference of two spherical illumination sources (surfaces of constant interference phase $\phi = n2\pi$) is a family of hyperboloids of two sheets with foci at the two sources.[2] In the far field of the sources, the fringe surfaces are approximately plane and parallel to the mean illumination direction [Fig. 1(a)]. The fringe interval Λ is given by

$$\Lambda = \frac{2\pi}{|\Delta \mathbf{k}_S|} , \tag{1}$$

where $\Delta \mathbf{k}_S$ denotes the difference between the two illumination wave vectors. Figure 1(b) shows the contour fringes as they appear on a cube.

Invited Paper TD-102 received May 18, 1985; accepted for publication July 16, 1985; received by Managing Editor Aug. 2, 1985.

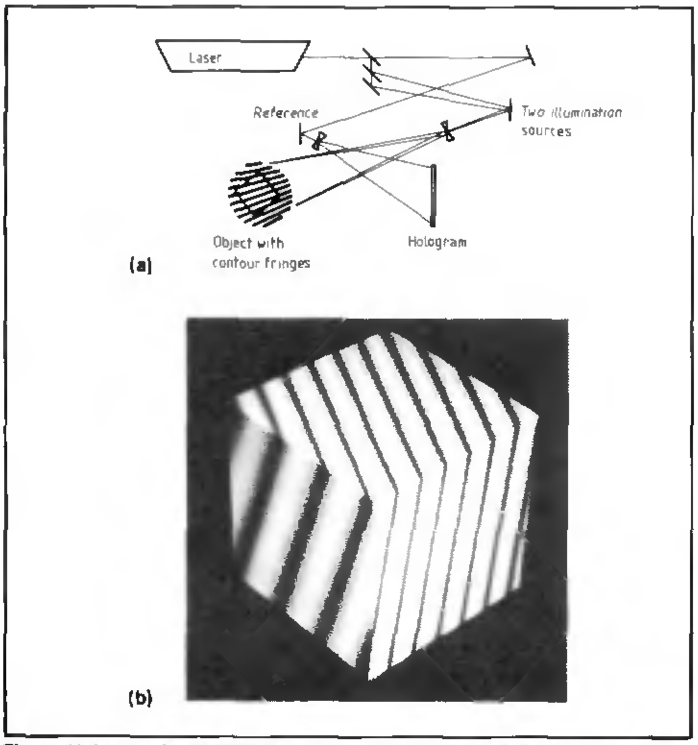

Fig. 1. Holographic contouring with two illumination sources. (a) Experimental arrangement; (b) contour fringes on a cube.

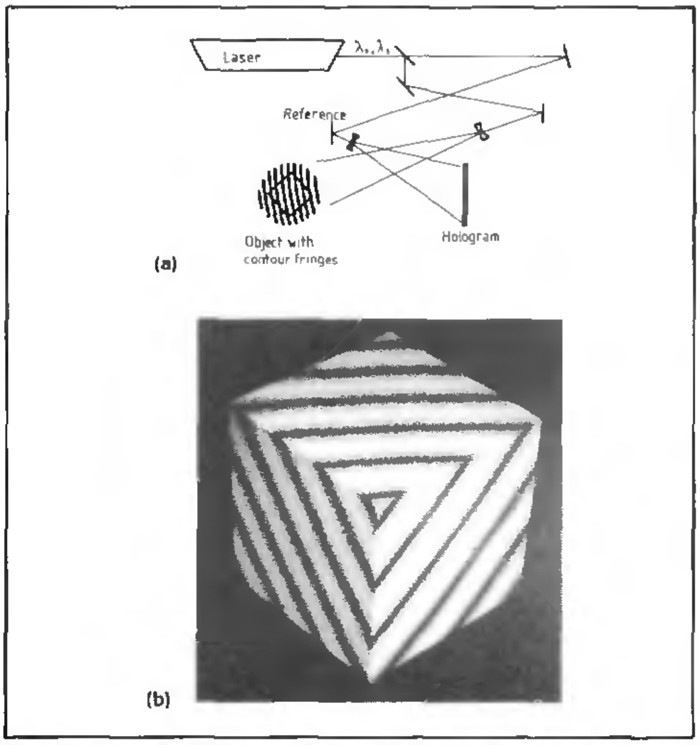

Fig. 2. Two-wavelength holographic contouring. (a) Experimental arrangement; (b) contour fringes on a cube.

Advantages of the two-source contouring are the simplicity of the experimental realization and the possibility of working in real time (without the hologram). The major drawback of this method is that the angle of incidence of the illumination on the object must be chosen relatively large in order to get reasonable sensitivity (cf. Sec. 4), which may produce shadowing on certain parts of the object.

2.2. Two-wavelength holographic contouring

The object under test is recorded holographically by double exposure using two different wavelengths.[1,6] Reconstruction of the hologram yields two superimposed images of the object. If the wavelength change $\Delta\lambda$ between the two exposures is small enough, the two reconstructions interfere and generate contour fringes on the object. This fringe pattern is a family of ellipsoids with foci at the illumination source and the observation point, respectively [Fig. 2(a)].[2] The fringe interval along the major axis of the ellipsoid is given by

$$\Lambda = \frac{\lambda^2}{2\Delta\lambda} , \tag{2}$$

where λ is the mean wavelength.

Figure 2(b) shows the contour fringes as they appear on a cube. The wavelength change has been realized by tuning the etalon (temperature) of the argon laser in order to select different longitudinal modes within the gain bandwidth of the green line ($\lambda = 514$ nm).[11] The corresponding frequency difference was 8 GHz, which yields a contour interval of $\Lambda = 2$ cm.

Some important difficulties with two-wavelength contouring are (a) the fringes can be produced only holographically; (b) large wavelength changes require special attention to the lateral displacement of the two reconstructed images (fringe contrast); and (c) the experimental realization of reproducible (or calibrated) wavelength changes is difficult and requires special equipment. The method is suited primarily for flat objects, where the fringes can be set parallel to the object surface and a small fringe spacing can be used to get high sensitivity.

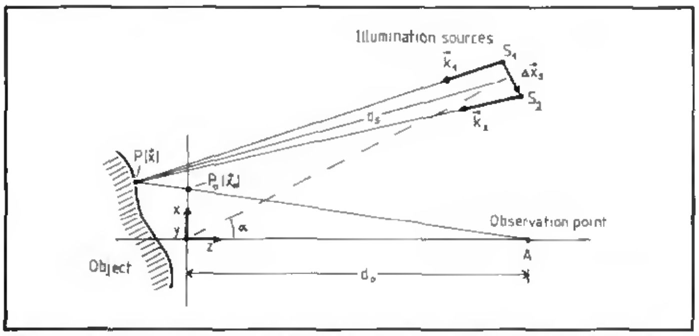

Fig. 3. Geometry for the interpretation of the contour fringes produced by two illumination sources.

2.3. Other methods

There are also other methods for contour fringe generation that are not treated here, namely, two-index holographic contouring,[7] which is very similar to the two-wavelength method, and all kinds of moire techniques.[1,10] Heterodyne and phase shifting techniques can be applied to most of them as well.[7,10]

3. INTERPRETATION OF FRINGES IN TWO-ILLUMINATION-SOURCE CONTOURING

3.1. Determination of object depth

In the following, the determination of the object shape from the measured interference phase of the contour fringe pattern will be discussed for the case of two different illumination directions. The contour fringes on the object are generated by interference of the two spherical waves of sources S_1 and S_2 (see Fig. 3). The interference phase $\phi(\mathbf{x})$ at the object point $P(\mathbf{x})$ is given by

$$\phi(\mathbf{x}) = k[d_1(\mathbf{x}) - d_2(\mathbf{x})] , \tag{3}$$

where $k = 2\pi/\lambda$ and where $d_i(\mathbf{x}) = [(\mathbf{x} - \mathbf{x}_i)^2]^{1/2}$ is the distance between $P(\mathbf{x})$ and the illumination source $S(\mathbf{x}_i)$ (cf. Fig. 3). Assuming that the separation $\Delta\mathbf{x}_s$ of the two sources is much smaller than the distance $d_s(\mathbf{x})$ from the sources to the object point $P(\mathbf{x})$, Eq. (3) can be replaced to a very good approximation by

$$\phi(\mathbf{x}) = \frac{k}{d_s(\mathbf{x})}\Delta\mathbf{x}_s \cdot \mathbf{x} + \phi_o , \tag{4}$$

where ϕ_o is a constant, generally unknown phase. In the experiment, ϕ_o is arbitrarily determined by assuming that $\phi(\mathbf{x}=0) = 0$.

The object is observed by an imaging system. The observation point A is defined by the center of the lens aperture, which is at a distance d_o from the object plane. The interference phase $\phi(\mathbf{x})$ at the object point $P(\mathbf{x})$ is measured at the conjugate image point $P_o(\mathbf{x}_o)$ (cf. Fig. 3). The geometrical relation between $\mathbf{x}$ and $\mathbf{x}_o$ leads to

$$x = x_o\left(1 - \frac{z}{d_o}\right), \quad y = y_o\left(1 - \frac{z}{d_o}\right), \tag{5}$$

where $\mathbf{x} = (x,y,z)$ and $\mathbf{x}_o = (x_o,y_o,0)$. Inserting Eq. (5) into Eq. (4), one gets

$$\phi(\mathbf{x}) = \frac{k}{d_s(\mathbf{x})}\left[(\Delta x_s x_o + \Delta y_s y_o)\left(1 - \frac{z}{d_o}\right) + \Delta z_s z\right] . \tag{6}$$

The wanted object depth, which is the z-coordinate of the point $P(\mathbf{x})$, is found from Eq. (6) to be

$$z = \frac{(d_s/k)\phi - (\Delta x_s x_o + \Delta y_s y_o)}{\Delta z_s - [(\Delta x_s x_o + \Delta y_s y_o)/d_o]} . \tag{7}$$

The separation $\Delta\mathbf{x}_s$ of the illumination sources can be determined indirectly by measuring the interference phase $\phi(\mathbf{x}_o)$ in the object plane $z = 0$ (cf. Sec. 2.2). In order to reduce the influence of systematic errors (cf. Sec. 4), the expression $(\Delta x_s x_o + \Delta y_s y_o)$ in Eq. (7) is replaced by $d_s(\mathbf{x}_o)\phi(\mathbf{x}_o)/k$:

$$z = \frac{d_s(\mathbf{x})\phi(\mathbf{x}) - d_s(\mathbf{x}_o)\phi(\mathbf{x}_o)}{k\Delta z_s - [d_s(\mathbf{x}_o)\phi(\mathbf{x}_o)/d_o]} . \tag{8}$$

Thus, the object depth z in Eq. (8) depends essentially on the difference between the actual contour phase $\phi(\mathbf{x})$ and the previously measured reference phase $\phi(\mathbf{x}_o)$ for the plane $z = 0$. Note that the distance $d_s(\mathbf{x})$ between $P(\mathbf{x})$ and the illumination sources also depends on z. Therefore, Eq. (8) must be solved by iteration.

3.2. Determination of the separation of illumination sources

The distance vector $\Delta\mathbf{x}_s$ between the illumination sources is found from the interference phase $\phi(\mathbf{x}_o)$ observed on a plane screen in the object plane. The measured interference phases $\phi_x(x_o)$ and $\phi_y(y_o)$ along the x_o- and y_o-axis, respectively, can be fitted to the theoretical phase functions with Δx_s and Δy_s as parameters:

$$\phi_x(x_o) = \frac{kx_o}{[(x_s-x_o)^2 + y_s^2 + z_s^2]^{1/2}}\Delta x_s \equiv \chi(x_o)\,\Delta x_s ,$$

$$\phi_y(y_o) = \frac{ky_o}{[x_s^2 + (y_s-y_o)^2 + z_s^2]^{1/2}}\Delta y_s \equiv \chi(y_o)\,\Delta y_s , \tag{9}$$

where $\mathbf{x}_s = (x_s,y_s,z_s)$ are the coordinates of the illumination sources. Along the x_o-axis, the interference phase will be measured at the sampling points $x_o^{(n)}$. Least squares fitting of the measured phase data $\phi_x(x_o^{(n)})$ yields

$$\Delta x_s = \frac{\sum_n [\chi(x_o^{(n)})\,\phi_x(x_o^{(n)})]}{\sum_n \chi^2(x_o^{(n)})} . \tag{10}$$

Similarly, Δy_s can be determined from the measured phases $\phi_y(y_o^{(n)})$. However, in practice the two illumination sources will be chosen most often to lie in the horizontal plane $y = 0$, i.e., $\Delta y_s = 0$. The third component of $\Delta\mathbf{x}_s$ is found from geometrical considerations (cf. Fig. 3) to be

$$\Delta z_s = \frac{-(x_s\Delta x_o + y_s\Delta y_o)}{z_s} . \tag{11}$$

4. ACCURACY

The accuracy of the object contour determination depends mainly on the errors in the interference phase measurement. Other sources of errors, such as image distortion and aspherical illumination beams, are effectively compensated for by referring to the calibration phase map obtained from a plane reference object, as described in Sec. 3.1 [Eq. (8)]: The calculation of the object contour is not based on the absolute phase in the contour fringe pattern, but on the phase difference between the object and the reference plane. Thus, for the evaluation of Eq. (8), exact knowledge of the wavefronts of the two illumination sources is not important. Deviations from the theoretically expected phase $\phi(\mathbf{x}_o)$ due to image distortion and wavefront aberration in first-order approximation do not affect the object contour determination.

The errors for the determination of the object coordinate z will first be discussed for two-illumination-source contouring. For simplicity, both illumination sources are assumed to be in the plane $y = 0$. The statistical error δz as a function of the phase measurement error $\delta\phi$ is found by differentiating Eq. (7) and inserting Eq. (11) to give

$$\delta z = \frac{d_s\delta\phi}{k(\tan\alpha + x_o/d_o)\Delta x_s} \simeq \frac{d_s}{k}\,\frac{\delta\phi}{\sin\alpha\Delta s} , \tag{12}$$

where α is the angle of the fringe planes with respect to the optical axis and where $\Delta s = (\Delta x_s^2 + \Delta z_s^2)^{1/2}$ is the distance between the illumination sources. Δs determines the fringe density on the object. The maximum fringe density will generally be limited by the detector resolution. Thus, it is not suitable to estimate an absolute error δz for the object contour measurement, but rather to indicate the error relative to the number of resolved points in the detected image and relative to the lateral object size. If N_f is the number of contour fringes across the object and L is the lateral extension of the object, one gets for the relative error $\delta z/L$ from Eq. (12)

$$\frac{\delta z}{L} = \frac{\delta\phi}{2\pi\,N_f\tan\alpha} . \tag{13}$$

To estimate the minimum error of a given system, N_f can be replaced by the ratio of the number of points resolved by the detector (pixels) and the minimum number of pixels within one fringe, necessary to get maximum fringe interpolation accuracy.

As numerical examples, the minimum relative error $\delta z/L$ for the object contour determination will be estimated for heterodyne and for quasi-heterodyne systems.[8] With both systems, typically 200 pixels can be resolved across the image. The minimum number of pixels within one fringe is assumed to be 10, and $\tan\alpha = 0.5$. For the quasi-heterodyne system, a phase measurement accuracy of 1/100 of a fringe is reasonable, which yields $\delta z/L = 10^{-3}$. With a heterodyne system, minimum phase errors of 1/1000 of a fringe have been obtained. This yields a maximum relative accuracy for contouring of $\delta z/L = 10^{-4}$.

Equation (12) shows that in order to get reasonable accuracy, the illumination angle α should not be chosen too small. On the other hand, even for $\alpha = 30°$ the error δz will be only twice as large as for the ideal case, where the contour fringes are parallel to the object plane. The choice of the angle of incidence α will normally be a compromise between good sensitivity and avoiding shadows on the object.

For two-wavelength holographic contouring, it is more difficult to give a formula analogous to Eq. (12), because the fringe pattern depends on the illumination and the observation geometry. For the special case of collimated object and reference waves, δz can be expressed as[6]

$$\delta z = \frac{\lambda^2}{\Delta\lambda(1 + \cos\alpha)} \frac{\delta\phi}{2\pi}, \tag{14}$$

where α is still the angle of incidence of the illumination beam. Again, the accuracy will be essentially limited by the number of contour fringes across the object that can be resolved by the detector. For very flat objects, two-wavelength holographic contouring can generate fringes parallel to the object surface without shadowing. Thus, small contour fringe separation can be used for high resolution of depth without getting high fringe densities in the image. However, for objects extended in depth, the absolute accuracy for the contour determination will be of the same order of magnitude for two-wavelength contouring as for two illumination sources. Therefore, taking into account its experimental advantages (cf. Sec. 2), in most applications two-source contouring will be preferred.

5. EXPERIMENTAL RESULTS

5.1. Holographic contouring with quasi-heterodyne fringe interpolation

Quasi-heterodyne interference fringe interpolation is based on stepwise shifting of the interference phase and video-electronic detection. The intensity in the interferogram is measured by a TV camera for at least three different, well-known mutual phases between the interfering wavefields. The interference phase then can be calculated accurately at any point in the interferogram, independent of mean illumination and local fringe contrast. The experimental arrangements and the capabilities of phase shifting techniques are extensively discussed in Refs. 8 and 12.

Figure 4 shows an experimental setup for two-illumination-source holographic contouring with quasi-heterodyne phase measurement. The two spherical object illuminations are produced by two laser beams of a small mutual angle passing through a common lens of short focal length. Switching from one beam to the other is realized by a removable mirror.

In double-exposure phase shifting holographic interferometry, two reference beams are required in order to have independent access to the phase between the two reconstructed wavefields. This means that for two-source holographic contouring, the object is recorded twice, with different object and reference beams each time. The simultaneous reconstruction of the hologram with both references produces a contour fringe pattern on the object, where the fringes can be shifted by acting on the mutual phase (or the optical path length) between the two reference beams.

The two reference sources are placed very close together.[8,13] This has the advantage that the sensitivity to hologram misalignment is small. Furthermore, the references close together produce a pattern of macroscopic, parallel interference fringes in the hologram plane, which can be used to control the relative phase of the reference waves. For this purpose, a twin-photodiode is placed in this fringe pattern, just beside the hologram plate. It detects a fringe maximum, and an integrating feedback loop stabilizes the interference phase with the help of a piezo-mounted mirror in one reference beam. The phase steps for the quasi-heterodyne fringe interpolation can be produced by simply translating the stabilizing photodiode.

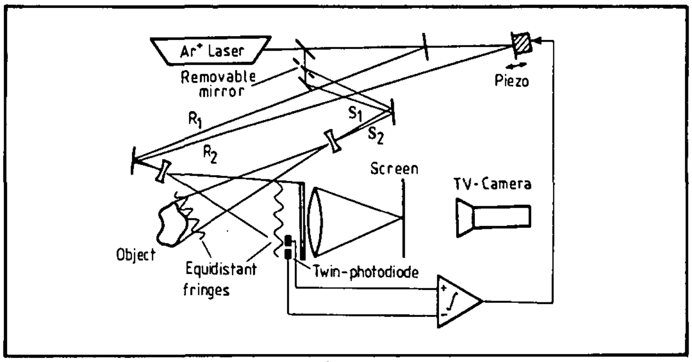

Fig. 4. Experimental setup for two-illumination-source holographic contouring using quasi-heterodyne interference fringe interpolation with video-electronic detection.

The virtual image of the hologram is projected onto a transparent screen where it is observed by a TV camera. The TV images for three phase steps (0°, 120°, and 240°) are digitized and sent to a microcomputer to calculate the interference phase and the object contour.

Figure 5 illustrates the contour measurement along a horizontal line across the edge of a cube [Fig. 5(a)].[12] Figure 5(b) shows one of the three intensity profiles through the fringe pattern. Note that the fringe contrast is reduced to about 50% due to the overlapping of the cross-reconstructions in two-reference-beam holography with reference sources close together.[8,13] Figures 5(c) and 5(d) show the measured interference phase and the corresponding object contour. The separation of the two illumination sources was 60 μm, and the contour fringe spacing on the object was 8.5 mm. The angle of incidence of the object beam with respect to the optical axis was $\alpha = 27°$. Assuming a phase interpolation error of 1/100 of a fringe,[8] the accuracy of the depth measurement can be estimated from Eq. (13) to be $\delta z/L = 1/500$ or $\delta z = 0.2$ mm rms.

Contour fringes with two illumination beams can also be generated in real time, i.e., without holographic recording, which makes the optical setup easier (cf. Secs. 5.2 and 5.3). One advantage of holographic recording is that a hologram provides higher intensity in the reconstructed image, which may be helpful when using low-power lasers. Another advantage of holographic contour fringe generation is that it is possible to do contouring in exactly the same setup as used for holographic deformation analysis, simply by adding one removable mirror to provide the second illumination beam (cf. Fig. 4).

5.2. Real-time contouring with quasi-heterodyne fringe interpolation

As mentioned above, contour fringes from two illumination sources also can be observed in real time, without holographic recording. Figure 6 shows the setup for real-time contour fringe generation and quasi-heterodyne phase measurement. The fringe stabilizing twin-photodiode is placed in the contour fringe pattern at the border of the illumination beams. The piezo-mounted mirror acts as a phase shifter in one of the two illumination beams. The TV-camera directly observes the object with the projected contour fringes.

Again, the object countour has been measured along a straight line across the edge of a cube (cf. Sec. 5.1). Figure 7 shows (a) the intensity profile through the fringe pattern and (b) the object contour calculated therefrom. The contour fringe spacing on the object was 7 mm; the angle of incidence of the illumination beam with respect to the optical axis was $\alpha = 24°$. Assuming a phase interpolation error of 1/100 of a fringe, the accuracy of the contour measurement can be estimated to be $\delta z/L = 1/630$ or $\delta z = 0.16$ mm.

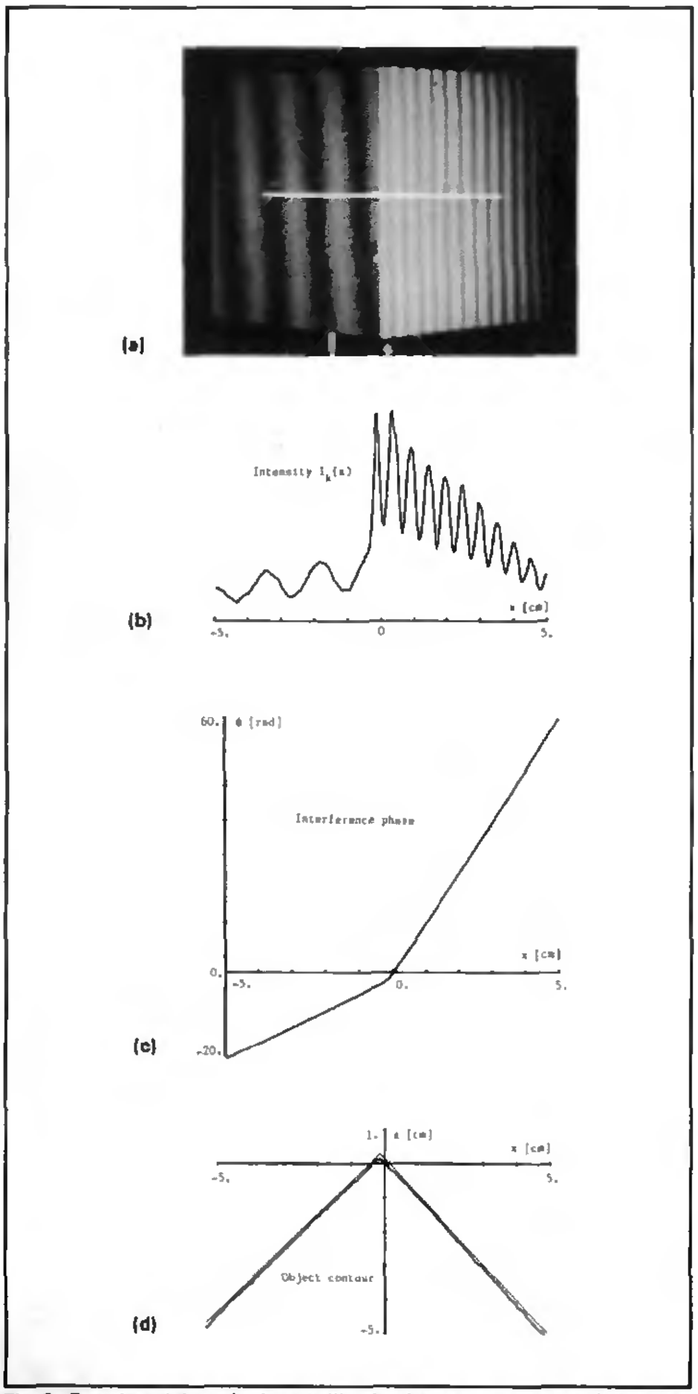

Fig. 5. Experimental results for two-illumination-source holographic contouring using quasi-heterodyne fringe interpolation with video-electronic detection. (a) Cube edge with contour fringes. (b) Intensity profile through the contour fringe pattern along white line above. (c) Measured interference phase. (d) Evaluated object contour.

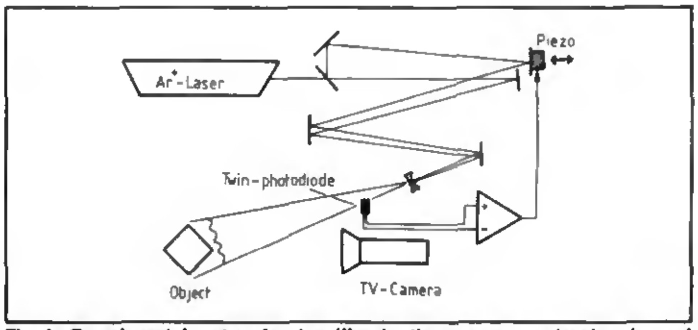

Fig. 6. Experimental setup for two-illumination-source contouring in real time using quasi-heterodyne interference fringe interpolation with video-electronic detection.

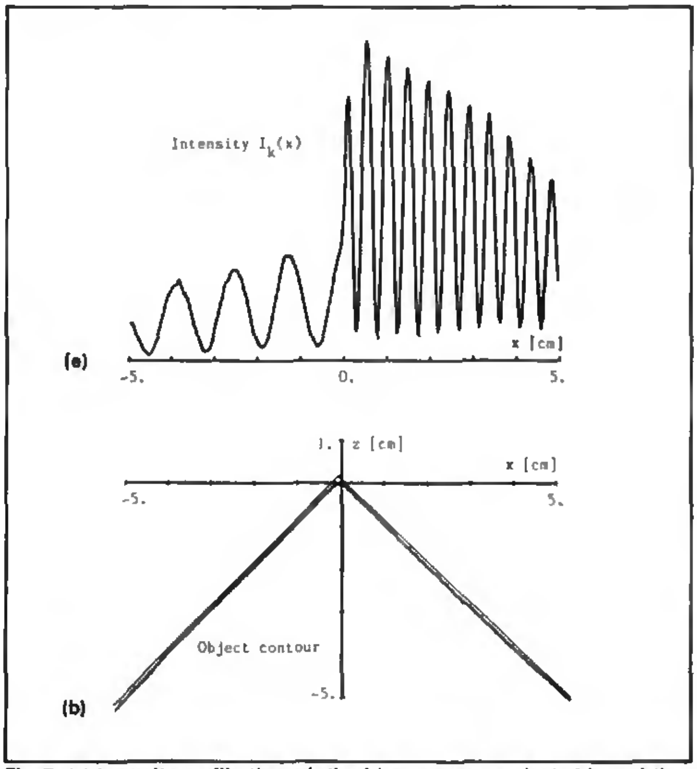

Fig. 7. (a) Intensity profile through the fringe pattern projected in real time from two illumination sources on a cube edge [Fig. 5(a)]. (b) Object contour evaluated with the quasi-heterodyne system.

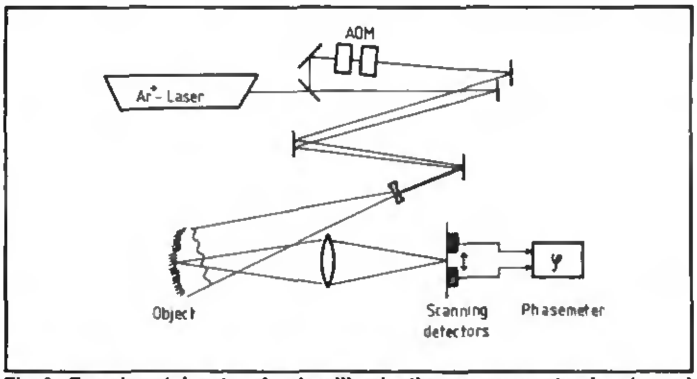

Fig. 8. Experimental setup for two-illumination-source contouring in real time using heterodyne phase measurement in the image of the object.

5.3. Real-time contouring with heterodyne phase measurement

Figure 8 shows the experimental arrangement for real-time contouring with two spherical illumination sources and heterodyne fringe interpolation. Heterodyne phase measurement for holographic interferometry is extensively discussed in Refs. 8 and 14. A pair of acousto-optic modulators (AOMs), driven at 40 MHz and 40.1 MHz, respectively, produces a frequency shift of 100 kHz in one illumination beam, which makes the contour fringes move across the object at a speed corresponding to the beat frequency. The phase of the interference pattern is determined by scanning the image of the object with a photodetector and measuring the phase of the beat frequency with respect to a reference signal. In practice, an array of three detectors (fiber bundles, which feed the light to three photomultiplier tubes) is used to determine two phase dif-

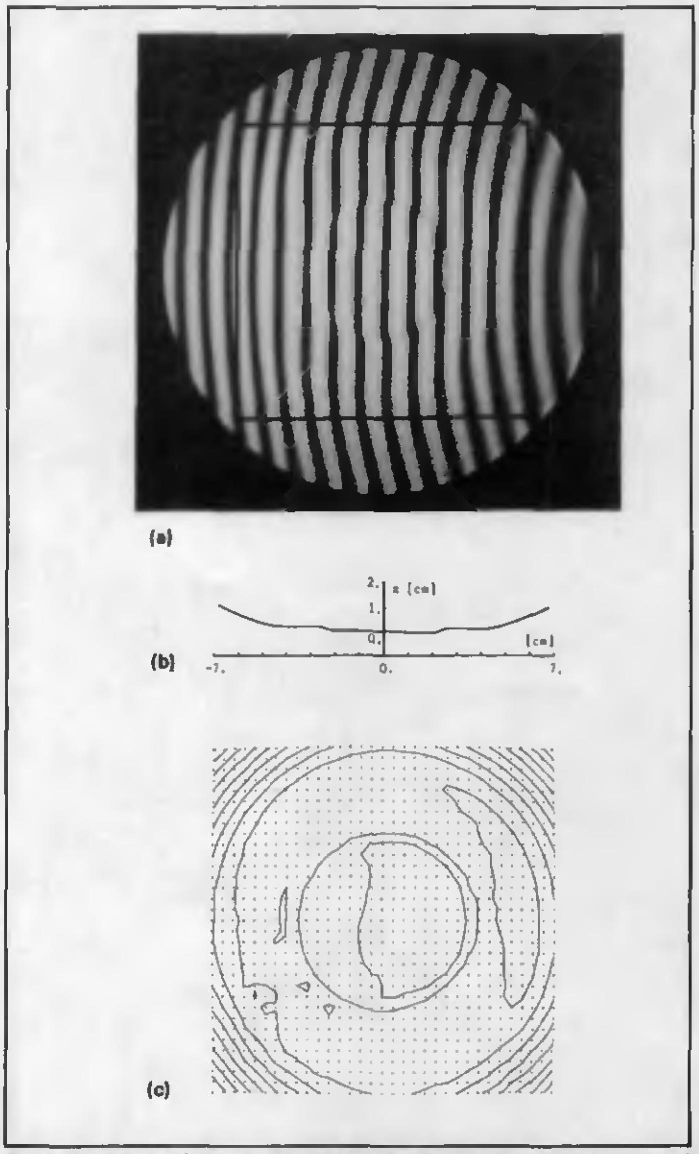

Fig. 9. Experimental results for two-illumination-source contouring in real time using heterodyne phase measurement. (a) Contour fringes on the object (a white painted saucer). The object contour has been determined inside the indicated square area. (b) Measured object profile along a diagonal of the square area. (c) Lines of equal height (separated by 1 mm in depth) based on a grid of 33 x 33 measurements at 3 mm separation.

ferences in two orthogonal directions, rather than the interference phase itself. The latter can be calculated easily and accurately by summation of the measured differences along a given path.

Figure 9 illustrates a result of heterodyne contouring on a saucer of 15 cm diameter. Figure 9(a) shows the contour fringes on the object. The fringe spacing was 9 mm, and the angle of incidence of the illumination beam was $\alpha = 27°$. The interference phase has been measured on a grid of 33×33 points of 3 mm separation within the square area indicated in Fig. 9(a). Figure 9(b) shows the object profile evaluated from the measured interference phase along the diagonal from the lower left to the upper right corner of this area. In Fig. 9(c) the lines of equal height with an interval of 1 mm are plotted. Assuming a phase interpolation error of 1° rms, the accuracy of the contour measurement can be estimated to be $\delta z/L = 1/1500$ or $\delta z = 0.06$ mm rms.

6. CONCLUSIONS

Heterodyne and quasi-heterodyne techniques for interference phase measurement have been successfully applied to two-illumination-source contouring. Both techniques provide high accuracy and fully automated measuring. The use of computers for data acquisition and processing offers the possibility of evaluating contour fringe patterns produced by very general optical geometries, i.e., nonplane and arbitrarily oriented fringe surfaces. A simple optical setup with two spherical illumination sources has been used for contour fringe generation. Experimental results are presented for 3-D object shape measurements, using holographic contour fringes as well as real-time projected fringe patterns. The accuracy for object depth measurement is typically 0.2% of the lateral extension of the object. An important application of one of the described methods is the determination of the object geometry, needed for holographic displacement and strain analysis, in exactly the same optical setup and with the same electronic equipment as used for quantitative holographic interferometry.

7. REFERENCES

1. J. R. Varner, "Holographic and Moiré Contouring," in *Holographic Nondestructive Testing*, R. K. Erf, ed., Chap. 5, Academic Press, New York (1974).
2. H. P. Hildebrand and K. A. Haines, J. Opt. Soc. Am. 57(2), 155 (1967).
3. N. Abramson, Appl. Opt. 15(1), 200 (1976).
4. M. Yonemura, Appl. Opt. 21(20), 3652 (1982).
5. P. Benoit, E. Mathieu, J. Hormière, and A. Thomas, Nouv. Rev. Optique 6(2), 67 (1975).
6. C. M. Vest, *Holographic Interferometry*, Chap. 7.2, John Wiley & Sons, New York (1979).
7. P. Hariharan and B. F. Oreb, Opt. Commun. 51(3), 142 (1984).
8. R. Dändliker and R. Thalmann, Opt. Eng. 24(5), 824 (1985).
9. V. Srinivasan, H. C. Liu, and M. Halioua, Appl. Opt. 23(18), 3105 (1984).
10. J. C. Perrin and A. Thomas, Appl. Opt. 18(4), 563 (1979).
11. R. Dändliker, "Heterodyne Holographic Interferometry," in *Progress in Optics*, Vol. XVII, E. Wolf, ed., pp. 67–69, North Holland, Amsterdam (1980).
12. R. Thalmann and R. Dändliker, 1984 European Conference on Optics, Optical Systems and Applications, (ECOOSA '84), B. Bolger and H. A. Ferwerda, eds., Proc. SPIE 492, 299 (1985).
13. R. Dändliker, R. Thalmann, and J.-F. Willemin, Opt. Commun. 42(5), 301 (1982).
14. R. Dändliker, "Heterodyne Holographic Interferometry," in *Progress in Optics*, Vol. XVII, E. Wolf, ed., pp. 1–84, North Holland, Amsterdam (1980).

Automated evaluation of 3-D displacement and strain by quasi-heterodyne holographic interferometry

R. Thalmann and R. Dändliker

Institut de Microtechnique de l'Université
CH-2000 Neuchâtel, Switzerland

Abstract

The determination of 3-D displacement and strain by holographic interferometry for industrial applications is a problem still not resolved satisfactorily. Important requirements are: 1) simple optical arrangement requiring only one hologram recording, 2) fully automated fringe evaluation and data processing. The proposed arrangement with quasi-heterodyne (phase shifting) fringe interpolation and video-electronic detection offers fast and automated phase measurement with high accuracy. The 3-D information about the deformation is obtained by moving the TV-camera behind the hologram plate to get different directions of observation. If the object shape is known, the effects of image distortion due to perspective can be corrected by appropriate interpolation of the measured interference phases. In this paper, the optical setup and the data acquisition system will be described. The calculation of vector displacement and strain, including correction of the distortion by perspective, are discussed in detail. Finally, experimental results with an estimation of the accuracy for displacement and strain will be reported.

Introduction

Quasi-heterodyne (phase shifting) interference fringe interpolation with video-electronic detection [1,2] is a powerful technique for automated and quantitative evaluation of holographic interferograms. It provides precise interference phase measurement with high spatial resolution and a large number of data points, with an interpolation accuracy up to 1/100 of a fringe, independently of fringe position and variations of mean intensity and fringe contrast within the interferogram. The method can be applied to real-time,[3] double-exposure [1,2,4,5] and double-pulse [5] holographic interferometry, as well as to holographic contouring.[1,6,7]

In many applications of displacement (or vibration) measurements and especially for strain analysis, the knowledge of the interference phase alone is not sufficient to obtain quantitative results. For the quantitative evaluation of vector displacement and strain, at least three phase measurements with independent sensitivity vectors must be accomplished. In order to provide a simple holographic recording and reconstruction procedure, we propose a setup using only one holographic plate and one direction of illumination. The 3-D information is obtained by moving the TV-camera behind the hologram to get different directions of observation.

In this paper, the experimental arrangement for quasi-heterodyne holographic interferometry is shortly described. The theoretical and numerical fundamentals for the evaluation of vector displacement and strain are given. It is discussed in detail, how for non-planar objects the effects of image distortion due to perspective (different observation directions) can be corrected by appropriate interpolation of the measured interference phases. Finally, experimental results illustrate the performance of the described method.

Experimental arrangement

The experimental arrangement for quasi-heterodyne holographic interferometry with two reference sources close together and video-electronic detection is schematically shown in Fig.1. A detailed description can be found in Refs.1 and 2. For double-exposure holography with phase shifting fringe interpolation, two reference beams are required. During reconstruction a change of the relative phase between the two references allows to shift the fringes in the interferogram at will. In the quasi-heterodyne technique, this relative phase is changed step-wise, to at least three different values. Then the interference phase can be computed from the different measured intensity values at any image point with high accuracy, independently of mean intensity and fringe contrast variations. We propose an optical arrangement with the two reference sources very close together. This setup has the following advantage: First, the sensitivity for angular repositioning of the hologram is very low (only about 10°).[8] This makes it possible to reconstruct the hologram anywhere in a similar optical setup. Even holograms recorded by a ruby laser can be realigned for reconstruction with a He-Ne laser.[5] Secondly, the reference waves produce in the hologram plane a pattern of parallel macroscopic fringes which can be used to stabilize very efficiently the interference phase and to control accurately the shift of the mutual phase of the reference beams. The position of the fringe maximum is detected by a twin-photodiode and fed back to a piezo mounted mirror. The interferogram is detected by direct observation of the virtual image of the hologram with a CCD-camera. In order to get the 3-D information for the displacement vector, the camera is laterally moved behind the hologram plate. An alternative method would be the use of several fixed cameras at different places.

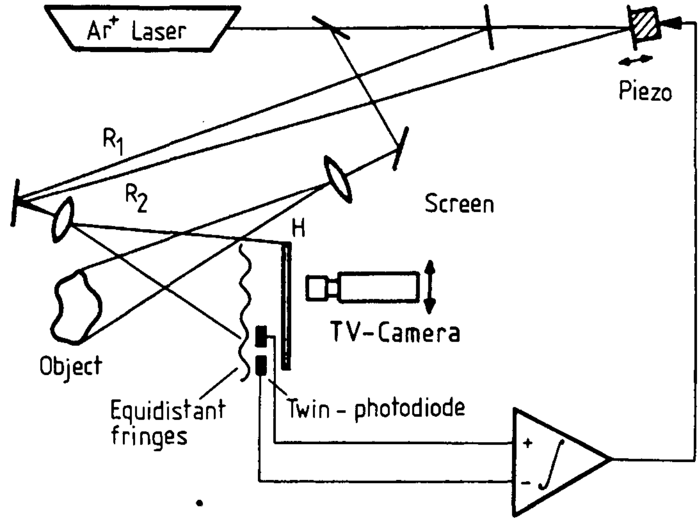

Figure 1. Schematic arrangement for quasi-heterodyne holographic interferometry with two reference sources close together, fringe stabilization and video-electronic detection.

Evaluation of 3-D displacement and strain

Determination of the displacement vector

The geometry of the optical setup is sketched in Fig.2. The origin of the (x,y,z)-coordinate system is chosen on the object surface, with the z-axis parallel to the mean observation direction. The object is illuminated from the point source $S(\vec{x}_S)$ and observed from the observation point $A(\vec{x}_A)$ behind the hologram plate. The observation point is determined by the center of the pupil of the TV-camera lens. The object shape is described by the coordinates of the points $\vec{x}_o$ or by the function $z_o = z_o(x_o,y_o)$.

For each object point $\vec{x}_o$, the interference phase is measured for N different observation points $A_n(\vec{x}_A^{(n)})$. The interference phases ϕ_n (n = 1,..,N) and the displacement vector $\vec{u}$ at the object point $\vec{x}_o$ are related by

$$\phi_n = k\ (\vec{g}_n \cdot \vec{u})\ , \tag{1}$$

where $k = 2\pi/\lambda$ is the wave number and $\vec{g}_n$ denotes the local sensitivity vector

$$\vec{g}_n = \vec{k}_S - \vec{k}_A^{(n)}\ . \tag{2}$$

$\vec{k}_S$ and $\vec{k}_A^{(n)}$ are the unity vectors of illumination and observation, respectively, given by

$$\vec{k}_S = (\vec{x}_o - \vec{x}_S)/|\vec{x}_o - \vec{x}_S| \quad \text{and} \quad \vec{k}_A^{(n)} = (\vec{x}_A^{(n)} - \vec{x}_o)/|\vec{x}_A^{(n)} - \vec{x}_o|\ . \tag{3}$$

Equation (1) can be written in matrix form as

$$\vec{\Phi} = k\ G\ \vec{u}\ , \tag{4}$$

with the N-dim. vector $\vec{\Phi} = (\phi_1,..,\phi_n)^T$ and the Nx3 matrix G with $G_{nk} = (\vec{g}_n)_k$. Note that the matrix G is different for each object point. If the interference phase is measured for more than N = 3 independent observation directions, the system of linear equations (4) is overdetermined. Its best solution in the sense of least squares is found by symmetrization:[9]

$$H\ \vec{u} - \vec{\Psi} = 0\ , \tag{5}$$

with the 3-dim. vector $\vec{\Psi} = G^T\vec{\Phi}$ and the symmetrical matrix $H = k\ G^TG$. Equation (5) can now be solved by trigonalization of the matrix H.

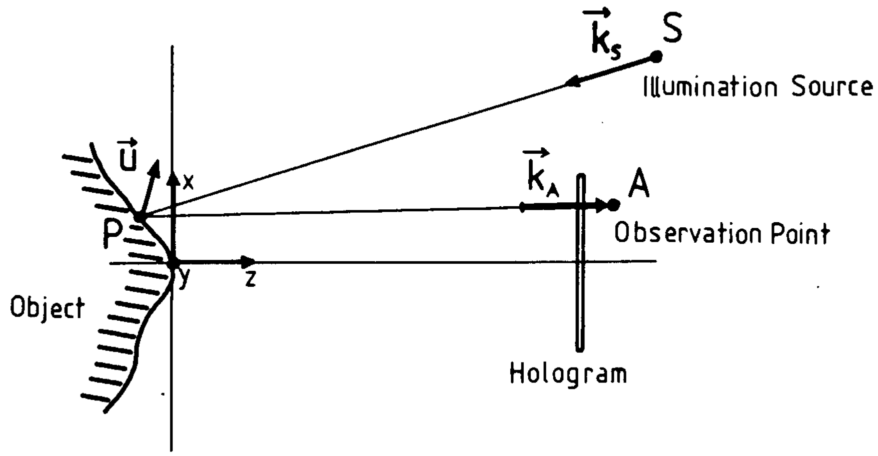

Figure 2. Geometry of the optical setup for hologram recording and observation.

Problem of the absolute fringe order

Generally the absolute fringe order is unknown and can not be determined directly from the interferogram. But there are several methods to overcome this problem, e.g.:
- by knowledge of an object point without displacement (fixation, vibration node);
- by holographic observation of the deformation in real time and fringe counting;
- by solving the system of Eqs.(4) with the absolute phase as fourth unknown (at least four different observations necessary).

None of these methods to determine the absolute phase gives accurate results. For in-plane displacement and strain analysis, however, the knowledge of the relative phases between the different observation directions is most important. It is the fringe stabilization used in the described quasi-heterodyne system (Fig.1) which assures the correct relative phases between successive observations under different viewing directions. This is anoter advantage of fringe stabilization compared to other phase shifting methods for interference phase measurement. However, fringe interpolation provides the interference phase only modulo 2π. Thus, for large in-plane displacements, the relative fringe order between the different directions of observation has to be established by counting the fringes for one selected object point, while the TV-camera is moved from one position of observation to the next. If several fixed cameras are used, a reference point on the object, for which the in-plane displacement is small enough so that the phase changes less than π (half of a fringe) between the different observation directions, should be known a priori.

Determination of surface strain

The surface strain is determined by the derivatives of the in-plane displacement vector components along the object surface. Because of measuring errors, the numerical calculation of these derivatives is only meaningful, if one takes the average over a relatively large number of measured points and thus reduces the spatial resolution. There are two possible approaches, a global one (a) and a local one (b):

(a) The whole field of sampling points is interpolated with smoothing cubic spline functions. By the appropriate choice of a weighting parameter, the degree of smoothing can be arbitrarily influenced. The derivatives can then be calculated from the spline functions at any desired point. This is certainly the best way to determine the derivatives of the displacement vector and thus the strain, but it requires a large amount of calculation and memory space, especially for two-dimensional data fields, because the computation is a global one. Furthermore, this method is only applicable for plane object surfaces, because the derivatives are calculated in a fixed coordinate system and can therefore not be determined along a curved surface.

(b) The strain can be determined locally at some positions of interest only. The in-plane derivatives are calculated in the tangential plane to the object surface at the corresponding point by two-dimensional linear least square fitting of the displacement vector components through the point and its neighbours. The number of sampling points to be taken into account for this fit will be chosen as a function of the accuracy of the displacement measurement and the desired spatial resolution. This procedure is described in detail in Ref.10 for 5 points, but it can be easily extended to an arbitrary number of points.

In comparison, the first approach (a) provides a better spatial resolution for comparable degree of smoothing (averaging of statistical measuring errors) and it suppresses completely the high frequency noise, whereas the second method (b) has the advantage to be performed locally and requires therefore much less calculation effort.

Distortion of the image due to change of perspective

The image of a non-planar object is distorted due to perspective by the change of observation direction. For an automated evaluation of displacement and strain, this effect has to be corrected, i.e. corresponding points of the different distorted images have to be associated with a common object point.

Calculation of the image distortion

Figure 3 illustrates the distortion of the image due to a change of perspective: To each defocussed object point P correspond different points P_n in the conjugate image plane (x/y) for different observation points $\vec{x}_A^{(n)}$. This image distortion can be entirely characterized by a vector field $\vec{\varepsilon}(\vec{x})$, which describes the difference between the distorted and the reference image: $\vec{\varepsilon}$ is the vector from the reference point P_1 to the distorted point P_n (cf. Fig.3). As a reference, the image observed through the center of the hologram plate along the optical axis can be used, for instance.

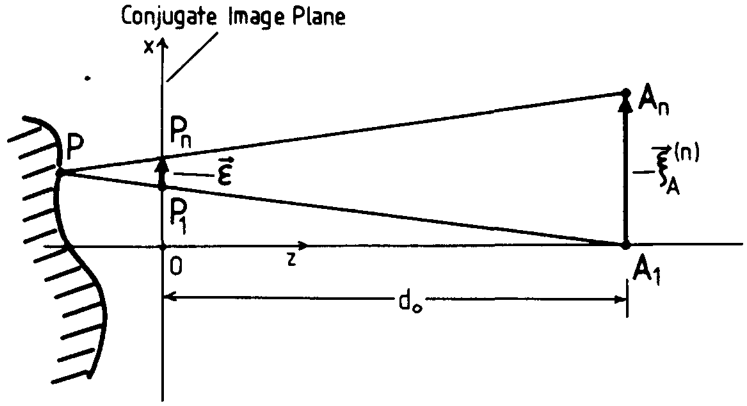

Figure 3. Image distortion $\vec{\varepsilon}$ due to a change of perspective: for different observations A_n the same (defocussed) object point P yields different points P_n in the conjugate image plane.

For the case of a simple parallel displacement of the TV-camera by the vector $\vec{\xi}_A^{(n)}$ to the position A_n, one obtains

$$\vec{\varepsilon} = \frac{z_o}{z_o - d_o}\,\vec{\xi}_A^{(n)} \tag{6}$$

In a general case, the camera will be displaced to an arbitrary position in space, tilted with respect to the z-axis and its focalization may be changed too. The image distortion can then be defined and calculated in a similar way as given above.

Correction of the image distortion by interference phase interpolation

For correct evaluation of the displacement, the measured phase maps in the different images corresponding to different observation directions must be referred to a common reference image.[10]

In a first step, the images are laterally shifted so that the images of the origin O are superimposed. The effect of image distortion is corrected by appropriate interpolation of the phase maps, as shown in Fig.4: ϕ_1 and ϕ_n are the interference phases measured from the observation points A_1 and A_n, respectively. The phase functions are sampled at the grid

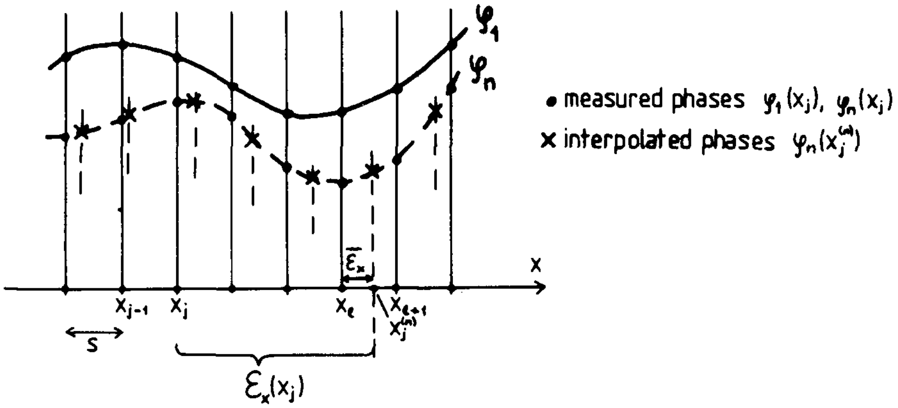

Figure 4. The effects of image distortion are corrected by appropriate interpolation of the interference phases ϕ_n at the common object points.

points $\vec{x}_i$, which are the pixels of the TV-camera. To determine the interference phases $\phi_n(P_i)$ associated with the same common object point P_i, the measured phase values $\phi_n(\vec{x}_i)$ are linearly interpolated at the point $\vec{x}_i^{(n)} = \vec{x}_i + \vec{\varepsilon}^{(n)}(\vec{x}_i)$:

$$\phi_n(\vec{x}_i^{(n)}) \equiv \phi_n(x_j^{(n)}, y_k^{(n)}) = \phi_n(x_l, y_m) + \bar{\varepsilon}_x \frac{\phi_n(x_{l+1}, y_m) - \phi_n(x_l, y_m)}{s} + \bar{\varepsilon}_y \frac{\phi_n(x_l, y_{m+1}) - \phi_n(x_l, y_m)}{s} , \quad (7)$$

where s is the separation of the measured points (spatial resolution of the camera), (x_l, y_m) is a grid point with

$$l = j + \mathrm{int}(\varepsilon_x(\vec{x}_i)/s) , \quad m = k + \mathrm{int}(\varepsilon_y(\vec{x}_i)/s) , \quad (8)$$

and $\bar{\varepsilon}_x$, $\bar{\varepsilon}_y$ are given by

$$\bar{\varepsilon}_x = s\,\mathrm{frac}(\varepsilon_x/s) , \quad \bar{\varepsilon}_y = s\,\mathrm{frac}(\varepsilon_y/s) . \quad (9)$$

int(.) denotes the integer and frac(.) the fractional part of a real number. The interference phase obtained this way can now be used to evaluate the displacement as described above.

Experimental results

All reported experiments have been carried out in two dimensions only, i.e. illumination source, observation points and investigated image points have been restricted to the x/z-plane (cf. Fig.2). Thus the objects were analyzed along a horizontal line only. Furthermore, only objects without (or with constant) displacement components in the y-direction were used. For all experiments, the TV-camera was translated directly behind the hologram and observations were made at three different positions with the coordinates x = 4 cm, 0, -4 cm, respectively. The number of analyzed points was for both objects 230, which corresponds to a spatial resolution of 0.43 mm and 0.61 mm for the investigated areas of 100 mm (tensile test specimen) and 140 mm (cylinder) diameter, respectively.

The expected accuracy for the determination of the displacement vector components depends essentially on the statistical error of the interference phase measurement. The phase error is mainly determined by the speckle noise [1] produced by the interference of the uncorrelated speckle patterns from the overlapping cross-reconstructions. The standard deviation of the statistical phase error is given by $\delta\phi = \sqrt{5/2N}$, where N is the number of speckles within the detector resolution (pixels). Due to the high spatial resolution of the utilized camera (CCD Sony XC-37) and thus the small number of speckles within one pixel, the intrinsic error of the phase measurement was 8° rms. For the accuracy of the displacement vector measurement, one has to distinguish between in-plane (u_i) and out-of-plane (u_o) components. From Eq.(4), one obtains for the two-dimensional case with symmetric illumination and observation

$$\delta u_o = \frac{\lambda}{\sqrt{2}\,(1 + \cos\alpha)} \frac{\delta\phi}{2\pi} , \quad \delta u_i = \frac{\lambda}{\sqrt{2}\,\sin\alpha} \frac{\delta\phi}{2\pi} , \quad (10)$$

where 2α is the angle between the marginal observation directions. For the experimental parameters given above and for a typical object to hologram distance of 70 cm, one obtains the numerical values δu_i = 140 nm and δu_o = 4 nm.

Tensile-test specimen

The aim of this experiment was to demonstrate the capabilities for in-plane displacement and strain measurement. The object (stretched aluminium specimen of 100x20x1 mm^3) was placed parallel to the x-axis at a distance of 50 cm to the TV-camera.

Figure 5(a) shows the interference pattern, Fig.5(b) the interference phases measured for the three observation directions and Fig.5(c) the evaluated displacement vector components u_x and u_z. u_x fits to a linear function, corresponding to a constant in-plane strain ε_{xx}, while u_z indicates a slight bending of the specimen, probably due to a deformation of the object fixation under the load. The absolute phase has been arbitrarily set to zero at the point x = -5 cm (fixed end) for the central observation direction. A change of this absolute phase would essentially produce a shift of the u_z component. Fig.5(d) shows the result of numerical differentiation of the in-plane displacement by fitting a smoothing cubic spline function to the values of u_x and taking the derivatives of the splines. Of course, it is impossible to distinguish between fluctuations due to measurement errors and real strain variations. An estimation of these fluctuations from Fig.5(d) indicates an accuracy for the strain measurement of $\delta\varepsilon$ = 8 μm/m rms. The spatial resolution of this kind of strain determination is determined by the degree of smoothing for the numerical fitting. It has been estimated to be 7mm, i.e. 16 sampling points. The experimentally determined value of $\delta\varepsilon$ is after all in good agreement with a numerical estimation based on the phase error $\delta\phi$, Eq.(10) and the given spatial resolution. Note that the accuracy $\delta\varepsilon$ for the strain would be significantly higher, if derivatives were taken in a two-dimensional field of measured points, because the number of points used for averaging is squared compared to the linear case for the same spatial resolution.

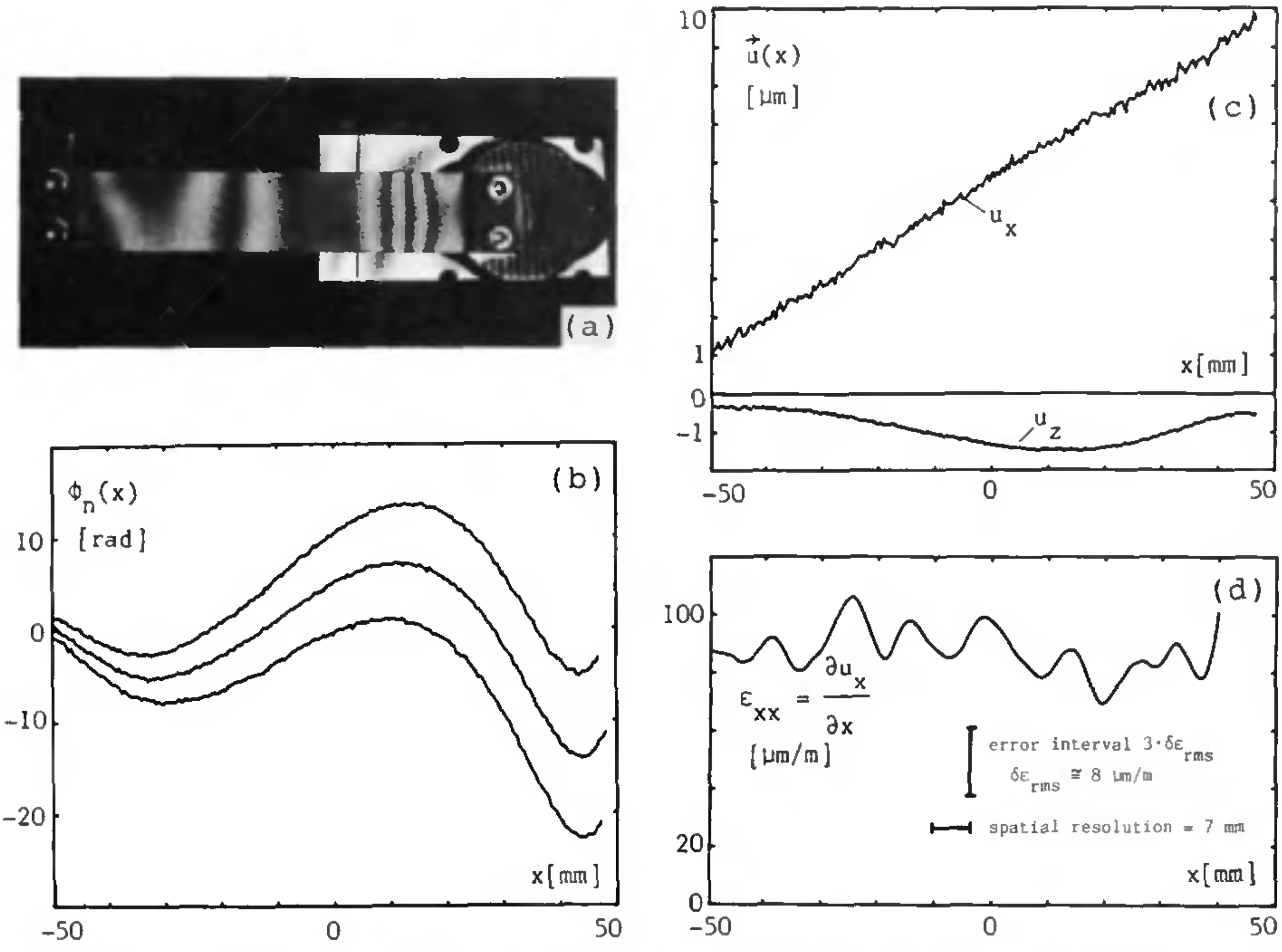

Figure 5. (a) Interference fringes on a tensile test specimen. (b) Interference phases measured from three different observation directions. (c) Evaluated in-plane and out-of-plane displacement vector components u_x and u_z. (d) In-plane strain ε_{xx} calculated by numerical differentiation of the u_x component.

Cylindrical pressure vessel

The second object investigated was a cylindrical aluminium vessel with a radius of R = 20 cm and a 5 mm thick wall, deformed by an internal pressure of about 1 atm. The front surface of the vessel was at a distance of 75 cm from the TV-camera.

Figure 6(a) shows the interference fringe pattern on the object. In Fig.6(b) the displacement vector components radial and tangential to the object surface are plotted, calculated from simulated interference phase data. The solid and dashed lines represent, respectively, the results calculated with and without correction for distortion due to perspective. The necessity of this correction is clearly demonstrated for the defocussed parts of the cylindrical surface: The front of the cylinder (coordinate $x \approx 0$) was in the conjugate image plane, whereas the extreme parts of the evaluated line were 29 mm out of focus (∿4% of the object distance). Figure 6(c) shows the measured radial and tangential components of the displacement, again with (thick line) and without (thin line) correction for the error due to perspective. The radial displacement of about 2 μm corresponds to a surface strain of $\varepsilon_{xx} = \Delta R/R = u_{rad}/R \approx 20$ μm/m.

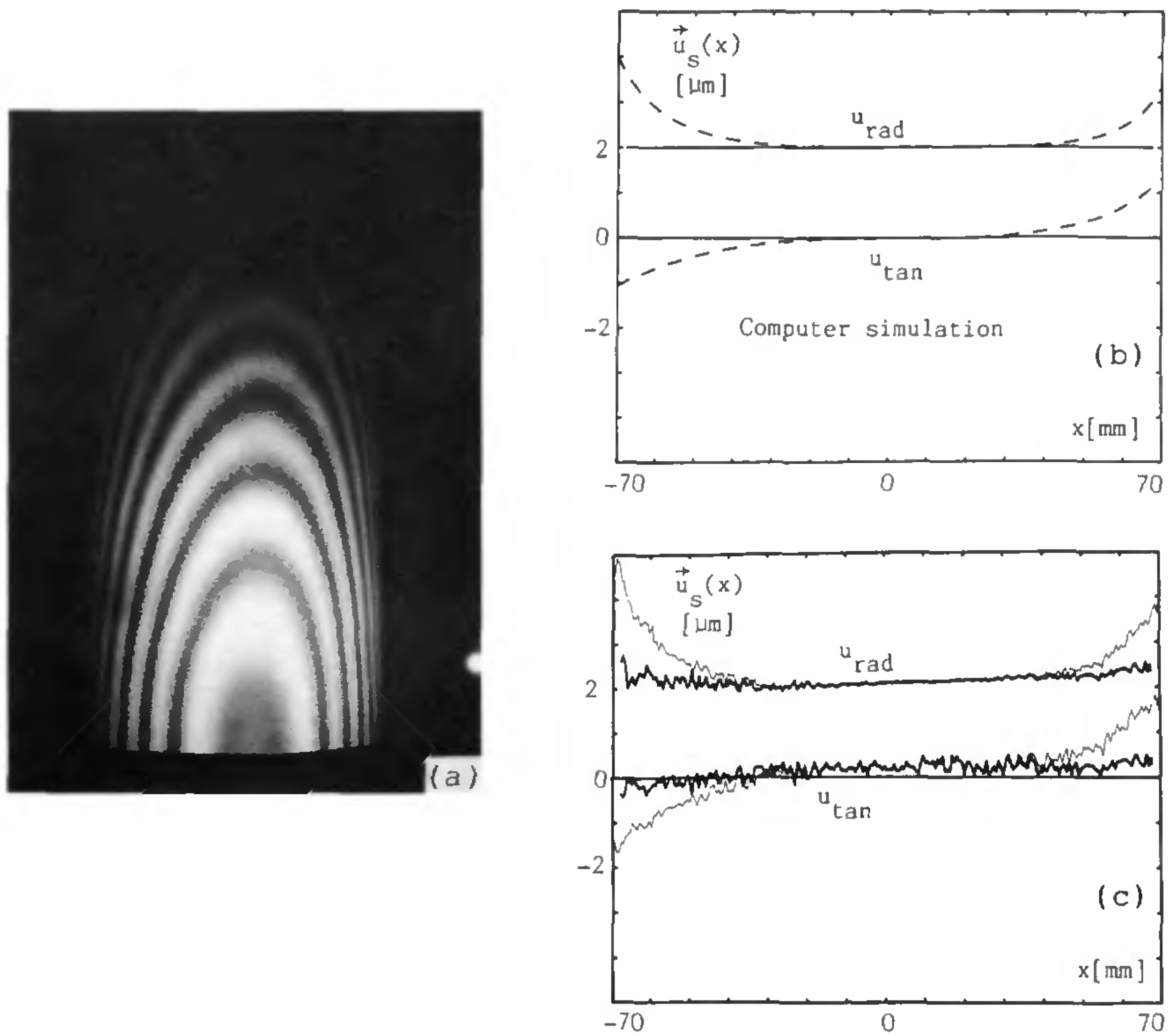

Figure 6. (a) Interference fringes on a cylindrical vessel under internal pressure. (b) Calculated displacement vector components radial and tangential to the object surface, evaluated from simulated interference phases with (solid line) and without (dashed line) correction for distortion due to perspective. (c) Displacements evaluated from measured phase values with (thick line) and without (thin line) correction of perspective.

Conclusions

The theoretical considerations as well as the experimental results show, that an evaluation of the 3-D displacement vector components from only one holographic plate is possible and leads to good results. Quasi-heterodyne fringe interpolation techniques allow the 3-D evaluation even for small changes of observation directions of a few degrees only. The importance and the success of the correction of image distortion due to perspective are clearly demonstrated by computer simulations and experimental results.

This work was supported by the Swiss National Science Foundation.

References

1. Thalmann, R., R. Dändliker, "High Resolution Video-Processing for Holographic Interferometry Applied to Contouring and Measuring Deformations", Proc. of SPIE, Vol. 492, pp. 299-306, 1984.
2. Dändliker, R., R. Thalmann, "Heterodyne and Quasi-Heterodyne Holographic Interferometry", Opt. Eng., Vol. 24, pp. 824-831, 1985.
3. Hariharan, P., B. F. Oreb, N. Brown, "Real-Time Holographic Interferometry: a Microcomputer System for the Measurement of Vector Displacements", Appl. Opt., Vol. 22, pp. 876-880, 1983.
4. Jüptner, W., Th. M. Kreis, M Kreitlow, "Automatic Evaluation of Holographic Interferograms by Reference Beam Shifting", Proc. of SPIE, Vol. 398, pp. 22-29, 1983.
5. Breuckmann, B., W. Thieme, "Computer-Aided Analysis of Holographic Interferograms Using the Phase-Shift Method", Appl. Opt., Vol. 24, pp. 2145-2149, 1985.
6. Hariharan, P., B. F. Oreb, "Two-Index Holographic Contouring: Application of Digital Techniques", Opt. Commun., Vol. 51, pp. 142-144, 1984.
7. Thalmann, R., R. Dändliker, "Holographic Contouring Using Electronic Phase Measurement", Opt. Eng., Vol. 24(6), 1985.
8. Dändliker, R., R. Thalmann, J.-F. Willemin, "Fringe Interpolation by Two-Reference-Beam Holographic Interferometry: Reducing Sensitivity to Hologram Misalignement", Opt. Commun., Vol. 42, pp. 301-306, 1982.
9. Stetson, K. A., "Matrix Methods in Hologram Interferometry and Speckle Metrology", NATO Advanced Study Institute on Optical Metrology, July 1984, Viana de Castelo, Portugal, (NATO ASI Series, Martinus Nijhoff Publishers, The Hague, 1985).
10. Dändliker, R., R. Thalmann, "Determination of 3-D Displacement and Strain by Holographic Interferometry for Non-plane Objects", Proc. of SPIE, Vol. 398, pp. 11-16, 1983.

Reprinted from Journal of the Optical Society of America A, Vol. 3, page 972, July 1986

Statistical properties of interference phase detection in speckle fields applied to holographic interferometry

Ruedi Thalmann and René Dändliker

Institut de Microtechnique de l'Université de Neuchâtel, CH-2000 Neuchâtel, Switzerland

Received November 15, 1985; accepted February 19, 1986

Quantitative evaluation of holographic interferograms requires high-resolution interference phase measurement with heterodyne or quasi-heterodyne methods. The presence of speckles in the interferogram of objects with diffusely scattering surfaces gives rise to a statistical error for the phase measurement. The statistical properties of interference detection in speckled images are theoretically investigated, and the resulting phase errors are rigorously calculated. The mean-square phase error is inversely proportional to the number of detected speckles. In addition, it depends on the decorrelation of the interfering speckle fields, owing to transverse displacement or coherent background. The number of speckles and the phase error are experimentally determined and compared with theory.

1. INTRODUCTION

The interference between laser speckle fields is essentially used in two coherent optical measurement techniques, namely, in speckle interferometry and in holographic interferometry. Applications are deformation analysis of objects with diffusely scattering rough surfaces, detection of refractive-index variations of transparent media placed in front of a diffuse background, and contour fringe generation on rough surfaces. Both techniques, holographic and speckle interferometry, are based on the same principle: the detection of interference between speckle fields in an imaging system. In holographic interferometry the detector integrates over a relatively large number of speckles, whereas in speckle interferometric methods the speckles are chosen large enough to be resolved by the detector. In this paper, the statistical properties of the detection of interference between two (or more) speckle fields are investigated and applied to high-resolution interference phase measurement techniques in holographic interferometry.

The quantitative evaluation of holographic interferograms for displacement and deformation analysis of mechanical objects is quite limited when the classical techniques of locating fringe maxima and minima are used. For better accuracy and automated interferogram detection and processing, interference fringe interpolation methods are required. Electronic phase-shifting techniques such as heterodyne and quasi-heterodyne methods[1-3] offer interference phase measurement with high accuracy and spatial resolution. The phase measurement is independent of fringe position, variations of mean intensity, and fringe contrast in the reconstructed image. In double-exposure holography, a setup with two reference beams gives access to the relative phase between the two reconstructions. During reconstruction, a change of this relative phase permits the fringes in the interferogram to be shifted at will and thus permits the interference phase to be measured by optoelectronic means.

The presence of speckles in the image of objects with diffusely scattering surfaces gives rise to a statistical error for the measured interference phase. The interference of noncorrelated speckles (or noncorrelated parts of speckles) introduces a random contribution into the phase of the mutual intensity of the interfering wave fields. Partial decorrelation of the speckle pattern may be caused by the transverse component of the object displacement. In addition, uncorrelated speckle fields (e.g., resulting from overlapping cross reconstructions or diffusely scattered light from the hologram) may be superimposed upon the desired interfering reconstructions. This source of phase error is of particular importance in quasi-heterodyne holographic interferometry, in which two reference sources that are close together and thus have overlapping reconstructions offer several advantages for the optical setup.[2,3]

In this paper we describe the influence of speckle decorrelation on interference phase measurement. In Section 2, the fundamental statistical properties of the speckle pattern in an imaging system are discussed. Then the detection of intensity in a speckle field with a detector of finite size is investigated. The principle of fringe formation and heterodyning in holographic interferometry is discussed. In Section 3, the statistical errors that are due to the speckle noise in phase measurement with heterodyne detection are rigorously calculated for different situations. In all cases, the resulting phase error depends essentially on the number of speckles within the detector area. Finally, the number of detected speckles and the statistical phase measurement error are experimentally determined with the help of a heterodyne system and compared with theory.

2. SPECKLE STATISTICS FOR COHERENT IMAGE FORMATION

A. Autocorrelation of Amplitude and Intensity

In holographic interferometry, the interferogram is usually observed in the image of the holographically recorded virtual object. The statistical properties of the speckle field in the interferogram will therefore be calculated for an imaging geometry, as sketched in Fig. 1. The imaging lens is placed close behind the holographic plate. The virtual image of the object is reconstructed by one or several reference beams R.

The complex amplitude of the diffused light on the object

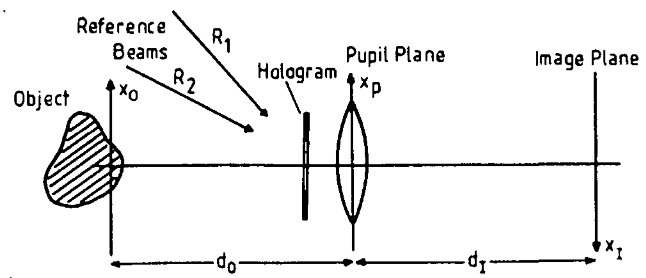

Fig. 1. Image-forming system for the reconstruction of a holographic interferogram.

surface is described by $O(\mathbf{x}_0)\rho(\mathbf{x}_0)$, where $O(\mathbf{x}_0)$ is the amplitude of the object illumination and $\rho(\mathbf{x}_0)$ is a stationary and Gaussian-distributed variable describing the surface roughness.[4] The amplitude in the coherent image of the object reconstruction is then given by the convolution integral[1,4]

$$V(\mathbf{x}_I) = \int d^2x_0 O(\mathbf{x}_0)\rho(\mathbf{x}_0)h(\mathbf{x}_I - \mathbf{x}_0), \qquad (1)$$

where $h(\mathbf{x}_I)$ is the impulse-response function of the imaging system (for the sake of simplicity, the magnification is assumed to be unity), which is essentially given by the Fourier transform of the aperture function of the imaging lens.[1,5]

The detection of the intensity in the coherent image with a detector of finite size involves the calculation of second-order statistics, which relates the statistical properties of different points within the speckle pattern.[1,5,6] For this purpose, the autocorrelation of the amplitude and the intensity in the image are calculated. For the amplitude, one obtains the twofold integral

$$\langle V(\mathbf{x}_I)V^*(\mathbf{x}'_I)\rangle = \iint d^2x_0 d^2x'_0 O(\mathbf{x}_0)O^*(\mathbf{x}'_0) \times \langle \rho(\mathbf{x}_0)\rho^*(\mathbf{x}'_0)\rangle h(\mathbf{x}_I - \mathbf{x}_0)h^*(\mathbf{x}'_I - \mathbf{x}'_0), \qquad (2)$$

where $\langle \cdot \cdot \rangle$ denotes the average over an ensemble of rough surfaces. The object amplitude is assumed to be slowly varying compared with the width of h and will therefore be taken out of the integral in all further calculations. For an object surface with sufficiently fine grain, the autocorrelation of ρ can be approximated by a Dirac function

$$\langle \rho(\mathbf{x})\rho^*(\mathbf{x}')\rangle = \delta(\mathbf{x} - \mathbf{x}'). \qquad (3)$$

So one gets for Eq. (2)

$$\begin{aligned}\langle V(\mathbf{x}_I)V^*(\mathbf{x}'_I)\rangle &\equiv C_V(\mathbf{x}_I, \mathbf{x}'_I) \\ &= |O(\mathbf{x}_0)|^2 \int d^2x_0 h(\mathbf{x}_I - \mathbf{x}_0)h^*(\mathbf{x}'_I - \mathbf{x}_0) \\ &= \langle I(\mathbf{x}_I)\rangle C_h(\Delta\mathbf{x}_I), \qquad (4)\end{aligned}$$

where C_h is the autocorrelation of the impulse-response function h and $\Delta\mathbf{x}_I = \mathbf{x}'_I - \mathbf{x}_I$. $|O(\mathbf{x}_0)|^2$ has been replaced by $\langle I(\mathbf{x}_I)\rangle = \langle V(\mathbf{x}_I)V^*(\mathbf{x}_I)\rangle$, since $C_h(0) = 1$.

The autocorrelation of the intensity is calculated in a similar manner by using the fourfold correlation of the surface roughness

$$\langle \rho(\mathbf{x})\rho^*(\mathbf{x}')\rho(\mathbf{x}'')\rho^*(\mathbf{x}''')\rangle = \delta(\mathbf{x} - \mathbf{x}')\delta(\mathbf{x}'' - \mathbf{x}''') + \delta(\mathbf{x} - \mathbf{x}''')\delta(\mathbf{x}' - \mathbf{x}''). \qquad (5)$$

Thus one gets

$$\langle I(\mathbf{x}_I)I(\mathbf{x}'_I)\rangle = \langle I(\mathbf{x}_I)\rangle\langle I(\mathbf{x}'_I)\rangle + |\langle V(\mathbf{x}_I)V^*(\mathbf{x}'_I)\rangle|^2, \qquad (6)$$

and, with Eq. (4),

$$C_I(\mathbf{x}'_I, \mathbf{x}_I) = \langle I(\mathbf{x}_I)\rangle^2[1 + |C_h(\Delta\mathbf{x}_I)|^2]. \qquad (7)$$

For a circular, binary pupil function of the imaging lens, the autocorrelation function C_h is given by the well-known Airy function[1]

$$C_h(x_I) = 2J_1(\pi x)/(\pi x) = \mathrm{Airy}(\pi x), \qquad (8)$$

where $x = x_I D/\lambda d_I$, D is the diameter of the lens pupil, and d_I is the image distance.

B. Measuring Intensity with a Detector of Finite Size

Normally, the detector for intensity measurement has an area that is much larger than the speckle size. Following Goodman,[6] the detected optical power P can be expressed by the integral of the intensity over the detector surface A_D, viz.,

$$P = \int_D d^2x_I I(\mathbf{x}_I) = \int d^2x_I D(\mathbf{x}_I)I(\mathbf{x}_I), \qquad (9)$$

where $D(\mathbf{x}_I)$ is a binary function representing the detector area, so that

$$\int d^2x_I D(\mathbf{x}_I) = A_D. \qquad (10)$$

The average contrast of the variations (or the reciprocal rms signal-to-noise ratio) of the detected power that is due to the speckle noise is defined as

$$\langle \delta P^2\rangle/\langle P\rangle^2 = (\langle P^2\rangle - \langle P\rangle^2)/\langle P\rangle^2. \qquad (11)$$

The average detected optical power is

$$\langle P\rangle = \int d^2x_I D(\mathbf{x}_I)\langle I(\mathbf{x}_I)\rangle = A_D\langle I\rangle. \qquad (12)$$

The second moment of P becomes

$$\begin{aligned}\langle P^2\rangle &= \iint d^2x_I d^2x'_I D(\mathbf{x}_I)D(\mathbf{x}'_I)\langle I(\mathbf{x}_I)I(\mathbf{x}'_I)\rangle \\ &= \int d^2\Delta x_I C_D(\Delta\mathbf{x}_I)C_I(\Delta\mathbf{x}_I), \qquad (13)\end{aligned}$$

where $C_D(\mathbf{x}_I)$ is the autocorrelation of the detector function $D(\mathbf{x}_I)$. Assuming the function $D(\mathbf{x}_I)$ to be binary and much larger than the speckle size and introducing Eqs. (7) and (12), one obtains

$$\langle P^2\rangle = \langle P\rangle^2\left[1 + \int d^2x|C_h(x)|^2/A_D\right]. \qquad (14)$$

The integral in Eq. (14) can be interpreted as the average area of a speckle correlation cell. This leads to the definition of the number of speckles N within the detector surface A_D[1,6], viz.,

$$N = A_D\Big/\int d^2x|C_h(x)|^2. \qquad (15)$$

With Eqs. (11), (14), and (15), the mean-square variation of the detected optical power is now found to be

$$\langle \delta P^2\rangle/\langle P\rangle^2 = 1/N. \tag{16}$$

For a binary aperture of the imaging lens one gets

$$\int d^2x|C_h(x)|^2 = (\lambda d_I)^2/A_P, \tag{17}$$

where d_I is the image distance and A_P is the area of the lens aperture. The number of speckles N can now be expressed in terms of the F-number of the lens as

$$N = A_D\pi(f/2\lambda F d_I)^2. \tag{18}$$

A reasonable definition for the average speckle size $(\Delta x)_s$ is obtained from the integral in Eq. (17), if one sets the value of this integral equal to the surface of a small disk with diameter $(\Delta x)_s$. For a circular lens aperture of diameter D one gets

$$(\Delta x)_s = (4/\pi)(\lambda d_I/D). \tag{19}$$

C. Interference Fringe Formation

In double-exposure holographic interferometry of diffusely scattering objects,[1,7] two object states (before and after deformation) are recorded holographically. According to Eq. (1), the complex amplitudes V_1 and V_2 of the two object reconstructions in the image are given by

$$V_k(\mathbf{x}_I) = \int d^2x_0 O_k(\mathbf{x}_0)\rho_k(\mathbf{x}_0)\exp\{i[\omega t + \phi_k(\mathbf{x}_0)]\}h(\mathbf{x}_I - \mathbf{x}_0), \tag{20}$$

where ω is the circular frequency of the optical wave. The deformation of the object between the two states 1 and 2 is described by the displacement vector field $\mathbf{u}(\mathbf{x}_0)$. The object illumination O_2 can thus be expressed in terms of O_1 by $O_2(\mathbf{x}_0) = O_1(\mathbf{x}_0 + \mathbf{u}_I)$, where $\mathbf{u}_I$ is the in-plane component of the displacement vector. The interference phase $\phi = \phi_1 - \phi_2$ is related to the object displacement by $\phi = \mathbf{g}\cdot\mathbf{u}$,[7] where $\mathbf{g}$ is the sensitivity vector that is determined by the geometry of object illumination and observation. For the interference phase measurement, the ac part of the intensity $|V_1 + V_2|^2$ is of interest; this is given by the complex interference term $V_1V^*_2$, also called mutual intensity I_{12}:

$$\begin{aligned} I_{12} = V_1(\mathbf{x}_I)V^*_2(\mathbf{x}_I) = \iint d^2x_0 d^2x'_0 O(\mathbf{x}_0)O^*(\mathbf{x}'_0) \\ \times \exp[i\phi(\mathbf{x}_0)]\rho(\mathbf{x}_0)\rho^*(\mathbf{x}'_0) \\ \times h(\mathbf{x}_I - \mathbf{x}_0)h^*(\mathbf{x}_I - \mathbf{x}'_0 + \mathbf{u}_I). \end{aligned} \tag{21}$$

Assuming again that $O(\mathbf{x}_0)$ and also $\phi(\mathbf{x}_0)$ are approximately constant within the width of h, one obtains for the mean mutual intensity

$$\langle I_{12}(\mathbf{x}_I)\rangle = \langle I(\mathbf{x}_I)\rangle\exp[i\phi(\mathbf{x}_I)]C_h(\mathbf{u}_I), \tag{22}$$

where $\langle I_1\rangle = \langle I_2\rangle = \langle I\rangle$. Equation (22) shows that the real part of the complex interference term depends sinusoidally on the interference phase $\phi(\mathbf{x})$ that gives rise to the fringe pattern in the image. $C_h(u_I)$ describes the magnitude of the interference term and thus the visibility (or contrast) of the fringes. Figure 2 shows the measured interference fringe contrast in a holographic interferogram recorded with two reference beams versus mutual in-plane displacement of the two interfering wave fields (cf. Appendix A and Ref. 2). The

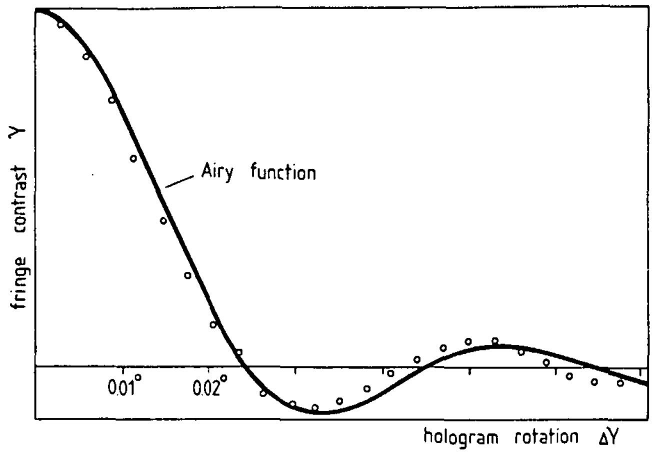

Fig. 2. Measured interference fringe contrast versus speckle decorrelation resulting from mutual in-plane displacement of two interfering speckle fields. The in-plane displacement is produced by hologram misalignment (rotation $\Delta\gamma$ around the hologram normal axis) in two-reference-beam holography.

solid line is the Airy function [Eq. (8)] that fits the experimental results. For in-plane displacements u_I comparable to the speckle size, the fringe visibility $C_h(u_I)$ vanishes. This effect can also be interpreted as delocalization of the interference fringes.[7]

D. Heterodyne Holographic Interferometry

In heterodyne holographic interferometry, the two object waves are recorded with different reference beams R_1 and R_2 (Fig. 1).[8] During reconstruction with both references simultaneously, the optical frequency ω of one of the two reference beams is shifted [e.g., with the help of acousto-optical modulators (AOM's)]. The mutual intensity is now varying sinusoidally at the beat frequency $\Delta\omega = \omega_1 - \omega_2$:

$$I_{12}(\mathbf{x}_I, t) = \exp(i\Delta\omega t)I_{12}(\mathbf{x}_I). \tag{23}$$

When the intensity in the interferogram is detected the interference phase can be measured electronically with high accuracy as the phase of a periodic signal, independently of local variations of the mean intensity and the fringe contrast.[1,3]

3. CALCULATION OF THE EXPECTED INTERFERENCE PHASE ERROR

A. Superposition of Two Wave Fields

First, the situation of two interfering wave fields shall be considered, as is the case in two-reference-beam holographic interferometry for well-separated reference sources.[1,2] The mutual intensity I_{12} is detected by an ac-coupled photodetector at the heterodyne frequency. The detector is averaged over many speckles, i.e., its surface is much larger than the average speckle size [cf. Eq. (9)]. The detected optical power is

$$\langle P_{12}\rangle = \int d_2x_I D(\mathbf{x}_I)\langle I_{12}(\mathbf{x}_I)\rangle. \tag{24}$$

The interference of noncorrelated speckles (or noncorrelated parts of speckles) gives rise to a random contribution to the phase of the complex mutual intensity I_{12}. The decorrelation of the two speckle patterns is due to the in-plane object displacement u_I. Since the detector averages over only a finite number of speckles, P_{12} differs from the (true) ensemble average $\langle P_{12}\rangle$ (cf. Fig. 3). The statistical phase measurement error that is due to the speckle noise can be calculated from the fluctuations of the detected power P_{12}. Assuming an average interference phase of $\langle\phi(\mathbf{x}_I)\rangle = 0$, $\delta\phi$ can be approximated by

$$\delta\phi \simeq \tan\delta\phi = \frac{\mathrm{Im}(P_{12})}{\mathrm{Re}(P_{12})} = \frac{\mathrm{Im}(P_{12})}{\langle P_{12}\rangle + \mathrm{Re}(P_{12} - \langle P_{12}\rangle)} \simeq \frac{\mathrm{Im}(P_{12})}{\langle P_{12}\rangle}. \quad (25)$$

Note that this approach is valid only if the correlated part in P_{12} is much greater than the uncorrelated part, i.e., if there are enough speckles within the detector area.

For the mean-square value of $\delta\phi$ one gets

$$\langle\delta\phi^2\rangle = \frac{\langle \mathrm{Im}^2(P_{12})\rangle}{\langle P_{12}\rangle^2} = \frac{1}{2}\frac{\langle |P_{12}|^2\rangle - \langle P_{12}{}^2\rangle}{\langle P_{12}\rangle^2}, \quad (26)$$

where we have assumed that $\langle I_{12}{}^2\rangle = \langle I_{12}^{*2}\rangle$, which is true for a real-valued autocorrelation function C_h.

The averages $\langle P_{12}\rangle$, $\langle P_{12}{}^2\rangle$, and $\langle |P_{12}|^2\rangle$ can now be evaluated with the help of the fundamentals presented in Section 2. $\langle P_{12}\rangle$ is obtained from Eq. (24) with Eq. (22) as

$$\langle P_{12}\rangle = \iint \mathrm{d}^2x_I D(\mathbf{x}_I)\langle I_{12}(\mathbf{x}_I)\rangle = A_D\langle I\rangle C_h(\mathbf{u}_I). \quad (27)$$

As in Eqs. (13) and (22), one gets

$$\langle P_{12}{}^2\rangle = \iint \mathrm{d}^2x_I\mathrm{d}^2x'_I D(\mathbf{x}_I)D(\mathbf{x}'_I)\langle I_{12}(\mathbf{x}_I)I^*{}_{12}(\mathbf{x}'_I)\rangle$$
$$= \int \mathrm{d}^2\Delta x_I C_D(\Delta\mathbf{x}_I)\langle I\rangle^2[C^2{}_h(\mathbf{u}_I) + C_h(\Delta\mathbf{x}_I + \mathbf{u}_I)C_h(\Delta\mathbf{x}_I - \mathbf{u}_I)] \quad (28)$$

and

$$\langle |P_{12}|^2\rangle = \int \mathrm{d}^2\Delta x_I C_D(\Delta\mathbf{x}_I)\langle I\rangle^2[C_h{}^2(\mathbf{u}_I) + C_h(\Delta\mathbf{x}_I)C_h(-\Delta\mathbf{x}_I)]. \quad (29)$$

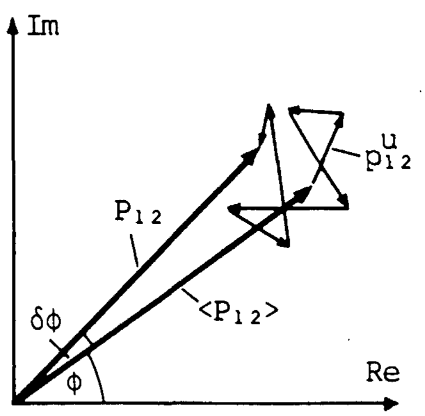

Fig. 3. Interference phase measurement error resulting from speckle noise. The power $p_{12} = p_{12}{}^c + p_{12}{}^u$ within each speckle is composed of a correlated and an uncorrelated part. The total detected power $P_{12} = \sum p_{12}$ differs from the (true) ensemble average $\langle P_{12}\rangle = \sum p_{12}{}^c$ and thus gives rise to the phase error $\delta\phi$.

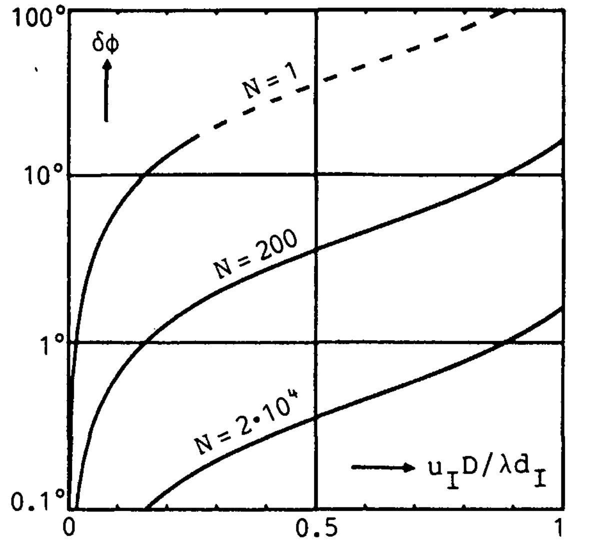

Fig. 4. Statistical phase error $\delta\phi$ for two interfering speckle fields versus normalized in-plane speckle decorrelation $u = u_I D/\lambda d_I$ for different numbers of speckles N within the detector area.

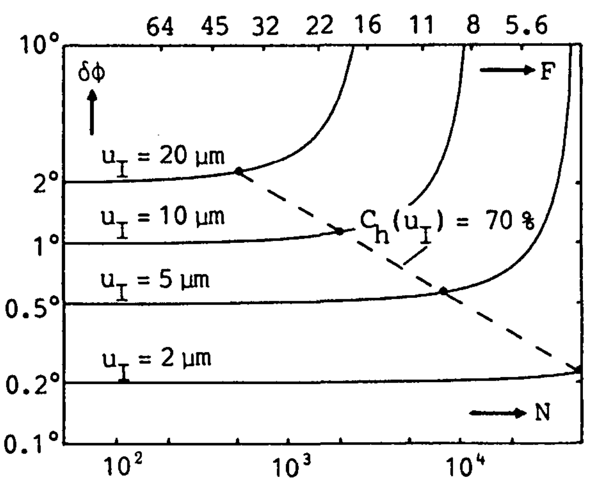

Fig. 5. Statistical phase error $\delta\phi$ versus number N of detected speckles for different in-plane displacements u_I. (Detector area A_D = 1 mm².)

From Eqs. (26), (28), and (29), one finds with Eq. (15) that

$$\langle \mathrm{Im}^2(P_{12})\rangle = (1/2)\int \mathrm{d}^2\Delta x_I C_D(\Delta\mathbf{x}_I)\langle I\rangle^2[C_h{}^2(\Delta\mathbf{x}_I) - C_h(\Delta\mathbf{x}_I + \mathbf{u}_I)C_h(\Delta\mathbf{x}_I - \mathbf{u}_I)]$$
$$= A_D{}^2\langle I\rangle^2[1 - C_h(2\mathbf{u}_I)]/(2N), \quad (30)$$

and, finally, for the rms phase error that is due to the speckle noise

$$\langle\delta\phi^2\rangle = \frac{1}{2N}\frac{1 - C_h(2u_I)}{C_h{}^2(u_I)}. \quad (31)$$

Figure 4 shows the statistical phase error $\delta\phi$ for two interfering speckle fields as a function of the speckle decorrelation (resulting from transverse displacement) for different number of speckles N within the detector area. For small in-plane displacements u_I, $\delta\phi$ tends to zero.

In Fig. 5, the statistical phase error $\delta\phi$ is plotted versus the number N of detected speckles for different in-plane displacements u_I. Through Eq. (18), the number of speckles is related to the F-number of the imaging lens. The figure shows that, over a wide range, the phase error that is due to the speckle noise for constant u_l does not depend on the lens aperture. The reason for this is that, when the lens aperture is closed, the reduction of the number of speckles, which increases the phase error [Eq. (31)], is compensated for by the increase of the average speckle size (and thus the fringe contrast), which reduces the phase error. For a given maximum in-plane displacement u_l, the optimum choice for the F-number (minimum phase error and brightest-possible image) is determined by the bend of the curves (dashed line in Fig. 5). The overall fringe contrast should therefore be better than approximately 70%.

B. Superposition of an Uncorrelated Background

A coherent background speckle field superimposed upon the two interfering wave fields introduces additional errors into the phase measurement. Such a background may be caused by scattering from the hologram plate or by overlapping cross reconstructions. It is assumed that this background consists of two uncorrelated speckle fields V_3 and V_4 at the optical frequencies ω_1 and ω_2, respectively, and that it has a relative amplitude A with respect to the two interfering fields V_1 and V_2. The total amplitude in the image then becomes

$$V(t) = V_1 \exp(i\omega_1 t) + V_2 \exp(i\omega_2 t) + A[V_3 \exp(i\omega_1 t) + V_4 \exp(i\omega_2 t)]. \qquad (32)$$

Since V_3 and V_4 are supposed to be generated by a diffusing surface and to pass through the same lens aperture of the imaging system as V_1 and V_2, they also follow the same speckle statistics.

The mutual intensity I_m, i.e., the ac part of the intensity $I = |\sum_k V_k|^2$ at the heterodyne frequency $\Delta\omega = \omega_1 - \omega_2$, is now given by

$$I_m = V_1 V^*_2 + A V_1 V^*_4 + A V_3 V^*_2 + A^2 V_3 V^*_4. \qquad (33)$$

A calculation of all significant integrals appearing in Eq. (26) leads finally to the statistical phase error

$$\langle \delta\phi^2 \rangle = \frac{1}{2N} \frac{1 + 2A^2 + A^4 - C_h(2u_l)}{C_h^2(u_l)}. \qquad (34)$$

In contrast to the case of Subsection 3.A, the minimum phase error (for $u_l = 0$) is not zero but rather

$$\langle \delta\phi^2 \rangle_{\min} = (2A^2 + A^4)/2N. \qquad (35)$$

C. Reference Sources Close Together: Superposition of Four Correlated Wave Fields

As mentioned above, the optical setup for heterodyne holographic interferometry requires two reference beams. The use of two reference sources that are close together offers some advantages, especially in quasi-heterodyne holographic interferometry: The repositioning sensitivity of the hologram plate is drastically reduced, and for stepwise phase shifting the interference phase can be efficiently stabilized.[2,3] The disadvantage of having the reference sources close together is that all four primary reconstructions are superposed,[2,8] namely, the two desired interfering reconstructions $V_1 = R_1R^*_1O_1$ and $V_2 = R_2R^*_2O_2$ and the two unwanted cross reconstructions $V_3 = R_2R^*_1O_1$ and $V_4 = R_1R^*_2O_2$. Figure 6 shows the four reconstructions on a television (TV) monitor of a double-exposure hologram of a bent cantilever beam for (a) well-separated reference sources and (b) reference sources close together with overlapping cross reconstructions. The intensity profiles generated by a video analyzer show the reduction of the fringe contrast by a factor of 2 because of the superimposed cross reconstructions.

For the calculation of the corresponding statistical phase error in case of reference sources that are very close together, the speckle patterns of the overlapping reconstructions cannot be considered to be completely uncorrelated, as was assumed in the preceding subsection. Each of the four wave fields V_k is described by Eq. (20) and the relations

$$O_2(\mathbf{x}_0) = O_1(\mathbf{x}_0 + \mathbf{u}_l), \qquad (36a)$$

$$O_3(\mathbf{x}_0) = O_1(\mathbf{x}_0 - \mathbf{v}_l), \qquad (36b)$$

$$O_4(\mathbf{x}_0) = O_2(\mathbf{x}_0 + \mathbf{v}_l) = O_1(\mathbf{x}_0 + \mathbf{u}_l + \mathbf{v}_l). \qquad (36c)$$

$\mathbf{v}_l$ denotes the lateral shift of the image that is due to reconstruction with the wrong reference.[8,9] The mutual intensity is again given by Eq. (33).

After the calculation of the numerous cross-correlating terms, one finds for the statistical phase error of the detected signal containing N speckles that

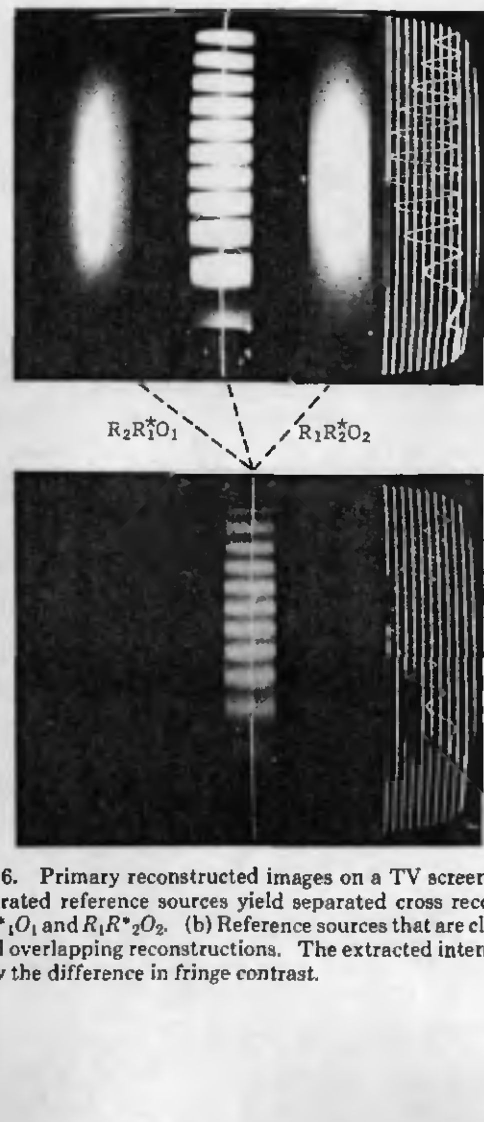

Fig. 6. Primary reconstructed images on a TV screen. (a) Well-separated reference sources yield separated cross reconstructions $R_2R^*_1O_1$ and $R_1R^*_2O_2$. (b) Reference sources that are close together yield overlapping reconstructions. The extracted intensity profiles show the difference in fringe contrast.

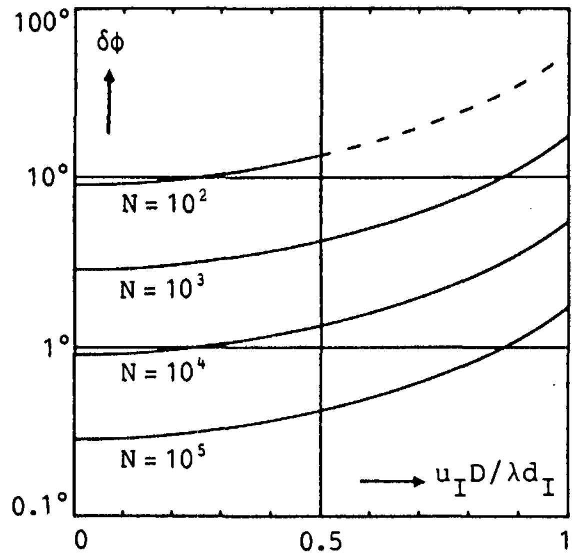

Fig. 7. Statistical phase error $\delta\phi$ versus normalized in-plane displacement for overlapping cross reconstructions.

$$\begin{aligned}\langle\delta\phi_2\rangle = [&6 + 8C_h(v_I) + 2C_h(2v_I) - 4C_h(2u_I + v_I)\\ &- 6C_h(2u_I + 2v_I) - 4C_h(2u_I + 3v_I)\\ &- C_h(2u_I + 4v_I) - C_h(2u_I)]\\ &\times \{2N[C_h(u_I) + 2C_h(u_I + v_I) + C_h(u_I + 2v_I)]^2\}^{-1}.\end{aligned} \tag{37}$$

Assuming that v_I is much larger than the speckle size $(\Delta x)_s$, all terms of C_h containing v_I can be neglected, and Eq. (37) can be rewritten as

$$\langle\delta\phi^2\rangle = \frac{1}{2N}\frac{6 - C_h(2u_I)}{C_h{}^2(u_I)}. \tag{38}$$

Again, the minimum error for $u_I = 0$ has a finite value, namely,

$$\langle\delta\phi^2\rangle = 5/2N. \tag{39}$$

Figure 7 shows the $\delta\phi$ of Eq. (38) versus the normalized in-plane displacement for different number of speckles N.

In the calculation of the phase error to get Eq. (37), the following term appears in the numerator:

$$\int d^2\Delta x_I C_D(\Delta \mathbf{x}_I) C_h{}^2(\Delta \mathbf{x}_I - \mathbf{v}_I). \tag{40}$$

For the evaluation of this integral, it has been assumed that the diameter of the detector is much larger than the width of C_h. For small v_I (reference sources very close together), this integral becomes $A_D{}^2/N$ [cf. Eq. (15)]. However, if v_I is larger than the detector diameter, this integral becomes zero. For the phase error $\delta\phi$ one then obtains

$$\langle\delta\phi^2\rangle = \frac{1}{2N}\frac{4 - C_h(2u_I)}{C_h{}^2(u_I)}, \tag{41}$$

which is exactly the same result as the one given by Eq. (34) for $A = 1$. This means that, if the corresponding speckle patterns of the overlapping cross reconstructions are laterally shifted by more than the detector aperture, they appear to be completely uncorrelated.

4. EXPERIMENTAL RESULTS

A. Experimental Setup and Concept of Phase-Error Measurement

The optical setup is sketched in Fig. 8. It is a classical arrangement with two reference sources for heterodyne holographic interferometry. The two references can be well separated (R_1 and R_2) or be close together (R'_1 and R_2). The AOM's introduce a frequency shift between the two references of $\Delta\omega/2\pi = 100$ kHz. The interferogram is observed in the image obtained with a $f/5.6$ Rodenstock repro lens of $f = 300$ mm. The interference phase is detected with the help of a twin detector consisting of two fiber bundles, each 1 mm in diameter, with their ends 3 mm apart in the image plane, that lead the light to two photomultipliers. The electronic signals are filtered at 100 kHz with a bandwidth of 10 kHz. Finally, the phase between the two signals is measured by a phasemeter with 0.1° resolution.

The phase error $\delta\phi$ is theoretically defined by the variance of the phase values observed at one point in the interferogram for different speckle patterns, i.e., for different states of the surface roughness. Of course, in practice it is not possible to determine the phase error this way. So interference phase differences $\Delta\phi_k$ between twin detectors (two fiber bundles) were measured at n different places in an interferogram with constant phase (no fringes, double-exposure hologram of a nondeformed object). From these measurements, the variance is calculated to obtain the rms error by

$$\delta\phi_{\exp} = \frac{1}{\sqrt{2}}\delta(\Delta\phi) = \left[\frac{\sum_{k=1}^{n}\Delta\phi_k{}^2 - \frac{1}{n}\left(\sum_{k=1}^{n}\Delta\phi_k\right)^2}{2(n-1)}\right]^{1/2}. \tag{42}$$

The factor $\sqrt{2}$ appears because the phase difference $\Delta\phi$ is the result of two independent phase measurements. The displacement of the twin detector between two consecutive measurements had to be kept small enough to avoid a systematic drift of the average phase difference. A shift of about 0.1 mm, i.e., 1/10 of the detector diameter, produced sufficiently independent statistical values. To determine the rms value, the phase was measured at 50 different positions. The temporal noise of interference phase measure-

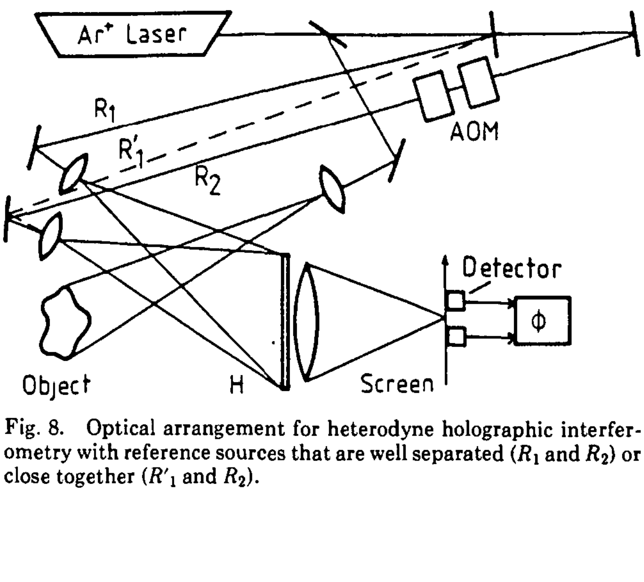

Fig. 8. Optical arrangement for heterodyne holographic interferometry with reference sources that are well separated (R_1 and R_2) or close together (R'_1 and R_2).

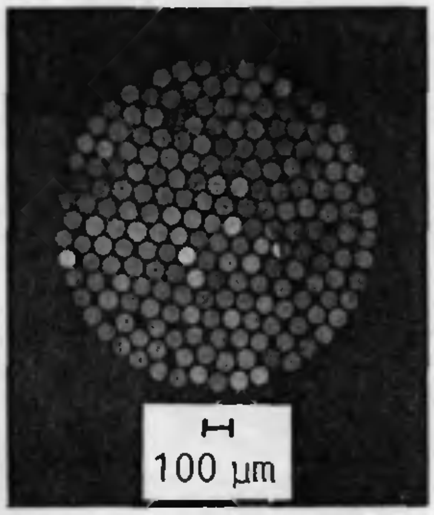

Fig. 9. Cross section of the fiber-bundle detector surface.

ment in heterodyne holographic interferometry is extensively discussed in Ref. 1. In the present experiment, the rms value of these fluctuations was found to be about 0.1°. This value was further reduced by taking the average over 20 measurements at each position to obtain $\Delta\phi_k$.

For an estimation of the reliability of the phase-error measurement, different factors have to be considered. As mentioned above, the second source of error of statistical nature, namely, the temporal noise, could be kept lower than 0.1°. The fact that the phases must be measured within an area of constant mean interference phase limits the number of independent phase measurements, because air turbulence always slightly changes the wave front of the object light between the two exposures of the hologram. The statistical uncertainty of the error determination can be estimated if the measured quantity (interference phase) is assumed to be Gaussian distributed. Then the relative variance $\sigma_{\delta\phi}$ of the error $\delta\phi$ depends on the number n of measurements as follows:

$$\sigma_{\delta\phi}/\delta\phi = 1/\sqrt{2n}. \tag{43}$$

In our case this means, for 50 measurements, an uncertainty of 10%. The observed reproducibility of the error determination did depend strongly on the experimental parameters, but 20% can be indicated as a typical value.

B. Number of Speckles within the Detector Area

To compare the measurements of the phase error $\delta\phi$ with the theoretically expected values, the number N of speckles within the detector area should be known exactly. The detector area is given by the cross section of the fiber bundle (Fig. 9), which consists of about 200 fibers, each with a diameter of 65 μm. This corresponds to a total detector surface of $A_D = 0.664$ mm^2.

The number N of speckles within A_D was determined in the following two ways:

(1) *Determination of the Speckle Surface.* The number N of speckles covered by the detector can be defined by the ratio of the detector area A_D and the surface of one speckle correlation cell [cf. Eq. (15)]. For a circular binary aperture of the imaging system, the integral over the autocorrelation C_h can be calculated, and the number of speckles can be directly expressed in terms of the F-number of the imaging lens [Eq. (18)]. If the aperture function of the lens is not well defined or if the F-number is not known exactly, the autocorrelation function C_h can be experimentally determined (cf. Fig. 2 and Appendix A).

In the present experimental setup, the measured width of $C_h(x_I)$ corresponds very well to the values obtained from the F-number of the imaging lens. For a lens with $f = 300$ mm and $F = 5.6$, 1:1 imaging, and $\lambda = 514$ nm, the speckle size $(\Delta x)_s$, as defined in Eq. (19), is found to be 7.4 μm. This yields for the detector shown in Fig. 9 a number of $N = 15700$ speckles within the detector area.

(2) *Determination of the Number of Statistically Independent Correlation Cells.* In principle, the number N of detected speckles can also be determined from the noise-to-signal ratio of the intensity measurement in the speckle field [cf. Eq. (16)]. But for large speckle numbers N the intensity variations are too small to be measured directly. It is more suitable to measure the fluctuations of the ac signal at the heterodyne frequency, since the ac power can then be measured over a large dynamic range with a spectrum analyzer in logarithmic scale.

W_c and W_u are the electrical ac output power of a detector placed in the interferogram for correlated and uncorrelated superposition of two speckle fields, respectively. It can be shown (cf. Appendix B) that the ratio of W_c and $\langle W_u\rangle$ is equal to the speckle number N within the detector area. In this way, it is possible to determine N without knowing the geometry of the optical setup (image formation system, detector area). The experimental difficulty is to ensure complete speckle decorrelation without significantly changing the experimental conditions with respect to the situation for correlated speckles and to obtain a statistically reliable mean value $\langle W_u\rangle$. From measurements for the detector described and a lens aperture of $F = 5.6$, the power ratio was found to be $\langle W_u\rangle/W_c = -42.6$ dB and thus $N = 18{,}200$.

In spite of the completely different experimental approach, the two methods, (1) and (2), yield within 15% the same result for the number of detected speckles. Because of its simplicity, method (1) has been used to determine the number of speckles in the reported experiments.

C. Phase-Error Measurements for Two Interfering Wave Fields

The statistical phase error $\delta\phi$ for two interfering wave fields (well-separated reference sources) has been measured as a function of the speckle decorrelation for different number of speckles N. The measurements were carried out as described in Subsection 4.A. The speckle decorrelation was realized by hologram misalignment (cf. Appendix A), which produces a mutual shift of the two object reconstructions and thus of the two (identical) speckle fields. Since the mechanical misalignment (rotation) of the hologram plate is too small to be precisely measured, the normalized speckle shift $u = u_I D/\lambda d_I$ is determined for each phase measurement from the actual interference fringe contrast [cf. Eqs. (22) and (8)]: The fringe contrast is normalized with respect to its maximum (typically 90% for perfect hologram alignment) and fitted to the Airy function (Fig. 2) to obtain its argument πu. The measurements are compared with the theoretical values of Eq. (31). The plots in Fig. 10 show the experimental results for the apertures $F = 5.6, 8, 11$, and 16, respectively.

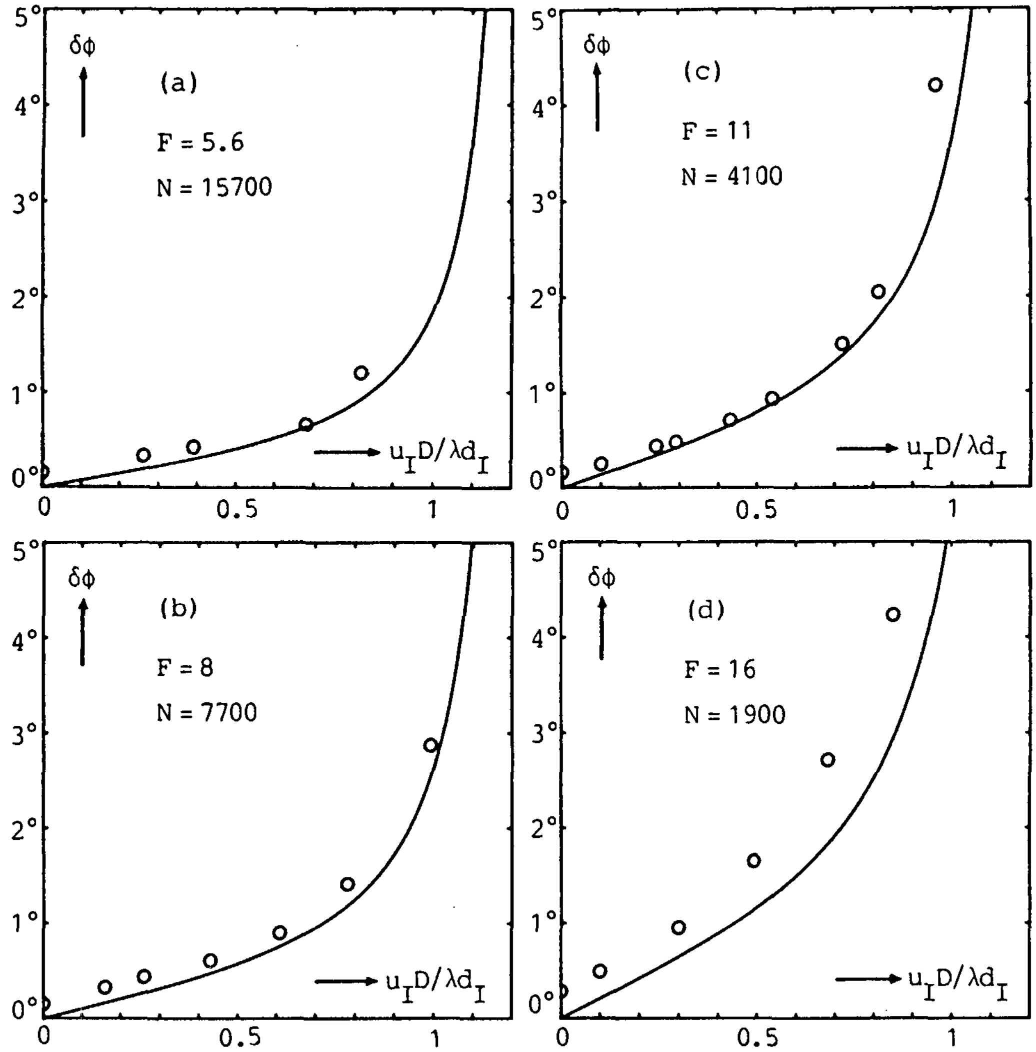

Fig. 10. Experimental verification of the statistical error $\delta\phi$ of phase measurement for two interfering speckle fields versus in-plane displacement u_I. N is the number of detected speckles, and F is the corresponding lens aperture.

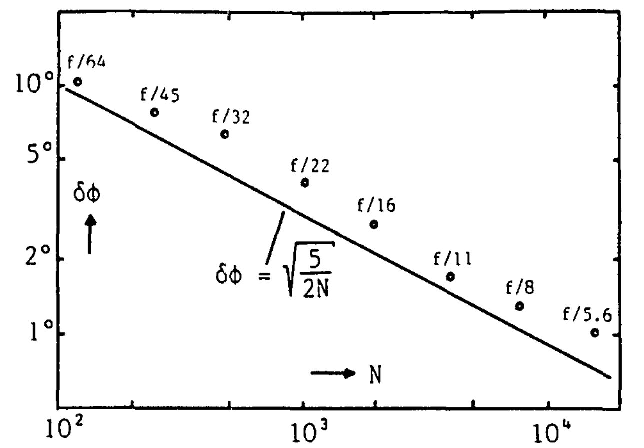

Fig. 11. Minimum statistical phase error $\delta\phi$, owing to speckle noise from overlapping cross reconstructions, is measured for different numbers N of detected speckles (i.e., different F-numbers).

D. Phase-Error Measurements for Overlapping Reconstructions

In the case of overlapping reconstructions, the statistical phase error varies only slowly with speckle decorrelation of the interfering wave fields (cf. Fig. 7). Therefore it was not possible to verify experimentally the theoretical behavior of the phase error versus transverse speckle shift [Eq. (38)]. The minimum value $\delta\phi = \sqrt{5/2N}$ of the phase error was measured for different number of speckles N, i.e., different lens apertures F. The results are shown in Fig. 11. The measured phase errors are systematically larger than the theoretical ones, but the $1/\sqrt{N}$ dependence is well established.

5. CONCLUSIONS

The statistical properties of intensity detection and its impact on interference phase measurement in speckle fields were investigated. The statistical error of the phase measurement that is due to speckle noise was theoretically calculated and experimentally verified for different situations. This error is caused by decorrelation of the interfering speckle patterns because of mutual transverse displacement or because of an additional uncorrelated background. The phase error is essentially proportional to $1/\sqrt{N}$, where N is the number of speckles within the detector area. When the above results are applied to holographic interferometry with high-resolution fringe interpolation, they show that the error that is due to decorrelated speckles is a basic limitation on the accuracy of deformation measurement of solid objects.[10] The phase error is of particular importance in quasi-heterodyne holographic interferometry with reference sources that are close together (overlapping cross reconstructions). This technique has also been applied to displacement and strain measurement.[11]

APPENDIX A

Measurement of the Autocorrelation Function $C_h(\mathbf{x}_I)$

Various statistical properties of a speckle pattern, such as the number of speckles within the detector area and the average speckle size, are based on the autocorrelation of the complex optical amplitude that is, for an imaging system, given by the autocorrelation C_h of the impulse response function h of the optical system [Eq. (4)]. The shape and width of C_h can be experimentally determined in a setup of holographic interferometry with two reference beams.

C_h describes the fringe contrast of two identical interfering speckle fields versus mutual transverse displacement (decorrelation). In holographic interferometry, this transverse speckle shift can be produced in a well-controlled manner, e.g., by misalignment of the hologram plate with respect to the two reference beams. During reconstruction, any rotation of a double-exposure hologram recorded with two different references produces a linear phase $\phi(\mathbf{x}_H)$ in the hologram plane [cf. Eq. (A4) and Refs. 1 and 2]. This phase $\phi(\mathbf{x}_H)$ can be decomposed into a phase $\phi_0(\mathbf{x}_0)$ in the object plane and a phase $\phi_p(\mathbf{x}_p)$ in the pupil plane,[1] where

$$\phi_p(\mathbf{x}_p) = \phi(\mathbf{x}_H)(d_0 - d_H)/d_0 = 2\pi(\mathbf{p}/\lambda)\cdot\mathbf{x}_H(d_0 - d_H)/d_0, \quad \text{(A1)}$$

where d_H is the distance between hologram and pupil plane and d_o is the object distance. The linear phase $\phi(\mathbf{x}_H)$ shows up as parallel fringes on the hologram plate (Fig. 12) and can be described by $(\mathbf{p}/\lambda)$, which is the number of fringes per unit length in the direction of $\mathbf{p}$. As a result of the shift theorem for Fourier transformation, ϕ_p produces in the image a mutual shift $\Delta\mathbf{x}_I$ of the two reconstructions of

$$\Delta\mathbf{x}_I = \mathbf{p}d_I(d_0 - d_H)/d_0 = \mathbf{p}M(d_0 - d_H), \quad \text{(A2)}$$

with the image magnification $M = d_I/d_0$.

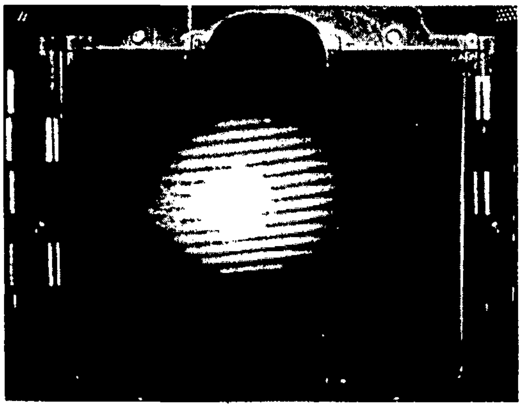

Fig. 12. Interference fringes on the hologram plate resulting from misalignment (rotation) of the hologram with respect to the two reconstructing reference beams.

The fringe contrast as a function of the speckle decorrelation $\Delta\mathbf{x}_I$ is given by [cf. Eqs. (8) and (22)]

$$C_h(\Delta\mathbf{x}_I) = 2J_1(\pi D\Delta\mathbf{x}_I/\lambda d_I)/(\pi D\Delta\mathbf{x}_I/\lambda d_I). \quad \text{(A3)}$$

The hologram can now be misaligned (rotated) until the fringe contrast vanishes completely. The corresponding fringe density $(\mathbf{p}_0/\lambda)$ on the hologram can then be easily measured. If the fringe distance is too large (small F-number), $\mathbf{p}_0$ can be calculated by using the relation[1]

$$\phi(\mathbf{x}_H) = [(\mathbf{k}_2 - \mathbf{k}_1) \times \omega]\cdot\mathbf{x}_H, \quad \text{(A4)}$$

where $\mathbf{k}_1$ and $\mathbf{k}_2$ are the wave vectors of the two reference beams on the hologram and $\omega = (\Delta\alpha, \Delta\beta, \Delta\gamma)$ describes the rotation of the hologram plate. $\mathbf{k}_2 - \mathbf{k}_1 = \Delta\mathbf{k}$ can be measured directly in the optical setup or determined indirectly by the linear phase function $\phi(\mathbf{x}_H)$ measured on the hologram plate for a large rotation angle ω.

For zero contrast of the interference fringes, the argument of the Airy function [Eq. (A3)] produces $\pi \times 1.22$. So one can now calculate the average speckle diameter [Eq. (19)] as

$$(\Delta x)_s = (4/\pi)(\lambda d_I/D) = (4/\pi)\Delta x_I/1.22 = 1.04 p_0 M(d_0 - d_H) \quad \text{(A5)}$$

and the number of speckles within the detector surface A_D by

$$N = A_D/[\pi(\Delta x)_s^2/4]. \quad \text{(A6)}$$

Experimental Results

The number N of detected speckles has been determined in this way for a setup with $d_0 = d_I = 60$ cm ($M = 1$), $d_H = 6.2$ cm, $A_D = 0.664$ mm^2, and $F = 5.6$. To determine the angular separation $\Delta k_x/k$ of the two references (sensitivity to misalignment), the hologram has been rotated by an angle $\Delta\gamma = 0.147°$, which yields $(p/\lambda) = 2.8$ fringes/cm (cf. Fig. 12), and, using Eq. (A4), one gets $\Delta k_x/k = 5.57 \times 10^{-2}$. The interference contrast in the image plane vanishes for a hologram rotation of $\Delta\gamma = 0.0135°$, and thus $p_0 = 1.31 \times 10^{-5}$. So one obtains, with Eqs. (A5) and (A6), $(\Delta x)_s = 7.4$ μm for the speckle diameter in the image plane and $N = 15{,}680$ for the number of speckles. This result corresponds very well to the $N = 15{,}740$ obtained from Eq. (18) for $F = 5.6$.

APPENDIX B

Average AC Power in Correlated and Uncorrelated Speckle Fields

The complex electric ac signal (current) in heterodyne detection of two interfering, frequency-shifted speckle fields for a detector covering N speckles can be written as

$$i(t) = \sum_n P_n \exp[i(\omega t - \phi_n)], \quad \text{(B1)}$$

where P_n is the mean optical power per speckle. If all the contributions $P_n \times \exp(i\phi_n)$ are correlated, the detected electrical ac power becomes

$$W_c = |i(t)|^2 = \sum_{n,m} P_n P_m = N^2 P_n^{\,2}, \quad \text{(B2)}$$

which corresponds to the total optical power on the detector.

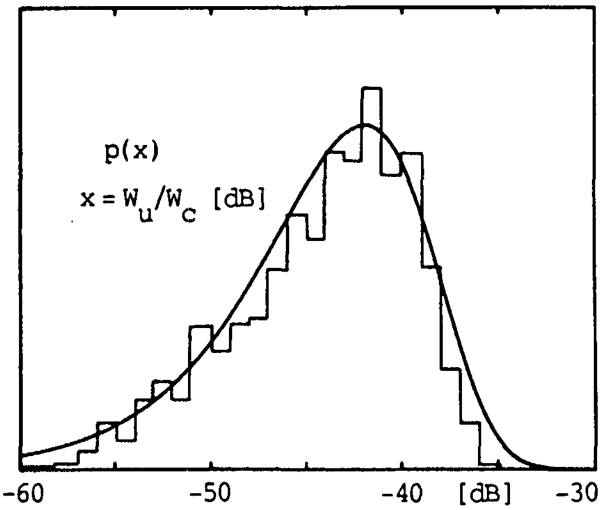

Fig. 13. Probability distribution of the ac power W_u detected from the interference of two uncorrelated, frequency-shifted speckle fields. W_u is represented in logarithmic scale [dB]. The histogram is based on 1000 measured values of W_u for statistically different speckle patterns.

For completely uncorrelated speckle fields, one obtains an average ac power of

$$\langle W_u \rangle = \left\langle \sum_{n,m} P_n P_m \exp[i(\phi_n - \phi_m)] \right\rangle = \sum_n P_n^{\,2} = N P_n^{\,2}. \tag{B3}$$

Thus the ratio of the correlated and the uncorrelated ac power is equal to the number of speckles within the detector area, viz.,

$$W_c / \langle W_u \rangle = N. \tag{B4}$$

Note that this number N of speckles measured in a coherent image is identical to the definition of N given in Eq. (15). This can be easily seen by setting $W = |P_{12}|^2$ for the electrical ac power and then calculating $W_c/\langle W_u \rangle$, using Eq. (29), for correlated ($u_I = 0$) and uncorrelated ($u_I \rightarrow \infty$) superposition of the two speckle fields.

The probability distribution of the uncorrelated ac power was calculated in Ref. 12 as

$$p(W_u) = (1/\langle W_u \rangle)\exp(-W_u/\langle W_u \rangle). \tag{B5}$$

Experimentally, the ac power is measured with a spectrum analyzer in logarithmic scale. Therefore one is interested instead in the probability distribution of W_u[dB] = 10 log ($W_u/\langle W_u \rangle$), which becomes[12]

$$p(x) = \frac{1}{10 \log e}\, 10^{x/10} \exp[-10^{x/10}], \tag{B6}$$

where $x = W_u$[dB]. This function is shown in Fig. 13.

W_c and W_u can be measured by heterodyne holographic interferometry for two situations that are nearly identical, except for the correlation of the speckle fields. A double-exposure hologram of a nondeformed object is recorded with two different reference waves. The ac power W_c is measured in the interferogram at the heterodyne frequency. Then the hologram is considerably misaligned to produce a mutual shift of the two reconstructions that is larger than the detector diameter. Now the two superimposed speckle patterns can be considered to be completely uncorrelated. W_u is measured repetitively, each time slightly changing the hologram position to produce statistically different speckle patterns. A histogram of W_u yields its probability distribution $p(x)$ (cf. Fig. 13). The maximum of $p(x)$, i.e., the most probable value W_u[dB], is equal to the mean value $\langle W_u \rangle$. Using Eq. (B4), the speckle number N can be calculated.

Experimental Results

The number N of speckles has been measured for the same experimental situation described in Appendix A. Figure 13 shows the measured histogram of W_u/W_c[dB] (it represents 1000 measured values of W_u). The mean value $\langle W_u \rangle / W_c$ has been calculated to be -42.6 dB (which yields $N = 18{,}200$) and is in good agreement with the value of $N = 15{,}700$ obtained in Appendix A.

ACKNOWLEDGMENT

This research was supported by the Swiss National Science Foundation.

REFERENCES

1. R. Dändliker, "Heterodyne holographic interferometry," in *Progress in Optics*, E. Wolf, ed. (North-Holland, Amsterdam, 1980), Vol. XVII, pp. 1–84.
2. R. Dändliker, R. Thalmann, and J.-F. Willemin, "Fringe interpolation by two-reference-beam holographic interferometry: reducing sensitivity to hologram misalignment," Opt. Commun. **42**, 301–306 (1982).
3. R. Dändliker and R. Thalmann, "Heterodyne and quasi-heterodyne holographic interferometry," Opt. Eng. **24**(5), 824–831 (1985).
4. S. Lowenthal and H. Arsenault, "Image formation for coherent diffuse objects: statistical properties," J. Opt. Soc. Am. **60**, 1478–1483 (1970).
5. J. W. Goodman, *Introduction to Fourier Optics* (McGraw-Hill, New York, 1968).
6. J. W. Goodman, "Statistical properties of laser speckle patterns," in *Laser Speckle and Related Phenomena*, J. C. Dainty, ed. (Springer-Verlag, Berlin, 1975).
7. C. M. Vest, *Holographic Interferometry* (Wiley, New York, 1979).
8. R. Dändliker, E. Marom, and F. M. Mottier, "Two-reference-beam holographic interferometry," J. Opt. Soc. Am. **66**, 23–30 (1976).
9. R. Thalmann and R. Dändliker, "High resolution video-processing for holographic interferometry applied to contouring and measuring deformations," Proc. Soc. Photo-Opt. Instrum. Eng. **492**, 299–306 (1984).
10. R. Dändliker and B. Eliasson, "Accuracy of heterodyne holographic strain and stress determination," Exp. Mech. **19**, 93–101 (1979).
11. R. Thalmann and R. Dändliker, "Automated evaluation of 3-D displacement and strain by quasi-heterodyne holographic interferometry," Proc. Soc. Photo-Opt. Instrum. Eng. **599** (to be published).
12. J.-F. Willemin, "Interférométrie hétérodyne de speckles: application à la mesure de vibrations mécaniques microscopiques," Ph.D dissertation (University of Neuchâtel, Neuchâtel, Switzerland, 1984), pp. 41–46.

to be published in: Appl. Opt. 26, ...(1987).

STRAIN MEASUREMENT BY HETERODYNE HOLOGRAPHIC INTERFEROMETRY

R. Thalmann and R. Dändliker

University of Neuchatel, Institute of Microtechnology,
CH-2000 Neuchatel, Switzerland

Abstract

Heterodyne holographic interferometry provides automated interference phase measurement with high resolution and allows the quantitative evaluation of 3D displacement and strain on solid objects. The fundamentals of heterodyning in double-exposure holography are reviewed and its possibilities and limitations are discussed in detail. Experimental results of strain measurement on a curved object surface are reported. Three double-exposure hologram recordings with different illuminations are used to get the vector displacement. Based on locally calculated derivatives of the displacement field, a sensitivity for the strain components of 1 μm/m with a spatial resolution of a few millimeters has been achieved. The features of heterodyne holographic interferometry are compared with those of quasi-heterodyne (phase stepping) fringe interpolation.

I. Introduction

The automated and quantitative evaluation of 3D displacement and strain from holographic interferograms requires accurate interference phase measurement independent of fringe position and intensity variations in the reconstructed image. In many interferometric arrangements, the heterodyne technique has become a powerful tool for high resolution interference fringe interpolation. In holographic interferometry, heterodyning has been successfully applied to surface deformation measurements of solid objects [1,2], measurements of phase objects [3] and surface contouring [4].

The aim of this paper is to demonstrate the performance and the theoretical and experimental limits of surface strain measurement by heterodyne holographic interferometry. After a brief introduction into the principle of heterodyning, the experimental arrangement is described. Then, the numerical evaluation of 3D displacement and strain from the holographic interferogram is explained. The limitations for the accuracy of the interference phase measurement are investigated in detail. Experimental results are reported for the determination of surface rotation and strain with double-exposure holography using a setup with three different illumination beams. Finally, the different methods of electronic fringe interpolation in holographic interferometry are compared and their fields of application are outlined.

II. Principle of heterodyne holographic interferometry

The application of the heterodyne technique in double-exposure holographic interferometry requires a setup with two reference beams [5] in order to have independent access to the relative phase between the two interfering reconstructions, which allows to shift the fringes in the interferogram. The two states of the mechanical object (before and after deformation), which shall be investigated by double-exposure holography, are recorded consecutively each with another reference wave on the same hologram plate. The simultaneous reconstruction with both reference beams yields four primary reconstructed images, the two desired interfering self-reconstructions and the two undesired cross-reconstructions [5]. To avoid disturbing overlapping of the different reconstructions, the two reference sources must be chosen on the same side of the object, with a mutual separation larger than the angular size of the object in the corresponding direction.

During reconstruction, the relative phase between the two references is shifted linearly in time by introducing an offset $\Delta\omega$ to the optical frequency in one of the two reference beams. Assuming that the two wavefields to be compared are given by

$$V_k(\vec{x}) = a_k(\vec{x}) \cos[\omega_k t + \phi_k(\vec{x})] \ , \tag{1}$$

the local intensity of their superposition becomes

$$I(\vec{x}) = |V_1 + V_2|^2 = a(\vec{x}) \{ 1 + m(\vec{x}) \cos[\Delta\omega t + \phi(\vec{x})] \} \ , \tag{2}$$

where $a(\vec{x})$ is the local mean intensity, $m(\vec{x})$ is the fringe contrast, and $\phi(\vec{x}) = \phi_1(\vec{x}) - \phi_2(\vec{x})$ is the phase difference of the two wavefields. Due to the optical frequency offset $\Delta\omega = \omega_1 - \omega_2$ during reconstruction, the superposition intensity is time dependent and the interference phase $\phi(\vec{x})$ can be detected as the phase of the beat frequency signal. Since the beat frequency $\Delta\omega/2\pi$ is chosen low enough (<100 MHz) to be resolved by the opto-electronic detector employed, the interference phase can be measured with high accuracy, independently of variations of the mean intensity and the fringe contrast, using an electronic phasemeter. This way, both the interpolation problem and the sign ambiguity of classical interferometry are solved.

III. Experimental arrangement

The experimental arrangement for double-exposure heterodyne holographic interferometry, as it has been used in the experiments reported here, is sketched in Fig.1. The setup is essentially based on the one described in Ref.1. The frequency difference $\Delta\omega/2\pi$ of 100 kHz between the two reference beams is realized by two commercially available acousto-optical modulators (AOM) in cascade to give opposite frequency shifts. During recording, both modulators are driven with 40 MHz, so that the net shift is zero. During reconstruction, one modulator is driven with 40 MHz and the other with 40.1 MHz, so that the net shift is the desired beat frequency of 100 kHz.

The interferogram is observed in the 1:1 image of the virtual object obtained with an f/5.6, f = 300 mm Rodenstock repro lens. The interference phase is determined by scanning an array of three detectors which measures the phase differences in two orthogonal directions in the image plane. The total phase $\phi(\vec{x})$ can be obtained afterwards by approriate integration. The detector array is realized by the ends of three fiber bundles, which feed the light to photomultiplier tubes. The beat frequency signals at 100 kHz are filtered with a bandwidth of 10 kHz, and the amplitudes are kept constant, independent of the intensity variations across the image, by a feedback control of the photomultiplier supply voltage. The phase differences between the detected signals are measured with zero-crossing phasemeters, which interpolate the phase angles to 0.1° and also count the multipes of 360° (fringe number). Note, that all electronic amplifiers and filters in the signal path should be carefully designed to avoid phase distortion that could reduce the accuracy of the phase measurement [6]. The detector array is mounted on a stepper motor driven stage to scan the image. Scanning and data acquisition is automated and computer controlled. The measuring time for one position, including the displacement of the detector head, is about 1 sec.

For the determination of vector displacement and strain, the interference phase caused by the object deformation must be measured for different sensitivity vectors, by changing either the observation, or the illumination directions, as explained in Sect.IV. In order to have a fixed imaging system and changes of the sensitivity vector which are large enough, we used a setup with three illumination sources. The deformation is recorded with three double-exposure holograms, each of them with another object illumination. For reasons of simplicity in the recording procedure and sensitivity to misalignment errors of the holograms, only one holographic plate is used. The different holograms are spatially multiplexed by rotating a symmetric aperture in front of the holographic plate. The three illumination sources (diverging lenses with f = -6 mm) are arranged around the optical axis as shown in Fig.2. The angle between the illumination directions and the optical axis is typically about 26°. Switching from one illumination source to the other is managed by removable mirrors mounted on precision translation stages [7]. First, the three holograms of the undeformed object state are recorded with the first reference wave on the appropriate part of the hologram plate, changing the illumination sources in the order 1, 2, and 3 (Fig.2). Then, the corresponding holograms of the deformed state are recorded with the second reference wave and the illumination beams 3, 2, and 1, respectively. Following this procedure, no repositioning of the removable mirrors between the hologram exposures is required. It is extremely important, that the optical setup as well as the object in its undeformed and its deformed state are stable during the whole recording procedure.

IV. Evaluation of displacement and strain

A. Determination of vector displacement

The interference phase ϕ and the displacement vector $\vec{u}$ at the object point $\vec{x}$ are related by [8]

$$\phi = k\,(\vec{g}\cdot\vec{u})\ , \tag{3}$$

where $k = 2\pi/\lambda$ is the wave number and $\vec{g}$ denotes the sensitivity vector

$$\vec{g} = \vec{k} - \vec{h}\ . \tag{4}$$

$\vec{k}$ and $\vec{h}$ are the unit vectors of observation and illumination direction, respectively, given by

$$\vec{k} = (\vec{x}_A - \vec{x}_o)/|\vec{x}_A - \vec{x}_o| \quad \text{and} \quad \vec{h} = (\vec{x}_o - \vec{x}_s)/|\vec{x}_o - \vec{x}_s|\ . \tag{5}$$

$\vec{x}_o$, $\vec{x}_A$, and $\vec{x}_s$ are the coordinates of the object point, the observation point, and the illumination source, respectively. It can be seen from Eqs.(4) and (5), that the sensitivity vector $\vec{g}$ is not constant along the object surface, but it depends on the coordinate $\vec{x}_o$. Therefore, $\vec{g}$ has to be calculated for each object point $\vec{x}_o$ independently.

To determine all three components of the displacement vector, three interference phase measurements from three hologram recordings with different illumination sources and thus different sensitivity vectors $\vec{g}_n$ are carried out. Equation (3) can be written in matrix form as

$$\vec{\Phi} = k\,\mathbf{G}\vec{u}\ , \tag{6}$$

with the 3-dim. vector $\vec{\Phi} = (\phi_1,\phi_2,\phi_3)$ and the 3x3 matrix $\mathbf{G}$ with $G_{nk} = (\vec{g}_n)_k$. Equation (6) can now be solved by trigonalization of the matrix $\mathbf{G}$. If the interference phase is measured for more than three independent sensitivity directions, the system of linear equations (6) is overdetermined. Its best solution is found by least squares fitting [9].

As mentioned in the preceeding Section, heterodyne holographic interferometry provides rather the measurement of phase differences $\Delta\phi_x$ and $\Delta\phi_y$ in the orthogonal directions x and y than the total interference phase $\phi(x,y)$ itself. For the evaluation of the displacement field, $\phi(x,y)$ can easily be calculated by summation of the measured phase differences along a given path. Obviously, with respect to the propagation of measurement errors, a simple summation procedure is not ideal. More sophisticated methods with least squares fitting for the summation of the interference phase are described in the literature (see e.g. Ref.10), but they all need extensive computations. However, for strain analysis this is not necessary, since the phase differences between the object points rather than the total phase are important.

B. Determination of surface strain and rotation

In-plane strain and rotation of the object surface can be determined by numerical differentiation of the displacement field in the tangential plane at each point. The grid of sample points on the surface of non-plane objects is generally distorted by perspective. Therefore standard finite difference methods cannot be applied. However, the required derivatives can be calculated by 2-dim. least squares fitting of the displacement vector components through the desired point and its nearest neighbours, as described hereafter.

The location of the sample points on the object surface are obtained by a central projection of the regular grid, which is defined by the interference phase measurement in the image, from the observation point onto the object surface. The derivatives shall be calculated in an arbitrarily chosen sample point, denoted by P_n. The object point P_n is taken as the origin of a new coordinate system (ξ,η), tangential to the surface at this point, with the ξ-axis in the x,z-plane. A certain number N of points P_i around P_n are selected, e.g. 4, 8 or even more, depending on the desired spatial resolution and the accuracy of the displacement measurement. The points P_i are projected onto the ξ,η-plane, where they form in general an irregular grid of points (ξ_i,η_i) (cf. Fig.3). The components of the displacement vector $\vec{u}$ are also expressed in the local coordinate system (ξ,η,ζ). For each component u_k of the displacement vector, a 2-dim. linear function

$$u_k(\xi,\eta) = u_k(0,0) + \xi\ \partial u_k/\partial\xi + \eta\ \partial u_k/\partial\eta \tag{7}$$

is established, which fits the values $u_k(\xi_i,\eta_i)$ at the N sample points best. Least squares fitting yields the first derivatives by solving the system of equations

$$\mathbf{B}\vec{v} = \vec{b} \tag{8}$$

where $\mathbf{B}$ is the symmetrical 3x3 matrix $\mathbf{B} = \mathbf{A}^T\mathbf{A}$ and $\mathbf{A}$ is the 3xN matrix

$$\mathbf{A} = \begin{pmatrix} 1 & \xi_1 & \eta_1 \\ \cdot & \cdot & \cdot \\ \cdot & \cdot & \cdot \\ \cdot & \cdot & \cdot \\ 1 & \xi_N & \eta_N \end{pmatrix} . \tag{9}$$

The vector $\vec{v}$ of the three unknowns and the constant vector $\vec{b}$ are defined by

$$\vec{v} = (u_k(0,0), \partial u_k/\partial\xi, \partial u_k/\partial\eta)\ . \tag{10}$$

$$\vec{b} = \mathbf{A}^T\vec{a}\ ,\ \text{with}\ a_i = u_k(\xi_i,\eta_i)\ ,\ i = 1,..,N. \tag{11}$$

Now, the in-plane strain ε and the rotation ω_ζ are given by

$$\varepsilon_{\xi\xi} = \frac{\partial u_\xi}{\partial\xi}\ ,\ \varepsilon_{\xi\eta} = \varepsilon_{\eta\xi} = \frac{1}{2}\left(\frac{\partial u_\xi}{\partial\eta} + \frac{\partial u_\eta}{\partial\xi}\right)\ ,\ \varepsilon_{\eta\eta} = \frac{\partial u_\eta}{\partial\eta}\ ,$$
$$\text{and}\ \omega_\zeta = \frac{1}{2}\left(\frac{\partial u_\eta}{\partial\xi} - \frac{\partial u_\xi}{\partial\eta}\right)\ . \tag{12}$$

The remaining components of strain and rotation, which are related to the out-of-plane derivatives of the displacement, can be calculated by using the mechanical boundary conditions for an object surface free from external forces [1,11].

C. Accuracy of surface strain determination

The accuracy for the determination of surface strain by holographic interferometry depends essentially on the error in the interference phase measurement. This has been investigated for heterodyne holographic interferometry in Ref.11.

To study the influence of interference phase errors on the evaluation of displacement and strain, one has to distiguish between relative phase errors (subsequently denoted by $\delta\phi$) and errors in the absolute phase ($\Delta\phi$). The former ones determine the accuracy for the measurement of the phase difference between two neighbouring points in the interferogram (sensitivity of phase measurement). This relative phase error is mainly of statistical nature. It is the essential limitation for surface strain determination. The absolute phase (absolute fringe order), on the other hand, is directly related to the change of the optical path length. Its uncertainty is the same all over the interferogram and limits mainly the determination of the displacement.

Although the accuracy for the different components of displacement and strain depends on the optical arrangement, it is appropriate to carry out an analytical estimation for a simple geometry. It shall be assumed, that three holographic interferograms with different illumination directions are evaluated. The illumination sources are arranged symmetrically around the optical axis, at a distance ℓ_s from the origin on the object surface. The illumination directions intersect the optical axis with an angle α and the observation direction is parallel to the optical axis (cf. Fig.2).

If the strain components are calculated by numerical differentiation of the displacement field, one obtains for the standard deviation of the surface strain as a function of the relative phase errors [12]

$$\delta\varepsilon = C \frac{\lambda}{\Delta x \sin\alpha} \frac{\delta\phi}{2\pi} \qquad (13)$$

where λ is the wavelength and the constant C has a value near 1, depending on the different components and the choice of the coordinate system. Δx denotes the base for the numerical differentiation of the displacement components and determines thus the spatial resolution of strain determination. Figure 4 shows the different $\delta\varepsilon$ versus the angle α for an interference phase measurement accuracy of 1°, i.e. $\delta\phi/2\pi = 1/360$, a spatial resolution $\Delta x = 3$ mm and $\lambda = 514$ nm. This corresponds very well with the results given in Ref.11.

The absolute phase (fringe order) is not known a priori from the measurement in the interferogram, therefore the measured interference phase contains an unknown additive constant. The problem can be overcome by refering to an object point without displacement (fixation, vibration node), or by interferometric observation of the deformation in real time and counting the fringes during the displacement. Whereas the knowledge of the absolute fringe order is indispensable for the determination of displacement, its influence on the surface strain components is very small. For the particular geometry described above, one obtains for the error of ε as a function of the uncertainty $\Delta N = \Delta\phi/2\pi$ of the absolute fringe order [12]

$$\Delta\varepsilon_{ii} = \frac{1}{\ell_S}\frac{\cos\alpha}{(1+\cos\alpha)}\lambda\,\Delta N_o \simeq \frac{1}{2}\frac{\lambda}{\ell_S}\Delta N_o\ . \tag{14}$$

where ℓ_s is the distance of the illumination sources from the object surface. For example, with $\lambda = 514$ nm and $\ell_s = 1$ m one gets $\Delta\varepsilon_{ii} \simeq \Delta N$ µm/m. Thus the error in strain determination due to an absolute phase error is in general negligible.

V. Sources of error in interference phase measurement

A. Two-reference-beam holography

Two-reference-beam holography requires special attention to the multiplicity of the reconstructed images and the influence of misalignment of the hologram with respect to the reference beams [5]. To avoid disturbing overlapping of the different reconstructions, the reference sources must be well separated. However, the consequence of large separation of the references is high sensitivity to repositioning errors. Small rotations of the hologram plate result in an additional mutual shift of the two reconstructed images (which causes speckle decorrelation and thus a reduced fringe contrast, cf. Sect.C) and a linear phase deviation in the interferogram [5,13]. The experimental practice shows [12], that in a typical setup with well separated reference sources and with a well designed hologram plate holder, it is possible to realign the hologram to achieve a fringe contrast of better than 80 % (for an f/5.6 imaging lens aperture) and a phase gradient in the interferogram of less than $2\pi\cdot10^{-3}\,\mathrm{mm}^{-1}$.

The use of an optical arrangement with reference sources close together, which would greatly reduce the sensitivity to misalignment [13], is not adequate in heterodyne holographic interferometry, because the resulting overlapping of the cross-reconstructions introduces a statistical interference phase error [14], which is significantly larger than the phase measurement accuracy which can be obtained by heterodyning.

B. Phase errors due to the electronics

In heterodyne holographic interferometry, the interference phase is measured electronically as the relative phase of two detector signals with a zero-crossing phasemeter. Fluctuations in the detected signals introduce a statistical phase error which depends on the signal-to-noise ratio of the detector signal, the heterodyne frequency and the integration time of the phasemeter [1]. Using photomultipliers with shot noise limited detection, a detector area larger than 0.1 mm^2 and an argon laser for hologram reconstruction, an SNR of 40 dB and a phase error below 0.1° can easily be achieved. Thus the electronic detector noise does usually not introduce any significant error to the phase measurement.

Attention must be paid to the cross-talk in the two acousto-optic frequency shifters. The rms value of the random phase error produced by the frequency cross-talk is given by $\delta\phi = \beta/\sqrt{2}$ [12], where β is the optical amplitude of the cross-talk component of the frequency ω in the frequency shifted beam at $\omega + \Delta\omega$. Using two independent quartz oscillators (with HF amplifiers) to drive the AOM's, we achieved $\beta^2 = -52$ dB and thus $\delta\phi = 0.1°$ rms.

C. Speckle decorrelation

The presence of speckles in the image of objects with diffusely scattering surfaces gives rise to a statistical error for the measured interference phase. The interference of non-correlated speckles (or non-correlated parts of speckles) introduces a random contribution to the phase of the mutual intensity of the interfering wavefields. Partial decorrelation of the speckle patterns may be caused by the transverse component of the object displacement.

The influence of speckle decorrelation on the interference phase measurement has been rigorously treated in Ref.14. The resulting mean square phase error due to the speckle noise as a function of the in-plane displacement component is given by

$$\langle\delta\phi^2\rangle = \frac{1}{2N}\ \frac{1 - C_h(2u_I)}{C_h^2(u_I)} \ . \qquad (15)$$

$\delta\phi$ is inversely proportional to the number N of speckles within the detector area. C_h is the autocorrelation of the point spread function h of the imaging system in the holographic reconstruction. For a circular pupil of the lens, C_h is given by the Airy function [1,14]. The phase error can be adequately reduced by increasing the detector surface and thus averaging over many speckles, at the expense of spatial resolution, of course. Figure 5 shows, for a given detector area of 1 mm^2, the statistical phase error $\delta\phi$ versus the number N of detected speckles for different in-plane displacements u_I as parameter. The number of speckles is related to the F-number of the imaging lens. The figure shows, that over a wide range the phase error for constant u_I does not depend on the lens aperture. The reason is that, when the lens aperture is closed, the reduction of the number of speckles which increases the phase error [Eq.(15)] is compensated by the increase of the average speckle size, and thus the fringe contrast, which reduces the phase error. For a given maximum in-plane displacement u_I, the optimum choice for the F-number (minimum phase error and brightest possible image) is determined by the bend of the curves (dashed line in Fig.5), which corresponds to a reduction of the optimum fringe contrast to about 70 %. The minimum phase error due to the speckle decorrelation is given by the simple relation

$$\lim_{N \to 1} \delta\phi = \sqrt{\pi/A_D}\ u_I = u_I/R_D, \qquad (16)$$

where A_D and R_D are the area and the radius of the (circular) detector aperture, respectively.

VI. Experimental results

A. Undeformed object and rigid body motion

The sensitivity and reliability of experimental strain determination can best be tested by measuring an undeformed object or an object undergoing only a rigid body motion. An aluminium plate, which can be rotated about its normal axis, has been investigated by a complete 3-D evaluation of three holograms with different object illuminations, as described in Sect.III. The interference phase has been measured on a grid of 15x15 sample points, 3 mm apart from each other. After the evaluation of the displacement vector field, the three surface strain components and the three rotation components have been calculated by numerical differentiation of the displacement field (cf. Sect.IV).

Table 1 shows the mean values and the standard deviations of strain and local rotation for the evaluated sample points of the undeformed object. The standard deviations (rms values) for surface strain and in-plane rotation are all about 0.2 µm/m, the mean values are all zero within the standard deviation error interval. The out-of-plane rotation ω_x is significantly different from zero due to a systematic deviation of the u_z component.

Table 2 shows the mean values and the standard deviations of strain and rotation evaluated on a plate with a small in-plane rotation of $\omega_z = 38 \cdot 10^{-6}$. The rotation has been chosen so small in order to have small enough in-plane displacement components (<1.5 µm) at the border of the evaluated surface area, which do not yet introduce a detectable statistical phase error due to speckle decorrelation (cf. Fig.5). Theoretically, all components, except the rotation ω_z, should be equal to zero. The measured rms errors are larger than for the undeformed object, but still of the order of a fraction of one micro-strain for a spatial resolution of 6 mm. Only the standard deviation for the ε_{yy} component is somewhat larger. Furthermore, the mean value of ε_{xx} is significantly different from zero. From an analysis of the 2-dim. phase and displacement fields, it can be seen that the deviations of the two normal strain components are rather of systematic nature and not due to statistical errors in the interference phase measurement.

The systematic deviations observed in the above experiments are mainly caused by repositioning errors of the hologram plate and atmospheric turbulences during hologram recording. The statistical interference phase measurement accuracy has been shown to be much better, namely of the order of 1/1000 fringe or 0.3° rms. This shows clearly, that limitations to strain determination in heterodyne holographic interferometry do not arise from limitations in the interference phase measurement technique, but rather from the interferometry itself, that is to say from the stability of the optical setup, air turbulences, zero order fringe errors, and inaccurately known geometrical data of the setup.

B. Cylindrical vessel with internal pressure

Another investigated test object was a cylindrical vessel loaded by internal pressure [11]. In this case, the strain has to be evaluated on a curved surface. The cylindrical vessel was an aluminium tube with a radius of R = 10 cm and a wall thickness of b = 5 mm (Fig.6). In the experiment described hereafter, the internal pressure difference was 2.6 bar.

For a curved object surface, it is adequate to introduce a surface oriented local coordinate system (ξ,η,ζ) at each observed object point. For the cylindrical object, the ξ-axis is chosen tangential to the surface at each point and perpendicular to the axis of the cylinder (η-axis) (cf. Fig.6). The displacement components, which are calculated in the laboratory coordinate system (x,y,z), are then transformed into tangential (u_ξ), axial (u_η), and radial (u_ζ) components. The surface strain components $\varepsilon_{\xi\xi}$, $\varepsilon_{\xi\eta}$, and $\varepsilon_{\eta\eta}$ are calculated by numerical differentiation of the displacement field in the surface oriented local coordinate system.

Figure 7 shows the interference fringe patterns of the three holograms, recorded with different illumination directions. The indicated rectangular area corresponds to the field of 31x5 sample points, for which the interferogram has been analyzed. In Fig.8, the measured phase functions along a horizontal line through the three interferograms are plotted. The absolute fringe order for each illumination direction has been determined from three corresponding real-time holograms of the cylinder deformation.

Figure 9 shows the experimentally determined displacement components along a radial section on the cylinder surface. The corresponding strain components are displayed in Fig.10. The reliability of the measurements has been checked by the evaluation of the interferogram for the same holographic recording on two interlaced grids of sample points (o and *, respectively). The standard deviation of the difference between the two measurements is of the order of 1 µm/m. These results illustrate impressively the power of heterodyne holographic interferometry. It is possible to determine all components of surface strain and rotation on a curved surface with an accuracy of about one micro-strain for a spatial resolution of a few millimeters.

VII. Conclusions

It is interesting to compare the features and the performance of heterodyne holographic interferometry and quasi-heterodyne [13,15,16] (step-wise phase shifting) techniques with video-electronic detection in view of their appropriate applications. Both, heterodyne and quasi-heterodyne techniques, offer automated data acquisition for a large number of sample points with high spatial resolution. The phase measurement is highly accurate, independent of variations of the mean intensity and the fringe contrast, and there is no sign ambiguity.

Heterodyne holographic interferometry offers very high accuracy for the interference phase measurement (better than 1/1000 of a fringe). The principle of heterodyning requires sophisticated electronic equipment, such as AOM's with HF drivers and phasemeters. The mechanical scanning of the image by photodetectors makes it slow (about 1 sec per point). Since the phase measurement accuracy can be very high, an arrangement with reference sources close together, which would introduce additional errors due to the overlapping of decorrelated speckles, is not adequate. Well separated reference sources, on the other hand, impose strong requirements to the stability of the optical setup and to the repositioning of the hologram. For recording and reconstruction, one and the same experimental setup has to be used.

The described arrangement, using three double-exposure hologram recordings with different illumination beams, provides surface strain measurement of extremely high resolution. For the strain components, obtained from the local derivatives of the experimentally determined displacement field, an accuracy of about 1 micro-strain with a spatial resolution of a few millimeters has been achieved. The determination of the displacement itself requires, however, in addition the knowledge of the absolute fringe order for each holographic interferogram, because the information on the mutual phase between the three interferograms is not directly available from the separately recorded holograms. The experimental results show clearly, that it is not the heterodyne fringe interpolation technique that limits the measurement accuracy, but rather air turbulence, hologram repositioning and speckle decorrelation due to large in-plane displacements.

Quasi-heterodyne holographic interferometry with TV-detection offers a moderate accuracy for the fringe interpolation (about 1/100 of a fringe), with all the advantages of phase shifting interferometry. An optical arrangement with two reference sources close together is nearly as simple and uncritical for the hologram recording and reconstruction as standard double-exposure holography. It requires no special instrumentation apart from a microcomputer with a video frame grabber, which is normally implemented in a standard image processing system. Data acquisition from the interferogram is very fast, even for a large number of sample points. With the experiental arrangement described in Ref.16, good results for 3-D dispacement analysis have been achieved. For the evaluation of surface strain, a typical sensitivity of about 10 µm/m with a spatial resolution of a few millimeters can be expected.

To summarize this comparison: Heterodyne holographic interferometry is well suited for scientific applications in laboratory environment, where the ultimate limits for strain determination are required. On the other hand, quasi-heterodyne holographic interferometry with TV-detection is suited for applications in industrial environment, for deformation and vibration analysis, where moderate accuracy is required. Note however, that this means moderate compared with heterodyne systems and that the capabilities of phase shifting techniques for displacement and strain measurement are anyway at least one order of magnitude better than those of conventional holographic interferometry.

References

1. R. Dändliker, "Heterodyne holographic interferometry", in Progress in Optics, Vol. XVII, E. Wolf, ed. (North Holland, Amsterdam, 1980), pp. 1-84.

2. R.J. Pryputniewicz, "Heterodyne holography applications in studies of small components", Opt. Eng. 24, 849-854 (1985).

3. P.V. Farrell, G.S. Springer, and C.M. Vest, "Heterodyne holographic interferometry: concentration and temperature measurements in gas mixtures", Appl. Opt. 21, 1624-1627, (1982).

4. R. Thalmann, R. Dändliker, "Holographic contouring using electronic phase measurement", Opt. Eng. 24, 930-935 (1985).

5. R. Dändliker, E. Marom, and F.M. Mottier, "Two-reference-beam holographic interferometry", J. Opt. Soc. Am. 66, 23-30 (1976).

6. J. Mastner and V. Masek, "Electronic instrumentation for heterodyne holographic interferometry", Rev. Sci. Instrum. 51, 926 (1980).

7. P. Hariharan, B.F. Oreb, and N. Brown, "Real-time holographic interferometry: a microcomputer system for the measurement of vector displacements", Appl. Opt. 22, 876-880 (1983).

8. see e.g., C.M. Vest, Holographic Interferometry, (John Wiley & Sons, New York, 1979), Chapt.2.

9. K.A. Stetson, "Matrix methods in hologram interferometry and speckle metrology", Nato Advanced Study Institute on Optical Metrology, July 1984, Viana de Castelo, Portugal, (NATO ASI Series, Martinus Nijhoff Publishers, The Hague, 1986).

10. B.R. Hunt, "Matrix formulation of the reconstruction of phase values from phase differences", J. Opt. Soc. Am. 69, 393-399 (1979).

11. R. Dändliker and B. Eliasson, "Accuracy of heterodyne holographic strain and stress determination", Exp. Mech. 19, 93-101 (1979).

12. R. Thalmann, "Electronic fringe interpolation in holographic interferometry, applied to deformation measurement of solid objects", Ph.D. thesis, (University of Neuchâtel, Switzerland, 1986).

13. R. Dändliker, R. Thalmann, J.-F. Willemin, "Fringe interpolation by two-reference-beam holographic interferometry: reducing sensitivity to hologram misalignement", Opt. Commun. 42, 301-306 (1982).

14. R. Thalmann and R. Dändliker, "Statistical properties of interference phase detection in speckle fields, applied to holographic interferometry", J. Opt. Soc. Am. A 3, 972-981 (1986).

15. R. Dändliker, R. Thalmann, "Heterodyne and quasi-heterodyne holographic interferometry", Opt. Eng. 24, 824-831 (1985).

16. R. Thalmann and R. Dändliker, "Automated evaluation of 3-D displacement and strain by quasi-heterodyne holographic interferometry", Proc. of SPIE, Vol. 599, 141-148 (1986).

Tables

Table 1. *Experimentally determined mean values and standard deviations of strain and rotation components from a holographic interferogram of an undeformed object.*

	ε_{xx}	ε_{yy}	ε_{xy}	ω_x	ω_y	ω_z
mean value [μm/m]	-0.25	0.23	-0.22	-0.26	0.01	-0.08
standard deviation [μm/m]	0.22	0.3	0.14	0.04	0.04	0.17

Table 2. *Experimentally determined mean values and standard deviations of strain and rotation components from a holographic interferogram of a rotated plate.*

	ε_{xx}	ε_{yy}	ε_{xy}	ω_x	ω_y	ω_z
mean value [μm/m]	-2.61	-1.43	-0.91	0.03	-0.92	38.0
standard deviation [μm/m]	0.71	1.35	0.71	0.3	0.5	0.68

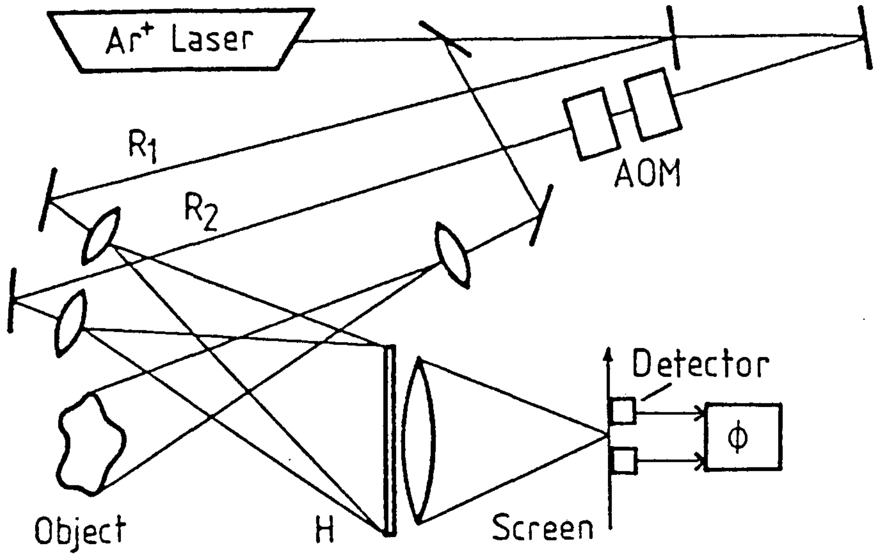

Fig.1. Arrangement for heterodyne holographic interferometry using two acousto-optic modulators to generate the frequency offset.

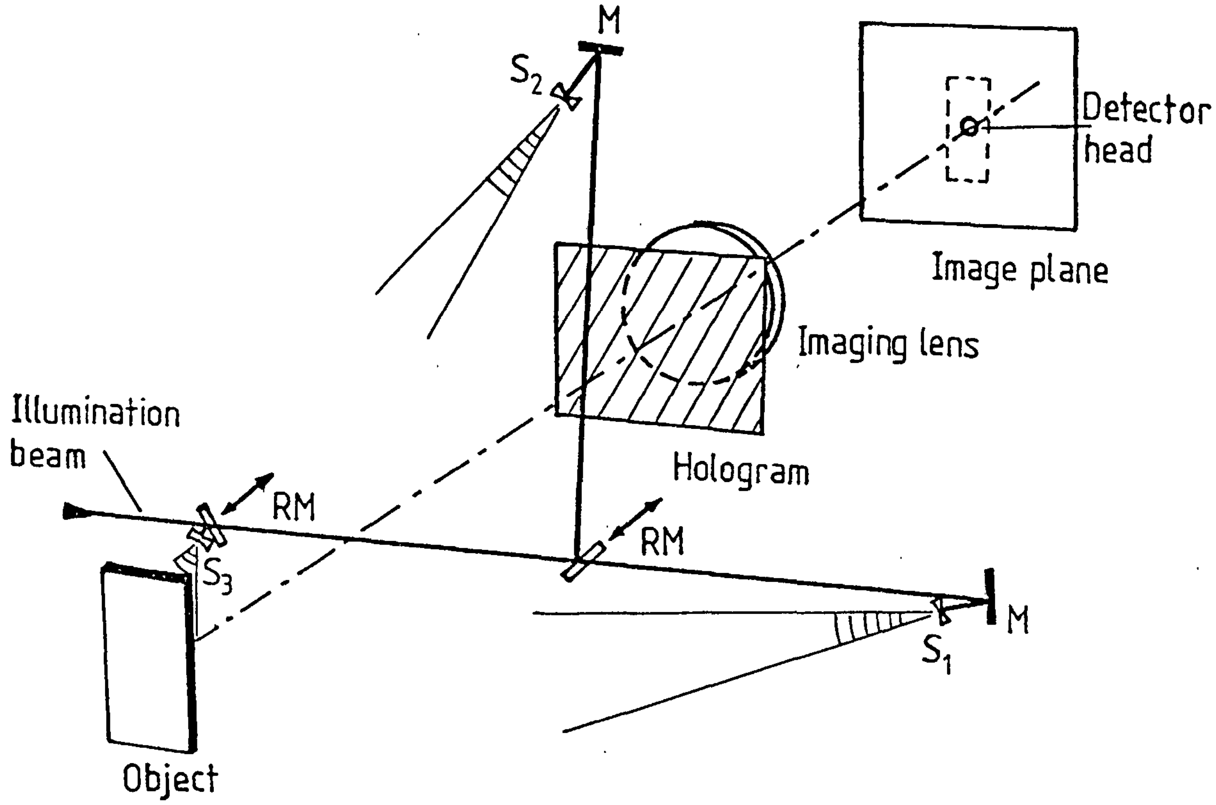

Fig.2. Schematic representation of the optical arrangement for hologram recording and observation. With the help of removable mirrors (RM), the illumination beam can be switched from source S_1 to S_2 and S_3 (diverging lenses).

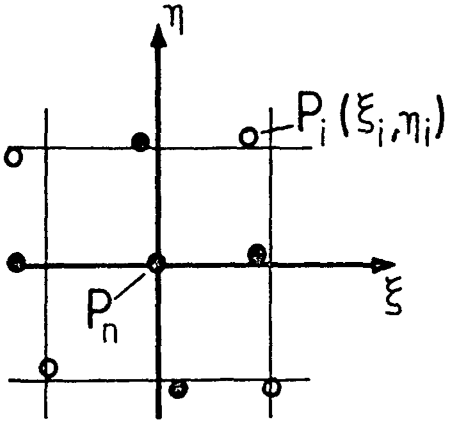

Fig.3. (ξ,η) is a plane tangential to the object surface at the point P_n. The derivatives of the displacement at P_n are obtained by fitting a 2-dim. linear function through P_n and its (4, 8 or more) nearest neighbours $P_i(\xi_i,\eta_i)$.

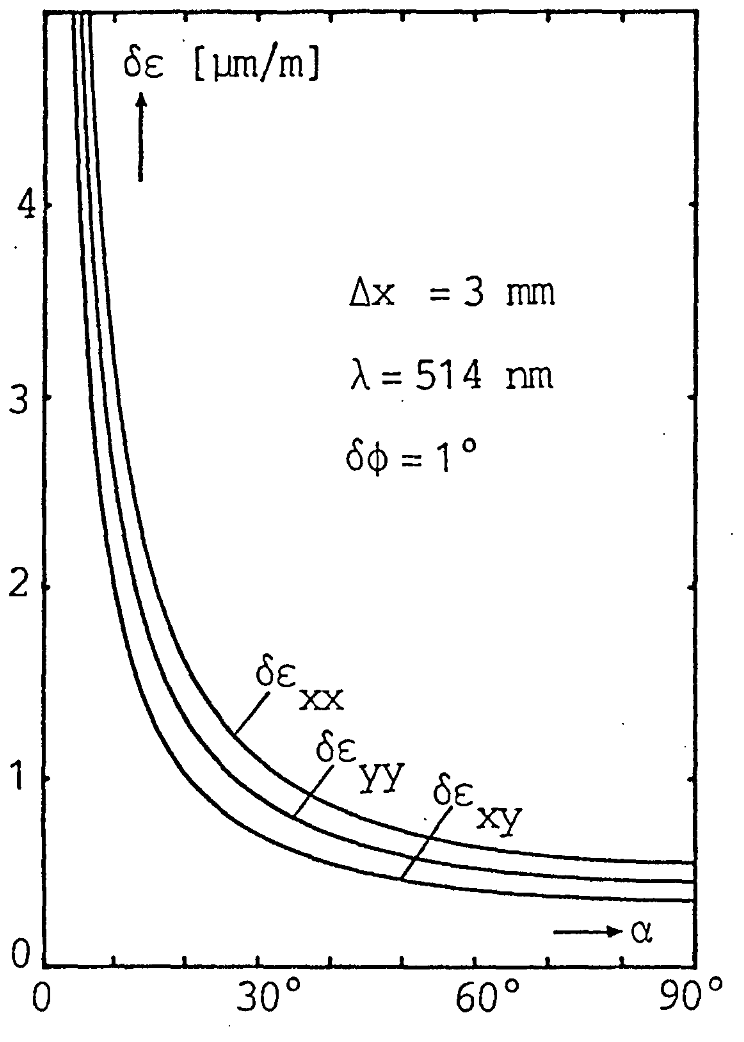

Fig.4. Accuracy of surface strain determination versus angle α between illumination and observation direction in the case of three symmetrically arranged illumination sources.

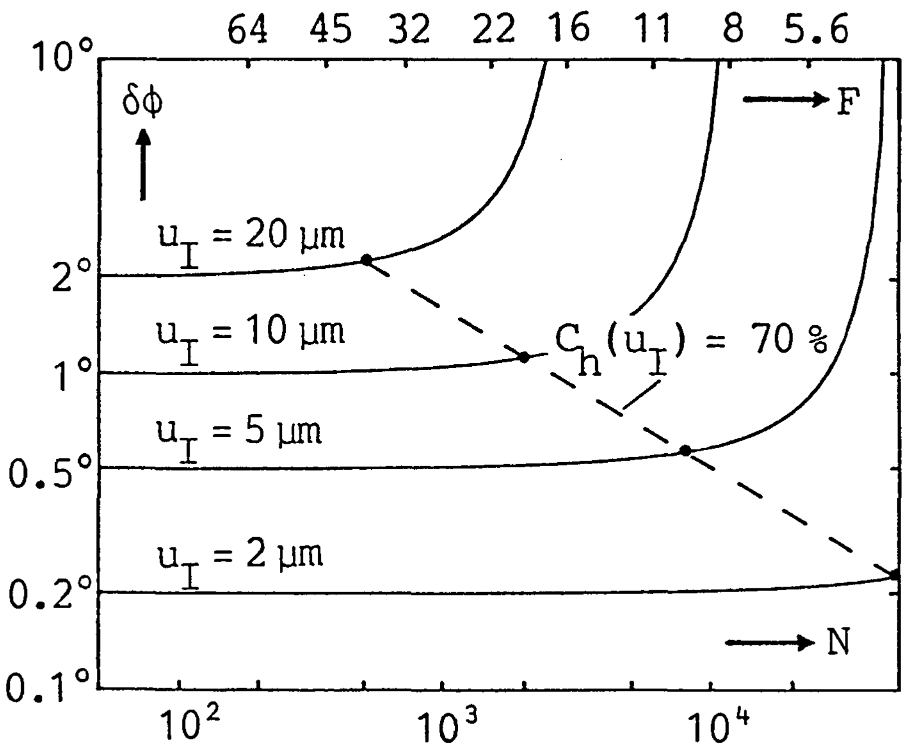

Fig.5. Statistical phase error $\delta\phi$ due to speckle decorrelation versus number N of detected speckles for different in-plane displacements u_I. (Detector area $A_D = 1\ mm^2$).

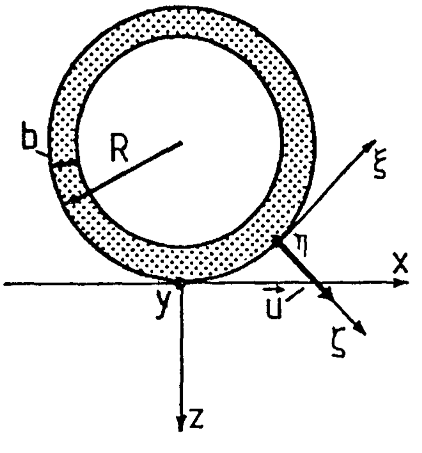

Fig.6. Cross-section through the cylindrical tube loaded by internal pressure. The displacement $\vec{u}$ and the strain along the curved surface will be represented in the local coordinate system (ξ,η,ζ).

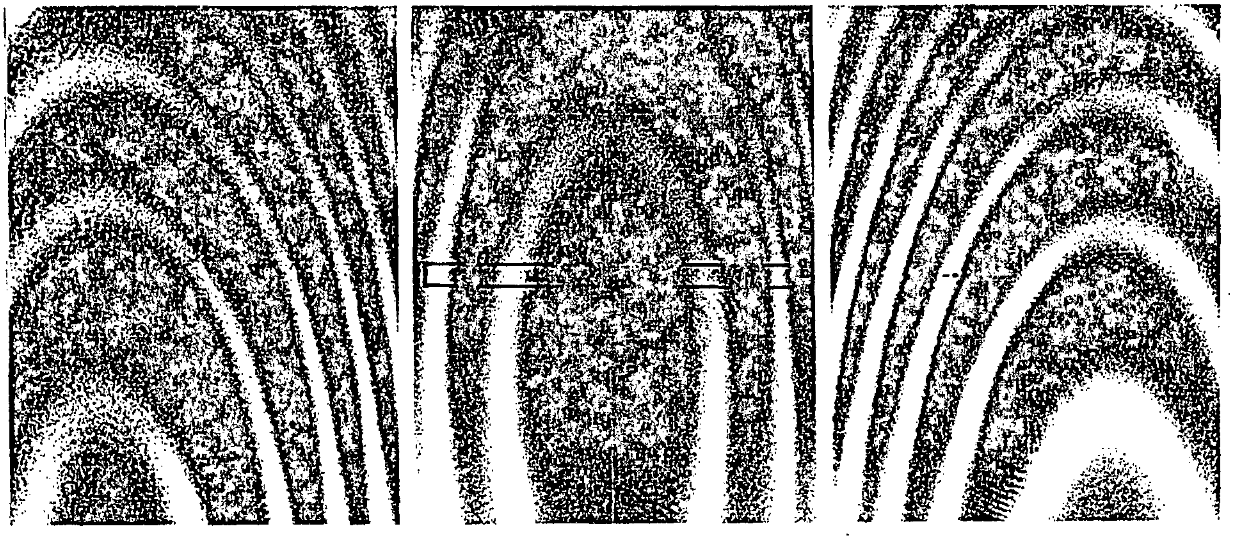

Fig.7. Interference fringe patterns on a cylindrical vessel deformed by internal pressure for three illumination directions. The rectangular field indicates the area, where the interferogram has been evaluated.

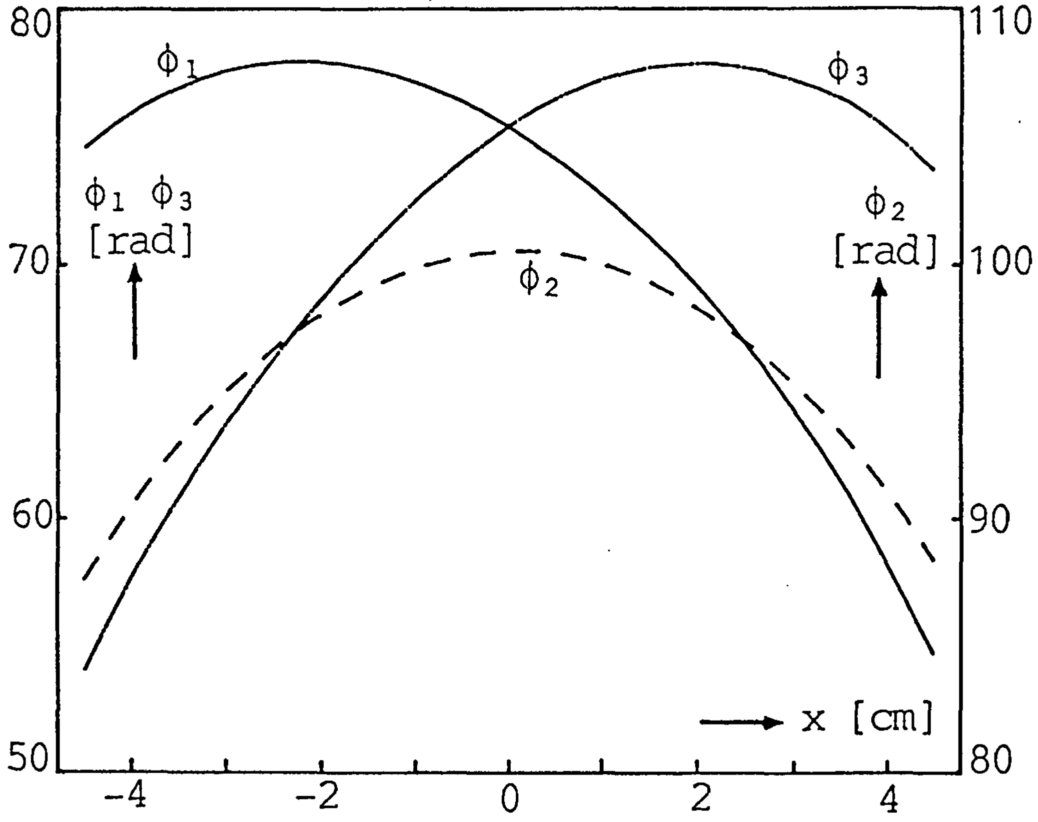

Fig.8. Measured phase functions along a horizontal line through the interferograms of Fig.7.

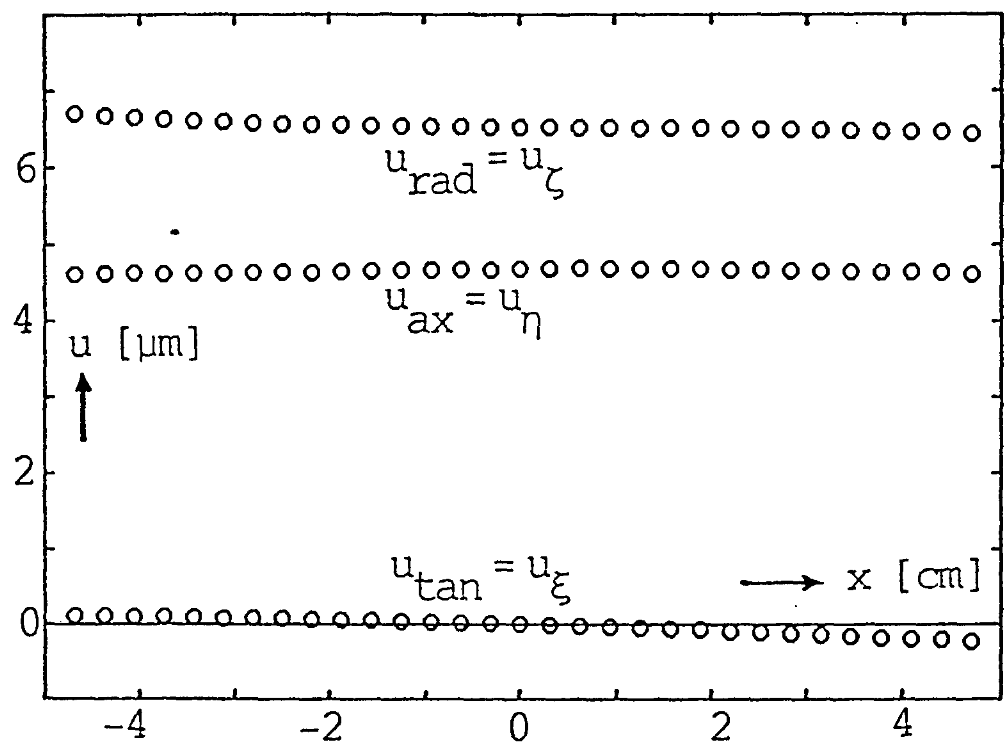

Fig.9. Experimentally determined radial, axial and tangential displacement components on the (curved) cylinder surface.

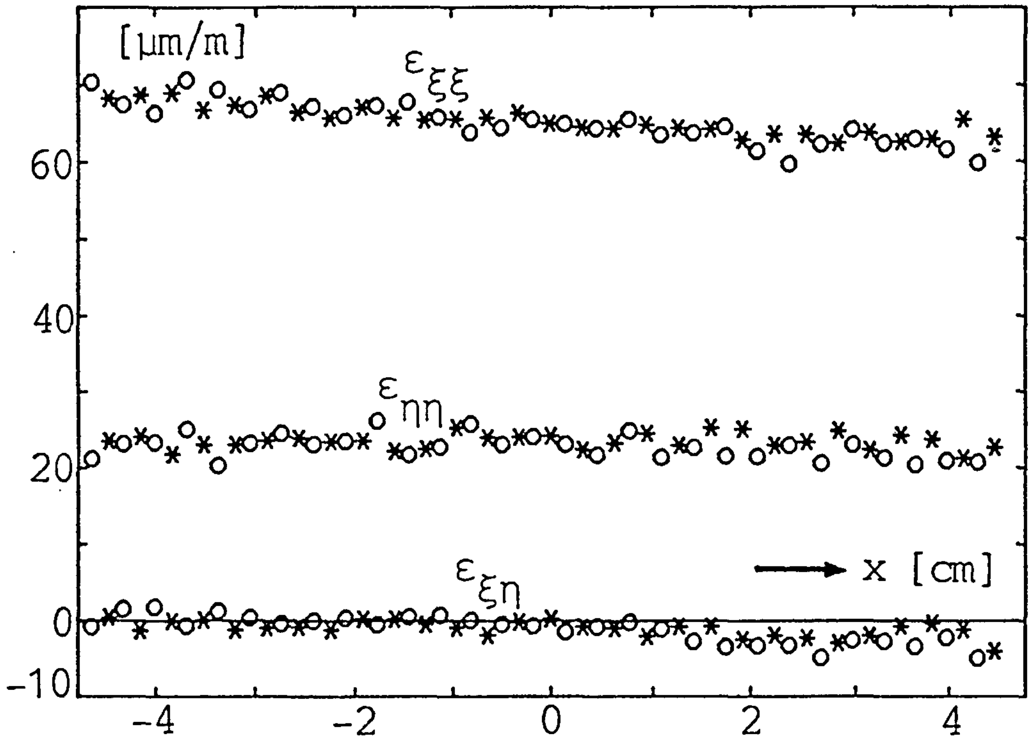

Fig.10. Experimentally determined surface strain components $\varepsilon_{\xi\xi}$, $\varepsilon_{\eta\eta}$, and $\varepsilon_{\xi\eta}$ of cylindrical vessel, evaluated from interference phases measured on two interlaced grids of sample points (o and *).

Liste de publications

- R. Dändliker, R. Thalmann, and J.-F. Willemin, "Fringe interpolation by two-reference beam holographic interferometry: Reducing sensitivity to hologram misalignment", Opt. Commun. 42, 301-306 (1982).

- R. Thalmann, R. Dändliker, "High resolution video-processing for holographic interferometry applied to contouring and measuring deformations", European Conference on Optics, Optical Systems and Applications, Proc. of SPIE492, 299-306 (1985).

- R. Dändliker, R. Thalmann, "Heterodyne and quasi-heterodyne holographic interferometry", Opt. Eng. 24, 824-831 (1985).

- R. Thalmann, R. Dändliker, "Holographic contouring using electronic phase measurement", Opt. Eng. 24, 930-935 (1985).

- R. Thalmann, R. Dändliker, "Automated evaluation of 3-D displacement and strain by quasi-heterodyne holographic interferometry", Optics in Engineering Measurement, Proc. of SPIE 599, 141-148 (1986).

- R. Thalmann, R. Dändliker, "Statistical properties of interference phase measurement in speckle fields, applied to holographic interferometry", J. Opt. Soc. Am. 3, 972-981 (1986).

- R. Thalmann, R. Dändliker, "Strain measurement by heterodyne holographic interferometry", to be published in Appl. Opt. 26, (1987).